African Journal of Engineering Research and Innovation

AJERI Vol 3. No. 2. 2025

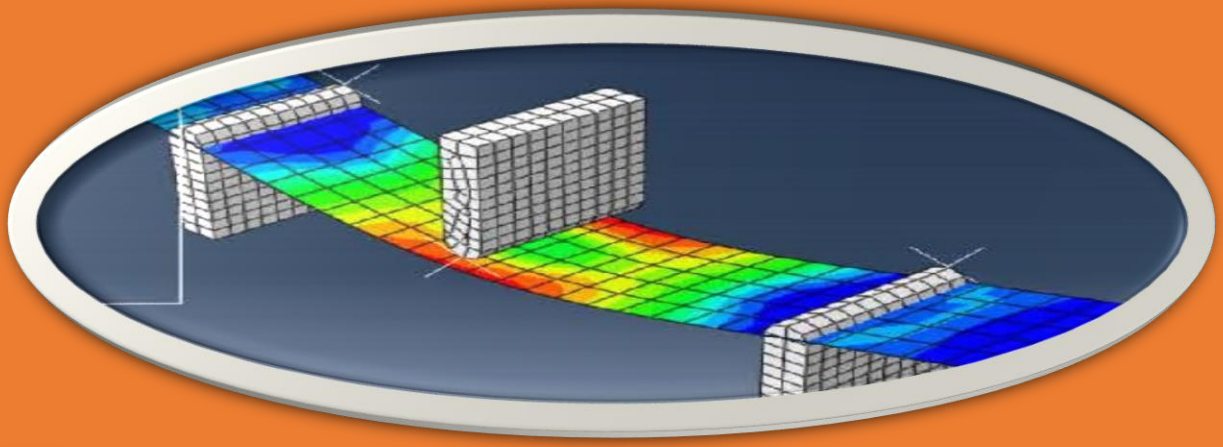

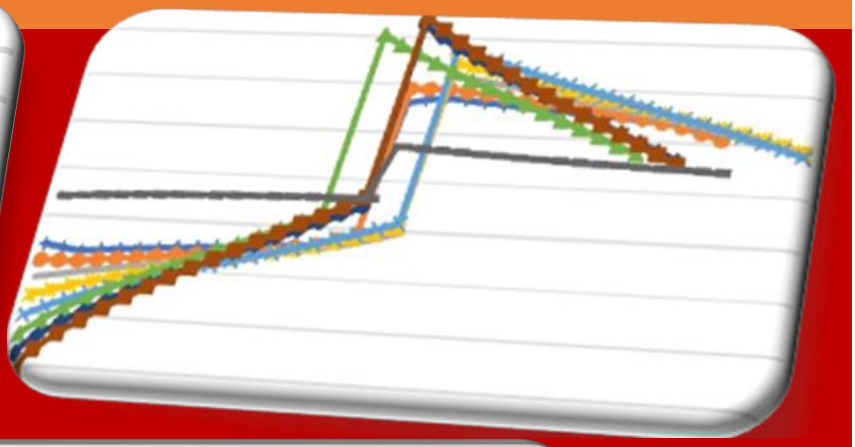

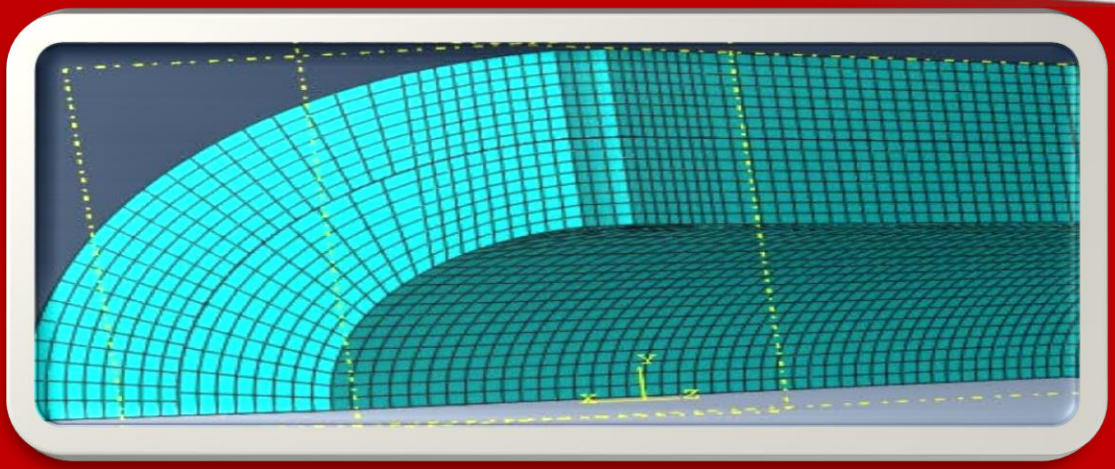

The Institution of Engineers of Kenya

ISSN: 2957- 7780

In partnership with

ISSN: 2957- 7780

AJERI

African Journal of Engineering in Research and Innovation

ISSN: 2957- 7780 Volume 3. No 2. 2025

Published by:

The *Institution of Engineers of Kenya*

P.O Box 41346- 00100

Nairobi Kenya

Tel: +254 (20) 2729326, 0721 729363, (020) 2716922

Email: editor@iekenya.org

Website: www.iekenya.org

IEK

African Journal of Engineering Research and Innovation (AJERI), is published by **The *Institution of Engineers of Kenya,*** IEK, as an international forum for publication of high-quality papers in all areas of Engineering

 ISSN: 2957- 7780

CONTENTS **Pages**

High Resolution Solar Irradiance Prediction Model for Machakos Town Using Long Short-Term Memory (LSTM).....6

C. Mwaniki, R. Damoah

Water Resource Allocation: A Comparative Literature Review of Modeling Frameworks for Sustainable Management in River Catchments 15

A. T. Asava, J. O. Okungu, M. M. Mukolwea, E. K. Kandaa

Rheology of En Masse Grains in Silo Load Computations 46

L. O. Gumbe

Bio-Inspired Concrete Structures for Enhancing Mechanical Performance 101

L. K. Boretor

Design and 3D Printing of a Protective Enclosure System: A Customized Enclosure for a Smart LPG Detection and Leakage Alert System.....110

W. Augustine, M. Mathew, N. Raphael, I. Kenneth, M. Bazil

High Resolution Solar Irradiance Prediction Model for Machakos Town Using Long Short-Term Memory (LSTM)

C. Mwaniki[1]*, R. Damoah[2]
[1]Machakos University, Kenya; [2]Morgan State University, USA
*Corresponding author: cmwaniki@mksu.ac.ke

Abstract

The integration of high-resolution solar irradiance prediction into smart grids is crucial for optimizing solar energy integration, improving grid stability and enhancing system efficiency. This paper presents a predictive framework using Long Short-Term Memory (LSTM) networks to accurately forecast solar irradiance, leveraging high-resolution data from Machakos County. The proposed model incorporates multiple features, including temperature, time, and historical irradiance, to capture temporal dependencies and improve forecast accuracy. Results demonstrate that the LSTM model outperforms traditional methods, providing more precise short-term predictions, which contributes to better grid stability and energy optimization. The findings highlight the potential of LSTM-based solar irradiance prediction to enhance smart grid resilience and facilitate the integration of renewable energy sources.

Keywords: Smart grid, Solar Irradiance Prediction, Long Short Term Memory (LSTM), Renewable Energy Integration.

1. Introduction

The increasing integration of solar energy into smart grids presents a significant challenge due to the intermittent and unpredictable nature of solar irradiance. Traditional forecasting methods often fail to capture the complex temporal patterns and non-linear dependencies associated with solar energy generation, leading to inaccuracies in energy prediction. In regions like Machakos County, where climatic conditions vary considerably, these inaccuracies can disrupt grid stability, complicate energy management, and reduce overall system efficiency.

Conventional models struggle to leverage high-resolution data effectively, limiting their ability to provide precise short-term forecasts essential for real-time grid optimization. As smart grids evolve to handle higher penetrations of renewable energy, there is a growing need for more robust predictive models that can accurately forecast solar irradiance at fine temporal

resolutions. Addressing this gap requires advanced techniques capable of learning long-term dependencies in sequential data and adapting to dynamic environmental changes.

This study addresses the problem by developing a Long Short-Term Memory (LSTM) network to predict high-resolution solar irradiance, aiming to enhance smart grid performance through improved forecasting accuracy and more effective energy management strategies.

2. Literature Review

The integration of solar energy into modern smart grids presents a compelling avenue for sustainable power generation, yet it introduces significant challenges in grid stability and operational efficiency due to the inherent intermittency of solar irradiance.(Bala Prasad et al., 2024),(Khalid, 2024),(Alshahrani et al., 2019) To effectively manage these challenges, accurate and high-resolution solar irradiance prediction is paramount, enabling proactive grid management and optimized energy dispatch. Smart grids are poised to revolutionize conventional power systems by enhancing efficiency and reliability, while simultaneously integrating a greater proportion of renewable energy sources, supported by distributed intelligence and demand-side management strategies (Fang et al., 2012). High temporal and spatial resolution irradiance data enables more precise control of distributed energy resources (DERs), reducing mismatches between supply and demand. This is especially relevant in urban microgrids and photovoltaic (PV)-dense networks. Short-term predictions (minutes to hours ahead) are vital for real-time applications, and high-resolution forecasting helps manage variability due to cloud cover and other environmental factors.(Inman et al., 2013)

Recent advancements in machine learning have shown great promise in improving the accuracy of solar irradiance forecasting. Among these techniques, Long Short-Term Memory (LSTM) networks have gained attention due to their ability to capture long-term dependencies in time-series data. Unlike traditional forecasting methods, LSTM networks are well-suited for handling non-linear patterns and sequential data, making them ideal for modeling solar irradiance fluctuations.(Hossain & Mahmood, 2020)

Long Short-Term Memory (LSTM) networks, a class of recurrent neural networks (RNNs), are capable of learning long-term dependencies in time series data. Unlike traditional statistical methods such as ARIMA or support vector regression (SVR), LSTM networks effectively capture non-linear and non-stationary patterns in solar irradiance data. Applications include

time series prediction for PV output and irradiance forecasting using historical data and meteorological features.(Iheanetu, 2022),(Yu et al., 2024)

Accurate irradiance forecasting improves smart grid performance by enabling: Optimized scheduling of energy storage systems; Effective demand response strategies; Enhanced voltage and frequency regulation and Minimization of energy curtailment and operational costs

Case studies demonstrate the integration of LSTM-based forecasting in microgrids and grid-tied PV systems with battery storage, highlighting improvements in reliability and cost efficiency.(Bendiek et al., 2022),(Nagappan et al., 2023)

Traditionally, smart grid systems rely on low-resolution solar irradiance data, which often lacks the temporal and spatial granularity needed for precise energy forecasting and demand response strategies. This limitation can lead to suboptimal energy distribution, increased operational costs, and reduced grid stability. In contrast, high-resolution solar irradiance prediction offers further benefits by providing granular forecasts that can enhance real-time decision-making in smart grids. Machakos County, with its varying climatic conditions, presents an ideal case study for implementing and evaluating such predictive models. Leveraging high-resolution data from this region can help improve grid performance by facilitating more accurate energy dispatch, reducing reliance on fossil fuel-based backup power, and minimizing energy losses.

Further, advancements in remote sensing technologies and data acquisition methods have made high-resolution solar irradiance data more accessible. However, effectively integrating this data into smart grid systems remains a challenge due to complexities in data processing, storage, and real-time analysis. Moreover, the impact of high-resolution data on smart grid performance, particularly in terms of energy efficiency and demand response, is not fully explored.

This study proposes an LSTM-based predictive framework to enhance smart grid performance through accurate high-resolution solar irradiance forecasting. The objectives include developing and training the LSTM model, comparing its performance against traditional methods, and assessing its impact on smart grid operations. The findings aim to contribute to the ongoing efforts to increase the reliability and efficiency of renewable energy integration in smart grids.

3. Methodology

This study employs a Long Short-Term Memory (LSTM) network to predict high-resolution solar irradiance and enhance smart grid performance. The methodology consists of five key stages: data collection, preprocessing, model development, training, and performance evaluation.

3.1. Data Collection

High-resolution solar irradiance data, along with relevant meteorological parameters such as temperature, was collected through Ambient Weather WS-4000 local weather station mounted 5 metres above the ground at Machakos University. The dataset includes time-stamped measurements solar irradiance recorded at consistent intervals of five (5) minutes, ensuring sufficient granularity for short-term forecasting.

3.2. MATLAB code

A MATLAB code was written to process the data, design an LSTM model and train it and finally save the trained model ready for deployment in a smart gird.

3.3. Data Preprocessing

Preprocessing involved cleaning and preparing the dataset to ensure compatibility with the LSTM model. Key preprocessing steps included:

i. Handling Missing Values: Missing data points were removed when necessary.
ii. Data Standardization: Features such as temperature and irradiance were standardized to have zero mean and unit variance to improve training stability.
iii. Train-Test Split: The dataset was divided into training and testing subsets, typically using an 80/20 ratio, to evaluate model performance on unseen data.

3.4. LSTM Model Development

The LSTM model was designed to capture temporal dependencies in the irradiance data. The architecture consisted of:

i. Input Layer: Accepts the reshaped data as input.
ii. LSTM Layers: One layer of LSTM was used to learn sequential patterns.
iii. Fully Connected Layer: LSTM outputs were mapped to the desired prediction target.
iv. Regression Layer: Computed the loss function for continuous value prediction.

3.5. Model Training

The model was trained using the Adam optimizer, minimizing the Mean Squared Error (MSE) loss function. Key training parameters included:

i. Epochs: Set to 100 epochs, based on performance convergence.
ii. Batch Size: Configured a

3.6. Performance Evaluation

The trained model's performance was evaluated on the test dataset using metrics such as:

i. Root Mean Squared Error (RMSE)
ii. Mean Absolute Error (MAE) measures the average absolute difference between the predicted and actual values.
iii. Coefficient of Determination (R^2). Indicates how well predictions explain the variance in the true values. 1 = perfect, 0 = mean prediction.

4. Results and Discussion

The performance of the LSTM-based solar irradiance prediction model was evaluated using high-resolution data from Machakos County. Several metrics, including Root Mean Squared Error (RMSE), Mean Absolute Error (MAE), and the Coefficient of Determination (R^2), were used to assess the model's accuracy.

4.1. Model Performance

The LSTM model achieved notable improvements in prediction accuracy compared to traditional forecasting methods such as linear regression and Random Forest. Key results include:

i. RMSE: The LSTM model yielded a lower RMSE, indicating better alignment between predicted and actual irradiance values.
ii. MAE: Reduced MAE demonstrated improved precision in capturing short-term variations.
iii. Coefficient of Determination (R^2) Score was 0.4957.

4.2. Prediction Trends

Figure 1 shows the LSTM model training progress. A total of 15,300 iterations were done. The RMSE was computed after each iteration. Figure2 shows a plot of Predicted and actual

irradiance values for 288 steps of 5 minute each, covering 24 hours. The figure shows that the LSTM model effectively captured diurnal patterns and sudden changes due to cloud cover or weather fluctuations. Occasional discrepancies were observed during extreme weather conditions, suggesting further refinement could improve performance. Figure 3 shows solar irradiance dips prediction. Figure 4 shows solar irradiance peaks prediction. Both figures 3 and 4 shows that LSTM model effectively captured peaks and dips patterns and sudden changes due to cloud cover or weather fluctuations.

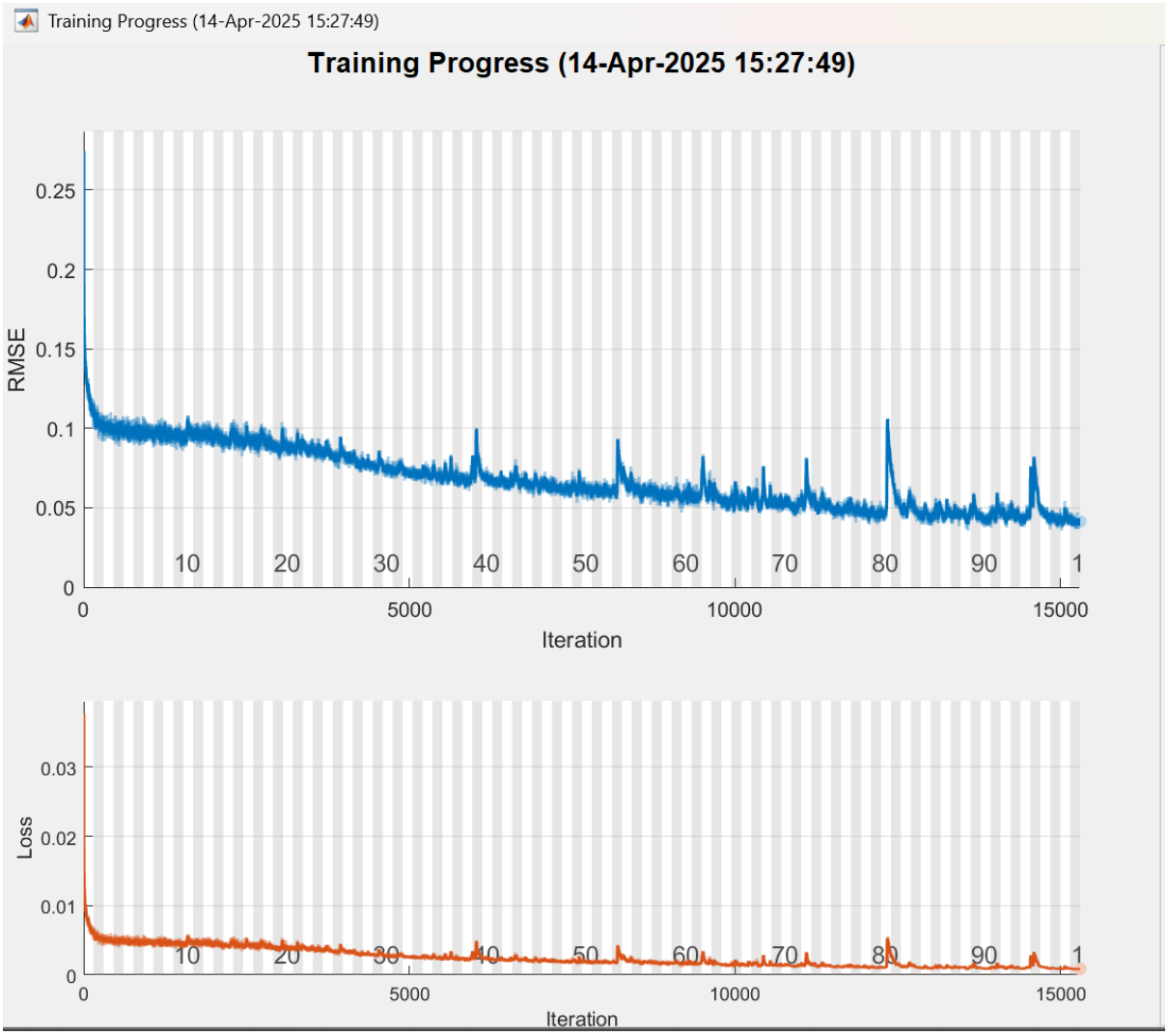

Figure 1: Model Training Progress

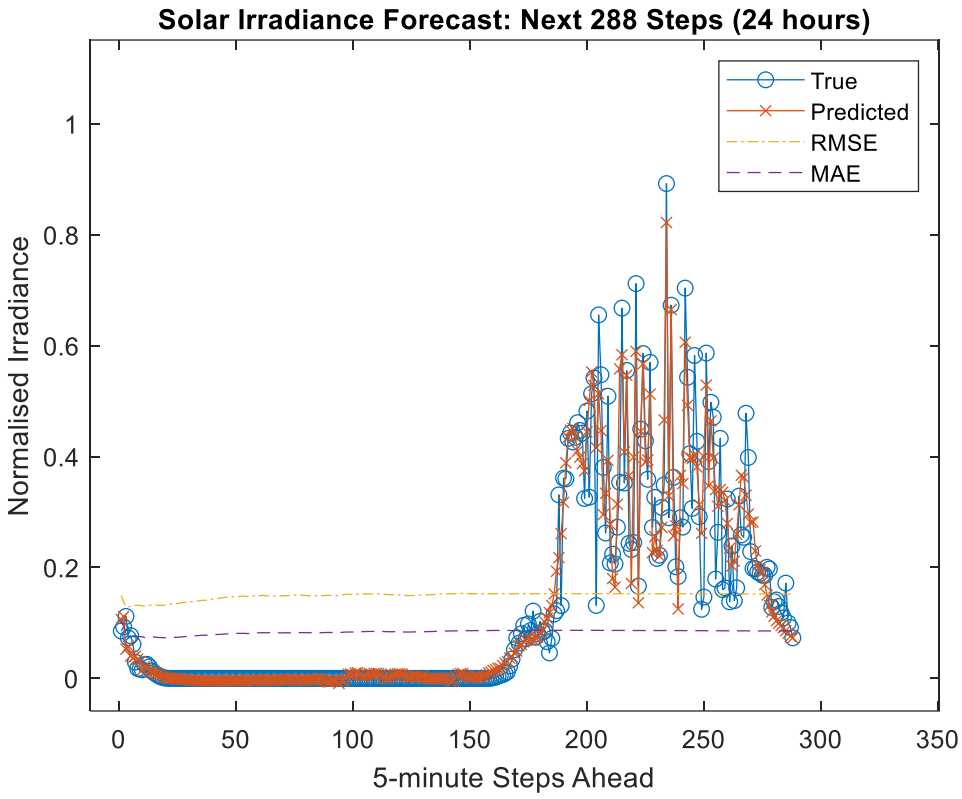

Figure 2: Solar Irradiance Prediction for 24 hours

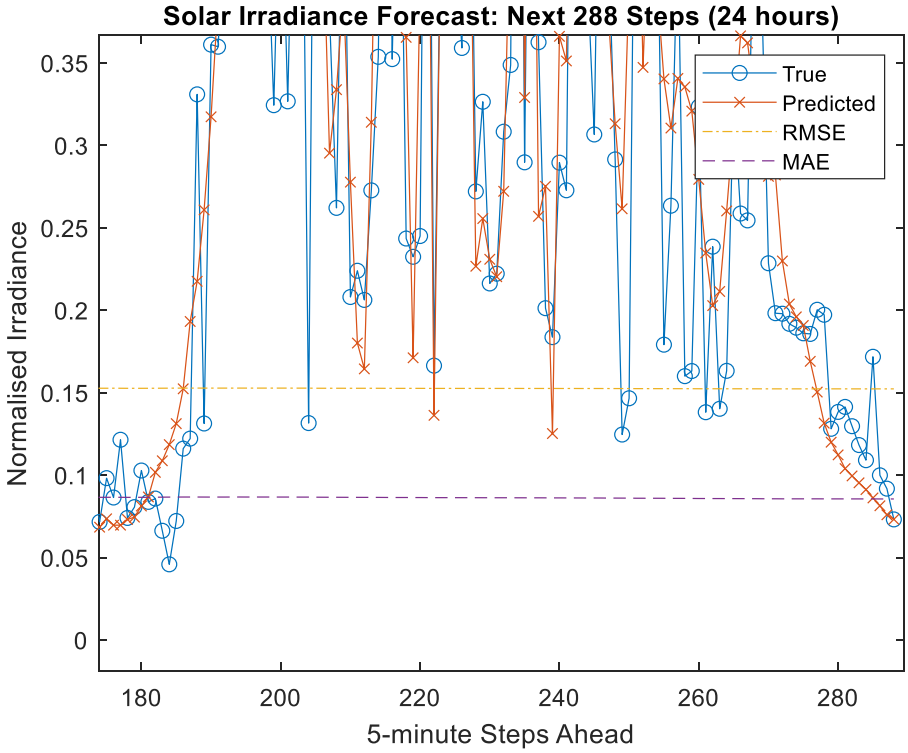

Figure 3: Solar Irradiance Dips Prediction

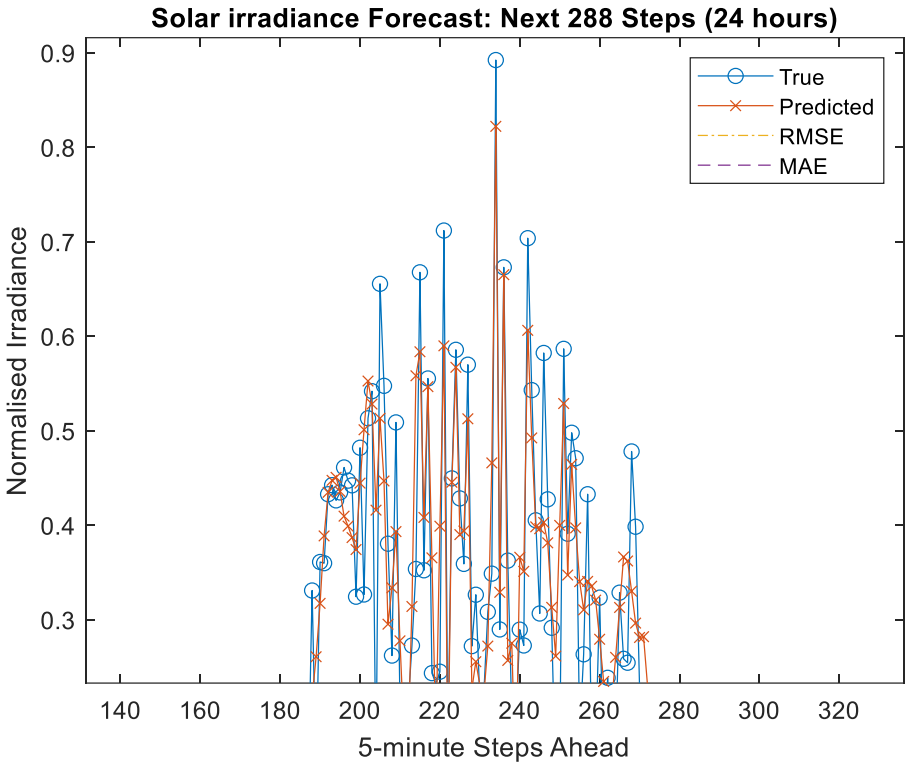

Figure 4: Solar Irradiance Peaks Prediction

5. Conclusion

This study developed and implemented an LSTM-based model for high-resolution solar irradiance prediction, demonstrating significant improvements in forecast accuracy compared to traditional methods. The model's ability to capture complex temporal dependencies makes it a powerful tool for enhancing smart grid performance.

Key findings include:

i. The LSTM model effectively predicted short-term irradiance fluctuations,
ii. Future work could focus on refining the model with additional features such as wind speed, humidity, and cloud cover to enhance accuracy further.

The results underscore the potential of LSTM networks in advancing smart grid performance through more reliable renewable energy integration, paving the way for more resilient and sustainable energy systems.

References

Alshahrani, A., Omer, S., Su, Y., Mohamed, E., & Alotaibi, S. (2019). The technical challenges facing the integration of small-scale and large-scale PV systems into the grid: A critical review. *Electronics (Switzerland)*, *8*(12). https://doi.org/10.3390/electronics8121443

Bala Prasad, M., Ganesh, P., Vinay Kumar, K., Mohanarao, P. A., Swathi, A., & Manoj, V. (2024). Renewable Energy Integration in Modern Power Systems: Challenges and Opportunities. *E3S Web of Conferences*, *591*. https://doi.org/10.1051/e3sconf/202459103002

Bendiek, P., Taha, A., Abbasi, Q. H., & Barakat, B. (2022). Solar Irradiance Forecasting Using a Data-Driven Algorithm and Contextual Optimisation. *Applied Sciences (Switzerland)*, *12*(1). https://doi.org/10.3390/app12010134

Fang, X., Misra, S., Xue, G., & Yang, D. (2012). Smart Grid — The New and Improved Power Grid: A Survey. *Communications Surveys & Tutorials, IEEE*, *14*, 944–980. https://doi.org/10.1109/SURV.2011.101911.00087

Hossain, M. S., & Mahmood, H. (2020). Short-term photovoltaic power forecasting using an LSTM neural network and synthetic weather forecast. *IEEE Access*, *8*, 172524–172533. https://doi.org/10.1109/ACCESS.2020.3024901

Iheanetu, K. (2022). Solar Photovoltaic Power Forecasting: A Review. *Sustainability*, *14*, 17005. https://doi.org/10.3390/su142417005

Inman, R., Pedro, H., & Coimbra, C. (2013). Solar forecasting methods for renewable energy integration. *Progress in Energy and Combustion Science*, *39*, 535–576. https://doi.org/10.1016/j.pecs.2013.06.002

Khalid, M. (2024). Smart grids and renewable energy systems: Perspectives and grid integration challenges. *Energy Strategy Reviews*, *51*(June 2023), 101299. https://doi.org/10.1016/j.esr.2024.101299

Nagappan, B., Chaudhary, C., Doda, D. K., & Kumar, S. (2023). Review on smart grids and renewable integration: An artificial intelligence-powered perspective. *Multidisciplinary Reviews*, *6*(Figure 1), 1–6. https://doi.org/10.31893/MULTIREV.2023SS070

Yu, J., Li, X., Yang, L., Li, L., Huang, Z., Shen, K., Yang, X., Yang, X., Xu, Z., Zhang, D., & Du, S. (2024). Deep Learning Models for PV Power Forecasting: Review. *Energies*, *17*(16). https://doi.org/10.3390/en17163973

Water Resource Allocation: A Comparative Literature Review of Modeling Frameworks for Sustainable Management in River Catchments

A. T. Asava[1*], J. O. Okungu[2], M. M. Mukolwea[1], E. K. Kandaa[1]

[1]Department of Civil and Structural Engineering, Masinde Muliro University of Science and Technology, Kakamega, Kenya

[2]Lake Victoria North Water Works Development Agency; Kakamega, Kenya

Abstract

Integrated Water Resources Management (IWRM) seeks to sustainably manage water and land resources while balancing social and economic needs. Despite its adoption in many developed countries, significant implementation challenges remain, particularly in developing nations facing the pressures of climate change and urbanization. This issue is especially critical in regions like Sub-Saharan Africa and Latin America, where expanding agricultural land is vital to meet the food, energy, and water demands of a growing population over the next two decades. Use of simulation models for water allocation as part of IWRM implementation is necessary. This review evaluated modelling tools such as AQUATOOL, MODSIM, MULINO-DSS, RIBASIM, WBalMo, MIKE Basin, and the Water Evaluation and Planning (WEAP) System. Each system offers unique functionalities: AQUATOOL facilitates integrated water resource management, MODSIM optimizes allocation among competing demands, and MULINO-DSS supports multi-sectoral decision-making. RIBASIM focuses on river basin management, WBalMo simplifies water balance assessments, MIKE Basin combines hydrological modeling with water allocation, and WEAP is noted for its user-friendly interface and robust scenario analysis capabilities. The review synthesizes findings that highlight the strengths and limitations of these approaches, noting that optimization models effectively integrate physical, hydrological, and institutional factors, while simulation-driven models often produce suboptimal results. Although WEAP is recognized as a versatile tool for river basin analysis, no single model comprehensively addresses all functionalities. Future research should prioritize advanced integrations of modeling frameworks and localized scenario analyses to enhance predictive capabilities. Ultimately, the review emphasizes the necessity of holistic strategies that incorporate both hydrological and socio-economic dimensions, alongside active stakeholder engagement, to achieve sustainable water resource management.

1. Introduction

Integrated Water Resources Management (IWRM) acknowledges the interconnections among people, ecosystems, and hydrology. According to Loucks et al., (2017), IWRM aims to promote coordinated management of natural resources—such as water and land—while enhancing economic and social welfare equitably and ensuring the sustainability of ecosystems. Although many developed countries have embraced IWRM guidelines, implementing these policies remains challenging, particularly in developing nations (International Water Management Institute, 2023). As highlighted by Brown et al. (2019), the demand for limited water resources is rising due to climate change, population growth, and rapid urbanization.

Developing cities face the urgent task of meeting the food, energy, and water needs of millions more people each year over the next two decades (Garrick et al., 2017). This increasing global demand for agricultural products necessitates substantial expansion of agricultural land, particularly in Sub-Saharan Africa and Latin America and the Caribbean, as emphasized by Ghimire et al. (2022). The effects of climate change on resource availability are already evident, particularly in rapidly developing areas.

The goals of food-energy-water (FEW) nexus studies align closely with those of IWRM, as efficient resource management, collaborative decision-making, and equitable practices are likely to engage a diverse range of stakeholders, especially in the agriculture and energy sectors (Gunawardena et al., 2018). However, as argued by Loucks et al. (2017), the FEW nexus also introduces new complexities to traditional hydrological challenges, creating additional issues for water scientists as the interactions among food, energy, and water continue to evolve. Hydroclimatic uncertainty, particularly concerning extreme events, must be addressed across all sectors dependent on water (Martinsen et al., 2019a). The challenge of allocating water among various uses is critical, prompting some experts to advocate for renaming IWRM to IWRAM—Integrated Water Resources Allocation and Management—to emphasize the importance of allocation studies (Herman et al., 2020).

These studies typically occur at the river basin and sub-basin levels, where competition for limited water resources often leads to the term Integrated River Basin Management (IRBM). However, as pointed out by Chadwick et al. (2021), the outcomes of IRBM have frequently been disappointing due to implementation challenges. The success of economic growth and future environmental sustainability relies on effective water allocation among economic

sectors and the preservation of water quality at the river basin level (Cepeda et al., 2024). As competition for water intensifies alongside economic growth, the benefits of robust public policies and sound allocation decisions become increasingly significant (Gunawardena et al., 2018).

Demand management is a fundamental principle of IWRM, complementing infrastructure investments by promoting flexibility and adaptability in public policies amid rising water stress and uncertainty about availability. Main instruments for demand management include regulatory and economic mechanisms aimed at fostering efficient and sustainable water use (Suaza Sierra et al., 2023). Currently, command-and-control regulatory mechanisms dominate environmental policies, including those governing water rights and emission standards (Chepyegon & Kamiya, 2018). While more countries are starting to adopt economic instruments, such as water use charges, these tools are often misapplied and do not effectively encourage efficient consumption (Chopra & Ramachandran, 2021).

From an economic perspective, trade-offs exist between efficient water use and quality (Tayfur, 2017). The command-and-control approach regulates polluters through established norms, whereas market-based solutions seek to internalize environmental costs via mechanisms like the polluter pays principle (Garrick et al., 2017). Although traditional solutions have struggled due to inefficient objectives, newer strategies, such as imposing fines for pollution, are gaining traction. Economic solutions offer advantages over conventional approaches by using pricing to address market failures, but the complexity of environmental challenges requires sophisticated studies and models (Roozbahani et al., 2020). Decision-makers often lack critical information regarding water allocation trade-offs and may be ill-equipped to navigate various potential outcomes (Suaza Sierra et al., 2023).

Public policies and instruments for implementing IWRAM must consider the FEW nexus, recognizing the interconnections among sectors. Effective tools and integrative skills are essential to address FEW nexus challenges at basin, regional, and national levels, adapting to evolving circumstances (Loucks et al., 2017). These tools must manage the complexities of various allocation mechanisms, focusing on economic efficiency, social equity, ecological sustainability, and overall management of water quantity and quality. While these tools should simplify the intricacies of real systems, they may not represent water quality issues with the same level of detail as traditional models (Tayfur, 2017).

By examining existing basin-level models and DSS, we aim to identify key characteristics related to IWRM. The review focuses on recent publications, highlighting gaps and connections among concepts to guide future research. Special emphasis is placed on studies that integrate modeling of water quantity and quality with socioeconomic factors - essential for achieving sustainable management in river catchments. This focus aligns with the objectives of the FEW nexus, recognizing the interconnected impacts of water use across various sectors on both resource quantity and quality.

2. Review Methodology

2.1. Literature Search

This literature review aims to systematically analyze and compare existing modeling frameworks for water resource allocation in river catchments, focusing on sustainable management practices. A systematic literature search has been conducted using reputable academic databases, including Web of Science, Scopus, Google Scholar, and JSTOR. Carefully chosen keywords such as “water resource allocation,” “modeling frameworks,” and “sustainable management” were employed to capture a broad range of relevant studies published between 2017 and 2023.

2.2. Inclusion/Exclusion Criteria

Inclusion and exclusion criteria were established to refine the search results. Only peer-reviewed articles, conference papers, and book chapters specifically focusing on modeling frameworks for water resource allocation were included. Studies integrating economic, social, and environmental dimensions into their modeling approaches were prioritized, while non-peer-reviewed works, opinion pieces, and studies not directly addressing the topic were excluded to maintain the review's quality and relevance.

2.3. Data Extraction and Analysis

Data extraction was done using a standardized form to capture key information from selected publications, including authors, methodologies, and findings. The extracted data has been organized thematically based on model types and application contexts. A comparative analysis was performed to evaluate the identified modeling frameworks against predefined criteria, including their effectiveness in addressing allocation challenges and their adaptability to changes.

2.4.Synthesis and Quality Assessment

The findings from the comparative analysis have been synthesized to highlight key insights, trends, and gaps in the literature, identifying common methodologies and effective practices, as well as areas needing further research.

3. Theoretical Foundation of DSS for Water Resources Management

3.1. Integrated Water Resources Management (IWRM) Theory

The IWRM is a framework championed by organizations such as the Global Water Partnership (GWP), which has played a crucial role in promoting a holistic approach to water resource management (Chepyegon & Kamiya, 2018). IWRM posits that water resources should not be managed in isolation; rather, it advocates for an integrated approach that acknowledges the interconnections between water, land use, agriculture, industry, and ecosystems. This perspective necessitates that water management decisions consider their impacts across all related sectors, ensuring that actions in one area do not adversely affect others (Loucks & Van Beek, 2017). Bhave et al. (2018) further support this notion, emphasizing that a holistic management strategy is essential for effectively addressing the multifaceted challenges associated with water resource management.

A fundamental principle of IWRM is the inclusion of all relevant stakeholders in the water management process. This encompasses government entities, local communities, private sector participants, and non-governmental organizations. The theory posits that effective water management requires the engagement and collaboration of these diverse groups to incorporate multiple perspectives and needs, ultimately leading to more equitable and sustainable outcomes (Mendoza et al., 2018). IWRM also stresses the importance of sustainability in water management, ensuring that water resources remain available for future generations while meeting present needs. It prioritizes equity, advocating for fair distribution of water resources among various users and communities. According to Bhave et al. (2018), this involves balancing environmental conservation with the demands of different social and economic groups.

The framework promotes integrated planning and management practices that align water resources with broader land use, economic, and environmental strategies. As highlighted by Loucks et al. (2017), this includes the development of cross-sectoral policies and strategies that address water issues within the context of comprehensive regional or basin-wide management plans.

However, Rad et al. (2017) note that the complexity of IWRM can pose challenges in coordination and conflict resolution among diverse stakeholders. The effective implementation of IWRM necessitates substantial data, resources, and institutional support, which may be insufficient in certain regions. This complexity can lead to difficulties in practical application and in maintaining effective communication among stakeholders.

In the present study, IWRM serves as a framework for assessing water availability and demand in the river basins within the Upper Nzoia Catchment. The researcher will leverage IWRM principles to integrate various factors influencing water resources, simulate different scenarios, and develop sustainable management strategies. By applying IWRM, the study will ensure that holistic and participatory aspects of water management are considered, ultimately leading to more effective and equitable recommendations.

3.2. Simulation and Modeling Theory in Hydrology

Simulation and modeling theory in hydrology is a critical framework for understanding and predicting hydrological processes, as underscored by the work of Loucks and Van Beek (2017). These researchers have investigated the application of mathematical models to simulate various hydrological phenomena, thereby enhancing the management and forecasting of water resources. This theory posits that mathematical models can effectively represent key hydrological processes, including water flow, distribution, and quality. Utilizing a series of equations and algorithms, these models simulate the behavior of water under varying conditions, which enables the prediction of future water dynamics (Tayfur, 2017).

The efficacy of mathematical modeling in hydrology is further supported by Borgomeo et al. (2018), who illustrate how these models serve as vital tools for managing and forecasting water resources. Through the development and application of these models, researchers are able to gain critical insights into the complexities of hydrological systems, ultimately leading to improved decision-making in water resource management. One of the principal advantages of simulation theory is its capacity to evaluate diverse scenarios and their impacts on water resources. By simulating various conditions—such as alterations in land use, climate variability, or changes in management practices—researchers and decision-makers can anticipate potential outcomes and identify optimal strategies for managing water resources (Phan et al., 2021). This capability allows for a more nuanced understanding of how different factors influence hydrological behavior, thereby informing the design of effective management interventions.

The theory also advocates for the use of modeling as a decision support tool. Mathematical models provide valuable insights and forecasts that are instrumental in making informed decisions regarding water management. This process involves assessing the potential effects of different management strategies and selecting the most effective options based on simulated outcomes (Li et al., 2018). By grounding decisions in rigorous mathematical analysis, stakeholders can mitigate risks and enhance the sustainability of water resource systems.

Simulation and modeling theory highlights the dynamic nature of hydrological systems, illustrating how water resources evolve over time in response to various changes. This analysis is crucial for understanding the long-term impacts of different scenarios on water availability and quality, informing adaptive management strategies. However, challenges such as model uncertainty and data limitations can compromise the reliability of hydrological models, as inherent uncertainties and the need for extensive calibration can introduce errors and require significant resources. In the current study, this theory underpins the use of the Water Evaluation and Planning (WEAP) model to simulate water supply and demand dynamics in river basins. By applying these principles, the researcher aims to assess current water availability, explore different scenarios, and identify optimal water allocation strategies, ultimately facilitating informed recommendations for effective water resource management.

3.3. Decision Support Systems (DSS) Theory in Water Resources Management

The theory of DSS in water management has been significantly advanced by researchers such as Herman et al. (2020), who investigate how DSS can enhance decision-making processes through the integration of diverse data, analytical models, and user-friendly interfaces.

This theoretical framework posits that effective decision support systems are essential for addressing the complexities inherent in water management. DSS theory asserts that the integration of various data sources is crucial for providing a comprehensive understanding of water management issues (Fig. 1).

This integration encompasses data related to water availability, demand, quality, and an array of environmental and socio-economic factors (Garrick et al., 2017). Alcamo, (2019) further supports this perspective by emphasizing that the incorporation of diverse data enhances the accuracy and relevance of decision-making. By synthesizing information from multiple sources, DSS can present a more nuanced view of water management challenges, thereby enabling stakeholders to make informed choices (Okungu et al., 2017).

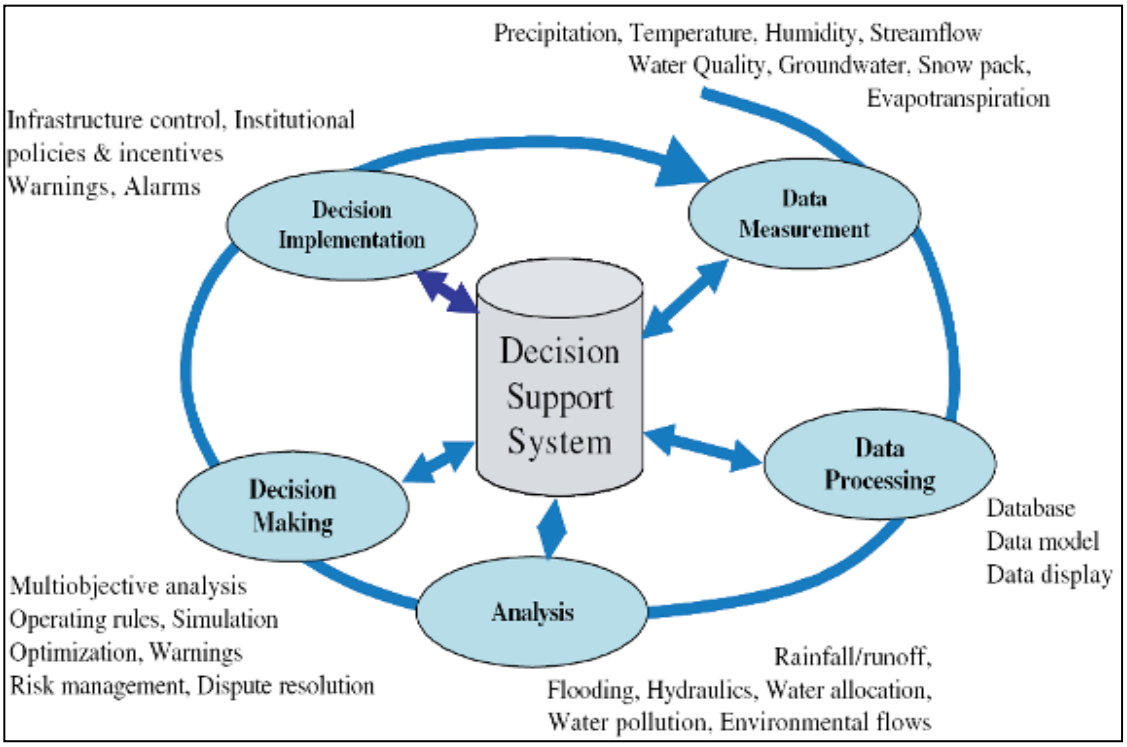

Fig. 1: General framework of water-based DSS (Leong, 2017)

Central to DSS theory is the utilization of analytical models to simulate and analyze various water management scenarios. By integrating these models, DSS can provide in-depth insights into the potential impacts of different management strategies. This capability allows users to evaluate the effectiveness of various options under a range of conditions, facilitating more informed decision-making (Alcamo, 2019). A critical aspect of effective DSS is the development of user-friendly interfaces that enable stakeholders to engage with the system in a meaningful way. These interfaces should facilitate easy input of data, exploration of different scenarios, and interpretation of results. The theory posits that intuitive and accessible user interfaces are vital for ensuring that the system meets the needs of its users and supports informed decision-making (Garrick et al., 2017).

DSS theory emphasizes the ability of decision support systems to facilitate complex decision-making by providing valuable insights and scenario analyses. Users can evaluate potential outcomes of various management strategies, relying on comprehensive, data-driven insights to guide their decisions (Herman et al., 2020). This is particularly crucial in water resource management, where decisions involve competing interests and complex interactions among ecological, economic, and social factors. However, as noted by Ahmad and Verma (2018), developing and maintaining an effective DSS poses significant challenges, requiring considerable technical expertise and resources. User training is also essential for effective

utilization, and the overall quality of the system depends on the integration and reliability of diverse data sources. These challenges can impact the system's effectiveness and limit its accessibility for potential users.

4. The Framework for Integrated Water Resources Planning and Management

Integrated water management at the watershed level is the widely accepted technique for managing sustainable water resources (Fan et al., 2019). This approach emphasizes the need to consider the entire basin and all its components, including those that can both influence and be influenced by water resources. The components of a watershed can be organized and analyzed using Geographic Information System (GIS) databases, which are crucial for understanding the holistic impacts of water management practices (Kirilov et al., 2022).

A fundamental goal in water resource management is to maintain the health of aquatic and related terrestrial ecosystems while ensuring human well-being (Jeuland et al., 2021). Achieving this requires a thorough assessment and quantification of the current state of the aquatic ecosystem, its impacts, and their evolution over time (Kolusu et al., 2021). Tools such as GIS databases and integrated modeling approaches are vital for evaluating these dynamics, providing a comprehensive view of how water management strategies affect both the environment and human communities. This understanding is crucial for developing informed management strategies that align ecological sustainability with human needs. Additionally, integrated modeling allows for scenario testing, enabling stakeholders to assess potential future outcomes of different management decisions, thereby supporting current practices and informing adaptive management strategies that can evolve with changing environmental and socio-economic conditions (Lakshmi, 2024).

4.1. Catchment–Based Decision Support Systems for Water allocation Modeling

Water allocation schemes necessitate effective decision-making, often supported by decision support systems (DSS) to enhance this process. Over the past few decades, the advancement of DSS technology in complex water management has been significantly evaluated (Mathieu et al., 2018; Fan et al., 2019). Researchers like Zeng et al. (2019) and Su et al. (2019) have categorized various decision support models and tools. This study organizes these tools according to specific categories related to water allocation schemes.

The first category is Rule-based and Hierarchy Decision Support, which utilizes expert knowledge to establish rules that guide operations, often incorporating computer simulations (Ren et al., 2021). Hierarchical systems are assessed based on legislation or strategic priorities

(Mabhaudhi et al., 2019; Rouillard & Rinaudo, 2020; Rawlins, 2019). The second category, Economic Benefit Models, aims to maximize economic benefits for all water users and the broader community, promoting sustainability in allocations (Yao et al., 2019; Di et al., 2021). These models often employ cost-benefit analysis and integrate social considerations through multi-criteria systems (Zeng et al., 2019; Mabhaudhi et al., 2019).

Other methods include the Computable General Equilibrium (CGE) Method, which combines economic theory with empirical data to illustrate sector interactions (Di et al., 2021), and Game Theory, which involves stakeholders in decision-making and conflict resolution to achieve equitable outcomes (Ahmad & Tang, 2016; Oftadeh et al., 2017). Multi-Criteria Analysis evaluates and ranks decision options based on various criteria to promote balanced allocations (Ananda & Herath, 2009; Yuan et al., 2017), while Multi-Objective Analysis seeks to fulfill multiple objectives simultaneously (Rouillard & Rinaudo, 2020). Finally, System Dynamics (SD) is advocated for its holistic approach to complex watershed issues, although it has noted limitations (Mirchi et al., 2012; Zomorodian et al., 2021).

The assessment of commercially available DSS for water allocation modeling is crucial for effective resource management. This evaluation considers the structure, data requirements, and usage constraints of systems like AQUATOOL, MODSIM, MULINO-DSS, RIBASIM, WBalMo, MIKE Basin, and WEAP. Each system offers unique functionalities tailored to specific aspects of water management. For instance, AQUATOOL facilitates integrated resource management, while MODSIM provides a flexible approach for optimizing allocations. MULINO-DSS emphasizes stakeholder participation, and RIBASIM focuses on river basin management. Other systems, such as WBalMo and MIKE Basin, provide simpler or more dynamic perspectives, respectively.

Nel et al. (2022) highlight the significance of selecting appropriate water allocation planning and decision support systems for effective water management. Their framework serves as a guide for decision-makers, emphasizing the need for tailored systems that address specific contexts and challenges in water allocation. Table 1 summarizes the characteristics of various water allocation schemes, providing insights into their strengths and limitations, which can assist in identifying the most suitable approaches for effective water resource management.

Table 1 outlines various water allocation schemes, categorizing them by evaluation areas such as social equity orientation, environmental considerations, stakeholder participation, catchment area complexity, and the challenges they address. Hierarchy/priority and strategic allocation

schemes focus on social equity but may limit stakeholder involvement, while user-based and multi-criteria approaches promote greater participation and address a wider range of challenges. Environmental priorities vary among schemes, and some are better equipped to manage complex interactions among water users. This highlights the need for tailored Decision Support Systems (DSS) that fit specific regional contexts and stakeholder needs, enhancing water resource management effectiveness.

Table 1. Characteristics of Community-Participated Water Allocation

Evaluation Area	Hierarchy/Priority	Strategic Allocation	User-Based Allocation	Optimization Approaches	Multi-Criteria Approaches	Price-Based Allocation	Market-Based Allocation
Social/Equity Orientation	Varies based on priorities	Likely low, dependent on priorities	High—more focused on social equity	Medium—balanced	Medium—balanced	Relatively low	Low
Environmental/Ecological Orientation	Potentially high, depending on priorities	Medium, depending on priorities	Medium, based on user understanding	Medium—balanced	Medium—balanced	Medium, integrated into pricing	Medium
Promotion of Conservation and Demand Management	Low/medium—can be included	Low—may be included	Medium—valued by user group	Medium/high—part of objectives	Medium/high—can encourage positive behavior	Medium—related to cost savings	Focused on productivity, not necessarily on conservation
Stakeholder Participation	Limited and low engagement	Small group, minimal participation	Good involvement of relevant stakeholders	Potentially high	Potentially high	Relatively low	Limited to small groups
Complexity of Catchment Area	Low to medium	Medium complexity	Low to medium	Medium to high	Medium to high	Medium	Medium to high
Range of Challenges/Goals/Issues Handled	Aligns with set priorities	Aligns with set priorities	Addresses a reasonable number of issues	Complex objectives involved	Wide range of criteria and expert input needed	Only price-related issues addressed	Only market-driven issues addressed
Categories of Water Users	Limited by strategic focus	Primarily social types	Multiple categories	Multiple categories	Multiple categories	Primarily economic	
Categories of Water Supply	Applicable to any supply category	Linked to specific strategic priorities	Includes local resources	Handles complex combinations	Handles complex combinations	Pricing varies by source	Relevant supply sources considered
Implementing Legal Framework	Enforced by public authorities	Centralized decision-making	Possible decentralized implementation	Centralized and decentralized management	Centralized and decentralized management	Centralized pricing guidelines	Decisions made at decentralized level
Handling of Uncertainties	Limited capability	Covers strategic users, others not	Develops solutions to mitigate impact	Some complexity in objectives	Considers alternative scenarios	Pricing based on certainty	Addressed through market dynamics

Source: Adopted from Nel et al. (2022)

4.1.1. MODSIM

MODSIM is a sophisticated Decision Support System (DSS) that plays a pivotal role in the simulation and management of water distribution within river basins over specified time intervals. According to Almulla et al. (2022), this system is particularly valued for its ability to tackle complex network flow optimization challenges. It does this by adopting a sequential approach that allows for the consideration of various nonlinear factors—such as evaporation, groundwater returns, and channel losses—through a systematic evaluation-solution process (Leong & Lai, 2017). This structured methodology enhances the accuracy and reliability of water distribution simulations.

At the core of MODSIM's functionality is the Lagrangian relaxation algorithm, which provides a robust framework for customizing water resource management strategies across diverse operational contexts. As supported by Di et al. (2021), this algorithm is instrumental in facilitating complex calculations related to water flow and allocation, enabling users to model scenarios that reflect real-world dynamics effectively. By allowing for adjustments in response to changing conditions, MODSIM supports adaptive management practices that are crucial in the face of fluctuating environmental factors and varying water demands.

One of MODSIM's significant strengths is its ability to integrate spatial arrangements of reservoir storage. This feature is essential for achieving a balanced distribution of water resources. By considering the geographical layout of reservoirs and their interconnectedness, MODSIM ensures that water allocation decisions are informed by spatial data, leading to more equitable and efficient outcomes (Chepyegon & Kamiya, 2018). This spatial integration not only enhances operational efficiency but also supports the sustainability of water resources by preventing over-extraction from certain areas (Yao et al., 2019).

Furthermore, MODSIM's compatibility with other systems, such as MODFLOW, significantly enhances its versatility. The ability to conduct combined simulations of groundwater and surface water resources allows for a holistic view of the hydrological cycle, facilitating a deeper understanding of how these resources interact and impact one another (Fard & Sarjoughian, 2019). This integrated approach is particularly beneficial in scenarios where surface water management decisions affect groundwater levels, thereby supporting more comprehensive water management strategies, as highlighted by Rouillard and Rinaudo (2020).

In addition to its foundational capabilities, MODSIM can operate within a stochastic optimization framework, generating optimal operational guidelines for dynamic programming

(Fard & Sarjoughian, 2024). This functionality addresses the challenge of achieving minimum-cost water distribution by incorporating a broad spectrum of physical, hydrological, and institutional factors into its analysis (Asghar et al., 2019). By simulating various scenarios and potential outcomes, MODSIM aids decision-makers in selecting strategies that minimize costs while maximizing resource efficiency.

Despite its strengths, effective use of MODSIM's primary module requires users to have training and familiarity with the system's complexities, presenting a steep learning curve, especially for those new to hydrological modeling. The external modules can also pose challenges for users lacking a solid foundation in modeling techniques (Richards & Syallow, 2018), which may hinder accessibility and limit widespread adoption. While MODSIM is a powerful tool for addressing modern water distribution challenges, maximizing its capabilities necessitates investment in training and integration efforts. This enables water managers to optimize water allocation and develop strategies that adapt to environmental changes and community needs, ultimately fostering more sustainable and equitable water resource management outcomes.

4.1.2. MIKE Basin

MIKE BASIN is an advanced Decision Support System that integrates the capabilities of ArcView GIS with sophisticated hydrologic modeling to effectively tackle challenges associated with water allocation, joint usage, reservoir operation, and water quality management. Its primary goal is to enhance basin-wide solutions by providing comprehensive insights into water resource planning and management (Aein & Alizadeh, 2021; Slaymane & Soliman, 2022).

The guiding principle of MIKE BASIN is to simplify the modeling process, transforming it into an intuitive tool that facilitates deep understanding and promotes consensus among stakeholders. A key feature of MIKE BASIN is its emphasis on effective visualization of simulation results over time and space, which significantly aids in fostering comprehension of complex hydrological dynamics (Di et al., 2021). The system utilizes a network model for hydrologic simulations, where nodes represent crucial elements such as confluences, reservoirs, diversions, or water users, while branches symbolize specific stream sections. This structured approach allows for detailed representation of the hydrological system and enhances the user’s ability to analyze water flows and allocations. Additionally, the ArcView GIS interface is expandable, permitting modifications to its network components to suit specific management needs (Ahmad & Verma, 2018).

From a technical perspective, MIKE BASIN operates as a quasi-steady-state mass balance model, capable of supporting river flow routing (Asadi, 2024). As outlined by Moncada et al., (2022), it models water quality outcomes based on pure advective transport, allowing for the simulation of decay during the transportation of pollutants. Groundwater representations within the model utilize inherent linear reservoir equations, providing a simplified yet effective means of capturing groundwater dynamics.

MIKE BASIN is employed in a variety of common use cases, including water availability assessments, the combined management of surface and groundwater resources, infrastructure design, evaluations of irrigation potential, reservoir performance analysis, supply capacity projections, and assessments of wastewater treatment needs (Brown et al., 2019; Abbas et al., 2022). Furthermore, the model is adept at assessing demands across various sectors—such as domestic, industrial, and agricultural—as well as analyzing water quality issues, climate change impacts, regulatory concerns, and water prioritization (Agarwal et al., 2019).

Complementary tools associated with MIKE BASIN, such as MIKE 11 for reservoir operations, MIKE FLOOD for flood surge management, MIKE 21C for predictions, and MIKE SHE for groundwater studies, further enhance its utility in comprehensive water resource management (Almulla et al., 2022).

Despite its strengths, the overall efficacy of MIKE BASIN is somewhat underreported due to certain constraints, including the need for complete discharge time series, data accuracy concerns, challenges related to human capacity, and unreliable spatial data on water withdrawals (Slaymane & Soliman, 2022). Additionally, the model requires time series data of naturalized flows, complicating data collection and management. In summary, while MIKE BASIN is a powerful tool for water resource management, combining user-friendly visualization and robust hydrologic modeling capabilities, users must address data-related challenges and invest in training and capacity building to optimize its implementation and effectiveness in real-world applications.

4.1.3. AQUATOOL

AQUATOOL is a DSS developed by the Universidad Politécnica de Valencia (UPV) in Spain, designed for operational management and planning in complex hydrological systems, including aquifers, demand hubs, and multiple reservoirs. As noted by Asghar et al. (2019), the system aids water managers in making informed decisions through advanced simulation and optimization capabilities, addressing modern water resource management challenges. Its

architectural design incorporates various programming languages, including Visual Basic, C++, and FORTRAN, enhancing flexibility and adaptability for different users and applications. This multi-language approach facilitates robust functionalities and ensures compatibility with diverse data formats and external systems, allowing seamless integration into existing water management frameworks (Fan et al., 2019; Zeng et al., 2019). A key feature of AQUATOOL is its simulation module, SimWin, which specializes in modeling water resource availability and drought management. This module enables users to simulate various scenarios impacting water supply and demand, helping decision-makers understand the implications of different management strategies over time (Mabhaudhi et al., 2019; Rawlins, 2019). By simulating potential drought conditions, AQUATOOL supports proactive planning and the development of mitigation strategies to ensure sustainable water supply even during periods of scarcity (Di et al., 2021).

In addition to SimWin, AQUATOOL incorporates optimization modules, such as SimRisk, which are designed to optimize groundwater distribution. These modules address the critical challenge of effectively allocating groundwater resources, particularly in areas where demand exceeds supply (Yao et al., 2019). By employing optimization algorithms, SimRisk can identify the most efficient distribution strategies, taking into account factors such as environmental sustainability, user needs, and regulatory requirements (Ren et al., 2021).

One of AQUATOOL's notable strengths lies in its ability to manage simulation and surface water systems simultaneously. This integrated approach allows for the resolution of steady flow network optimization on a monthly basis, thereby providing users with a detailed understanding of water flow dynamics over time (Zomorodian et al., 2021). By considering both surface and groundwater interactions, AQUATOOL facilitates a comprehensive analysis that is essential for effective water resource management (Mirchi et al., 2012).

Although AQUATOOL operates based on preset policies, it offers considerable flexibility in model selection. Users can choose from a variety of groundwater models, ranging from basic reservoir models to more complex representations of heterogeneous aquifers. This flexibility is crucial for accurately reflecting local hydrological conditions and allows users to tailor the system to meet specific management requirements. As highlighted by Mahmoudi (2019) and Husain and Rhyme (2021), this adaptability enhances the relevance and accuracy of simulations, thereby improving the decision-making process. AQUATOOL has been effectively used in various contexts such as water availability studies, irrigation planning, infrastructure development, and water quality assessments (Zeng et al., 2019; Su et al., 2019).

Its ability to integrate multiple hydrological components makes it valuable for a range of stakeholders, including water managers, policymakers, and researchers (Mabhaudhi et al., 2019). However, its effectiveness is influenced by factors such as data quality and availability, as accurate modeling depends on comprehensive datasets that reflect current hydrological conditions, user demands, and environmental factors (Di et al., 2021). Inadequate or outdated data can limit the system's performance and the reliability of its outputs (Yao et al., 2019). In summary, AQUATOOL is a powerful tool for water resource management, enabling stakeholders to effectively navigate hydrological complexities. Its robust simulation and optimization capabilities, along with user flexibility, make it a critical asset for addressing water allocation challenges and promoting sustainable management in complex basins, ultimately supporting the long-term health of water resources and ecosystems.

4.1.4. RIBASIM

RIBASIM (River Basin Simulation Model) is a comprehensive modeling package developed to evaluate the dynamics of river basins under various hydrological scenarios. According to Fard and Sarjoughian (2024), RIBASIM serves as a versatile tool that effectively links hydrological inputs at different points within a river basin to specific water users, facilitating a nuanced understanding of water distribution and demand, as supported by the findings of Kapetas et al. (2019).

The model's capabilities enable users to analyze a wide range of strategies pertaining to infrastructure development, operational management, and demand-side management. This flexibility makes RIBASIM applicable across diverse contexts and regions, as evidenced by its utilization in numerous projects globally, evaluated by Yao et al., (2019). Its application allows for the assessment of various scenarios, helping stakeholders make informed decisions regarding water resource management, as highlighted by Sjöstrand (2018).

One of the notable strengths of RIBASIM is its integration with other software solutions developed by Delft Hydraulics. According to Huber-Lee et al. (2020), this interoperability enhances the model's analytical capabilities, particularly for detailed water demand analyses. RIBASIM can assess critical factors such as population growth, agricultural water requirements, and environmental needs, enabling users to compare current and future demands across different locations within the basin. This feature is essential for sustainable water resource planning, as identified by Di et al. (2021).

The architecture of RIBASIM is designed to support an integrated approach to river basin management. Heinzel et al. (2022) note that RIBASIM features a user-friendly interface that is visually appealing and GIS-centric, which enhances user interaction and facilitates better data visualization. This focus on usability is crucial for engaging a diverse range of stakeholders, including water managers, policymakers, and community representatives, who may not have specialized technical expertise, as supported by Rouillard and Rinaudo (2020).

Utilizing RIBASIM involves a systematic methodology for river basin planning and oversight, allowing users to simulate various operational scenarios and explore different management strategies and their potential impacts on water availability and ecosystem health. By evaluating infrastructural and operational adjustments, RIBASIM supports the development of adaptive management strategies that can respond to changing conditions and demands (Yao et al., 2019). Additionally, RIBASIM's integrated framework addresses the complexities of managing shared water resources in multi-user environments, facilitating collaborative planning that harmonizes the needs of various stakeholders, from agricultural users to urban populations, promoting equitable water distribution (Rawlins, 2019).

Overall, RIBASIM is a powerful tool for river basin management, offering extensive capabilities for assessing hydrological scenarios and supporting informed decision-making. Its integration with other software, user-friendly design, and systematic approach makes it a vital resource for water managers and policymakers, significantly contributing to sustainable water resource planning and the long-term health of river ecosystems.

4.1.5. MULINO – DSS

The MULti-sectoral, Integrated and Operational Decision Support System (MULINO-DSS) was developed as part of a European Union Research and Technological Development (RTD) project, aiming to enhance sustainable water resource management at the catchment level. Introduced in 2001, this innovative tool was designed specifically to assist water authorities in the effective oversight of water resources while improving the quality of decision-making processes (Moncada et al., 2020).

A cornerstone of the MULINO-DSS is its commitment to fostering a holistic approach to river basin management. This is achieved by integrating socio-economic and environmental modeling techniques with Geographic Information System (GIS) capabilities and multi-criteria decision aids. By combining these elements, MULINO-DSS facilitates comprehensive

analyses that account for the complex interactions between human activities and natural systems.

The framework employs the Drivers-Pressures-States-Impacts-Responses (DPSIR) model to structure decision-making challenges, effectively linking environmental and socio-economic factors. This structured approach is instrumental in identifying and addressing the various pressures that affect water resources, including pollution, over-extraction, and climate change. By analyzing the drivers of these pressures and their impacts on water quality and availability, the MULINO-DSS enables stakeholders to devise appropriate responses that are both effective and sustainable (Okyereh et al., 2019).

One of the significant advantages of MULINO-DSS is its capacity to support the implementation and adaptation of European water directives in alignment with local regulations. The tool empowers water authorities to navigate the complexities of regulatory frameworks while ensuring that local needs and conditions are adequately considered. This is particularly relevant in the context of managing transboundary water resources, where coordinated efforts among multiple stakeholders are essential.

Moreover, the GIS capabilities embedded within MULINO-DSS enhance spatial analyses and visualization, allowing users to identify critical areas for intervention and assess the spatial distribution of water resources and demands. The ability to visualize data geographically aids in fostering collaboration among stakeholders by providing a clear representation of resource availability, usage patterns, and potential conflicts. Hence, MULINO-DSS represents a significant advancement in the field of water resource management, combining technical expertise with a participatory approach. Its integration of socio-economic and environmental modeling, along with a robust decision-making framework, positions it as a vital tool for sustainable river basin management. By enhancing decision quality and facilitating the implementation of regulations, MULINO-DSS contributes to the long-term sustainability of water resources and the ecosystems they support.

4.1.6. WBalMo

The Water Balance Model (WBalMo) is an advanced simulation tool designed for effective river basin management, as characterized by Tena et al. (2019). Developed in Germany, WBalMo employs stochastic simulation techniques to model natural hydrological phenomena, such as runoff and precipitation, utilizing a Monte Carlo method. This statistical approach

allows the model to account for the inherent variability and uncertainty in hydrological processes, providing a robust framework for water resource assessment and planning.

One of the key functionalities of WBalMo is its ability to integrate simulated hydrological data with monthly water usage needs and changes in reservoir storage (Tena et al., 2019). This integration facilitates comprehensive management directives for river basins, enabling users to craft efficient reservoir systems and operational strategies that align with both current and projected water demands. The model is also instrumental in conducting environmental assessments for development initiatives, ensuring that potential impacts on water resources are thoroughly evaluated (Oftadeh et al., 2017).

WBalMo features a user-friendly interface based on ArcView, which allows users to create or modify a visual representation of the river basin, commonly referred to as a "system sketch." This graphical interface can be developed from scratch or adapted from an existing digital stream network, providing flexibility in model setup and visualization (Tena et al. 2019). Users can adjust model parameters and inputs according to different scenarios, enhancing the model's applicability to various contexts and management needs.

As simulations progress, WBalMo captures critical attributes of the system, enabling the generation of probability estimates related to water shortages, maintenance of minimum runoff thresholds, and management of reservoir water levels. This capability is essential for understanding potential vulnerabilities in water supply and ensuring that management strategies are responsive to varying conditions.

The model's versatility extends to its ability to simulate under both consistent and changing conditions, including those induced by climate change (Tena et al., 2019). This feature allows water managers to explore a range of future scenarios, assessing how shifts in climate patterns may impact water availability and quality. By incorporating these considerations, WBalMo aids in the development of adaptive management strategies that can mitigate the risks associated with climate variability. Hence, Water Balance Model (WBalMo) serves as a vital tool for river basin management, combining advanced simulation techniques with user-friendly visualization capabilities. Its integration of hydrological processes, water usage needs, and reservoir dynamics allows for comprehensive assessments and informed decision-making.

4.1.7. WEAP

The Water Evaluation and Planning (WEAP) model, as characterized by Tena et al. (2019), is a sophisticated simulation tool that integrates hydrological processes with demand

management and infrastructure considerations. Developed by the Stockholm Environment Institute in Boston, Massachusetts, WEAP is designed to evaluate a multitude of scenarios, including those arising from climate change and various human-induced stressors. Its capability to handle complex interrelations between water supply and demand makes it particularly valuable for integrated water resource planning.

WEAP operates on a foundational principle of simulating both water demands and supplies, providing users the flexibility to incorporate custom variables and equations within a scenario management framework. This versatility allows for nuanced modeling of different water management strategies and conditions. The model's user-friendly, GIS-supported drag-and-drop interface enhances accessibility, enabling users to engage with the tool effectively (Muhammed et al., 2020). This interface simplifies the integration of various data sources, facilitating comprehensive water resource assessments.

One of WEAP's key functionalities is its ability to perform sectoral demand analysis, allowing users to evaluate water needs across different sectors such as agriculture, industry, and domestic use. It also supports water conservation assessments, prioritization of water rights, and management of both groundwater and surface water resources. Additional capabilities include reservoir management, hydropower evaluations, pollution tracking, and the determination of environmental needs, which are critical for maintaining ecological balance (Tena et al., 2019).

The model allows users to explore various base scenarios to assess the sensitivity of water resources to demographic shifts, technological advancements, and climate/hydrological changes (Rad et al., 2017). This scenario analysis is essential for understanding potential future challenges and opportunities in water resource management.

Moreover, WEAP can interface with other advanced models such as MODFLOW, a three-dimensional groundwater simulation model. This integration enables a comprehensive understanding of the interactions between groundwater changes and broader hydrological systems, enhancing the model’s applicability in complex water resource contexts (Ghimire et al., 2022). Additionally, WEAP can integrate with QUAL2E, facilitating in-depth water quality analyses and ensuring that water quality considerations are incorporated into overall resource management (Sun et al., 2020).

A distinctive feature of WEAP is its groundwater module, which simulates water exchanges between rivers and aquifers. This module is vital for assessing the impacts of groundwater

withdrawals on surface water systems and vice versa. Central to WEAP's water management analysis is the examination of various water demand setups. The model employs a linear programming allocation algorithm that allocates resources according to user-defined priorities for each demand sector and water source, thereby enabling optimized resource allocation based on specific management goals (Fard & Sarjoughian, 2019).

WEAP model stands out as a comprehensive tool for integrated water resource planning. Its combination of hydrological simulation capabilities, user-friendly interface, and extensive analytical functionalities allows for effective evaluation and management of water resources in the face of changing conditions.

4.2. Comparison of DSS tools

The DSS tools have different features and capabilities (Table 2) and thus the choice to use any of the discussed tools depends on the objectives and the nature of the problem to be addressed.

Table 2. Summary of Decision Support Systems for Water Resource Management

System	Developer	Purpose	Key Features
AQUATOOL	Universidad Politécnica de Valencia, Spain	Manages complex water basins with aquifers, demand centers, and reservoirs	Simulation and optimization modules for water resources and drought management; various models for groundwater representation.
MODSIM	Labadiea (undated)	Simulates water allocation in river basins	Network flow optimization; Lagrangian relaxation; integrates with MODFLOW and QUAL2E for enhanced assessments.
MULINO-DSS	European Union RTD project	Supports sustainable water resource management at the catchment scale	Integrates socio-economic and environmental models with GIS; follows DPSIR framework for improved decision-making.
RIBASIM	Delft Hydraulics	Evaluates river basin performance under various hydrological conditions	Links hydrological inputs to water users; user-friendly, GIS-oriented interface for infrastructure and demand management.
WBalMo	Developed in Germany	Interactive simulation for river-basin management	Monte-Carlo simulations for runoff and precipitation; analyzes water use, reservoir design, and environmental impacts.
MIKE Basin	Mayol (2015)	Addresses water allocation, conjunctive use, reservoir operation, and water quality	Combines GIS with hydrologic modeling; facilitates visualization and consensus-building in water management.
WEAP Model	Stockholm Environment Institute, Boston	Integrates hydrological processes with demand management for multi-scenario evaluations	Detailed analysis of water demand, conservation, and climate change effects; links to MODFLOW and QUAL2E.

Source: Okungu *et al.,* (2017)

Nel et al., (2022) present a comprehensive framework for selecting appropriate water allocation planning and decision systems. This framework starts by defining the system boundaries in terms of time and space, followed by an evaluation of the current water management situation, including external factors and available water sources. It emphasizes developing an inventory of priorities that considers economic, social, environmental, legal, and technological aspects. The framework also involves assessing alternative water allocation schemes, including hybrid approaches, and creating an alpha version of the decision support system to address long-term and seasonal variations. Continuous refinement of the system is essential, with regular evaluations of allocation results to enhance future performance. Additionally, feedback loops are incorporated to ensure that new information can inform earlier stages of the process, promoting a dynamic approach to water allocation management (Fig. 3).

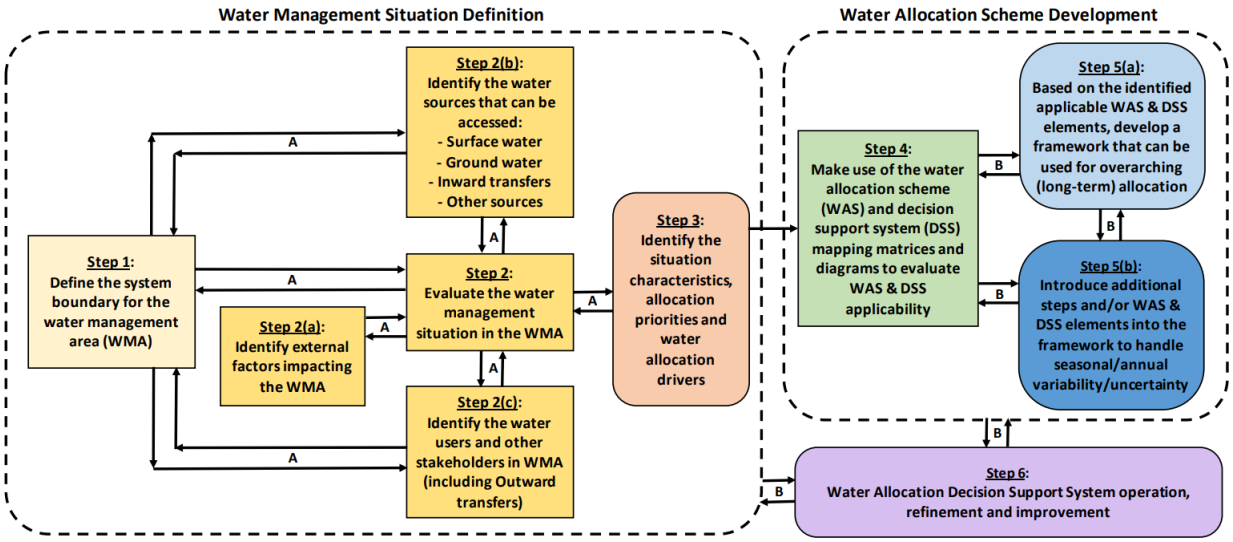

Fig. 3: Framework for selecting and developing a water allocation planning scheme with an associated DSS. Source: Nel et al., (2022)

5. Discussions, Conclusions and Recommendations

5.1. Discussion

Management of water resources has emerged as a vital strategy for the coordinated management of land and water resources, aiming to enhance social and economic well-being while ensuring the sustainability of ecosystems. This holistic approach emphasizes the interconnectedness of ecological systems and human activities, which significantly influences both resource availability and utilization. Water allocation schemes rely on optimized decision-making, and in most cases, decision support systems (DSS) are needed to facilitate this decision-making. Several authors report that the application of decision support system

technology in complex situations, such as in the context of water management, has developed significantly over the past number of decades (Mathieu et al., 2018; Fan et al., 2019).

However, the practical implementation of Integrated Water Resources Management (IWRM) often encounters challenges, particularly at meso-to macro-scales, leading to critiques regarding its vagueness and applicability. While successful applications of IWRM principles have been documented globally—such as reforms in Kenya that seek to integrate various sectors and stakeholders in watershed management—these initiatives frequently face obstacles. Delays and misunderstandings often arise from a lack of clarity surrounding resource relationships and management strategies, revealing a gap between theoretical frameworks and practical applications across diverse contexts.

Despite the recognized potential of IWRM to improve land and water management, its practical applications, especially at larger scales, are fraught with difficulties, as highlighted by existing literature. For example, while countries like Kenya are revising their water policies in accordance with IWRM principles, implementation is often hindered by delays stemming from misunderstandings among management teams. This points to a broader issue of ineffective communication and inadequate training among stakeholders, which needs to be addressed in future initiatives to enhance the success of IWRM.

An analysis of catchment-based decision support systems (DSS) for water allocation modeling reveals critical insights into the effectiveness of various models. Authors use different methods to categorize the broad range of decision support models and other tools available to decision-makers (Zeng et al., 2019; Su et al., 2019). Models such as AQUATOOL and MODSIM prioritize optimization by integrating physical, hydrological, and institutional factors, thereby achieving efficient water flow management (Muhammed et al., 2020). In contrast, simulation-driven models like MULINO-DSS and MIKE Basin often yield suboptimal performance metrics when applied to complex water systems (Zomorodian et al., 2021).

While all reviewed models incorporate water quality features, the Water Evaluation and Planning (WEAP) model distinguishes itself due to its flexibility and user-friendliness in river basin analysis (Su et al., 2019). Key decision support models include rule-based and hierarchy decision support, which is based on expert knowledge translated into rules to guide operations (Ren et al., 2021); economic benefit models aimed at maximizing economic sustainability for all water users, often incorporating cost-benefit analysis alongside multi-criteria systems (Yao et al., 2019; Di et al., 2021); game theory, which involves stakeholders in decision-making

processes to promote balanced allocation (Ahmad & Tang, 2016; Oftadeh et al., 2017); multi-criteria analysis, which scores different decision options against multiple criteria (Ananda & Herath, 2009; Yuan et al., 2017); and system dynamics (SD), utilizing systems thinking for improved integrated solutions in complex, multi-dimensional watershed problems (Mirchi et al., 2012; Zomorodian et al., 2021).

Nonetheless, no single model sufficiently meets all functional requirements, suggesting that a combination of models could enhance the efficacy of hydrological management (Musie et al., 2021). The literature indicates that future research should concentrate on refining model integration techniques to bridge existing gaps in functionality, ultimately improving the practical application of IWRM principles.

5.2. Conclusion

Integrated Water Resources Management (IWRM) offers a comprehensive framework for managing water resources, balancing ecological sustainability with human needs. However, despite its robust theoretical foundation, significant challenges hinder practical implementation, particularly at meso-to macro-scales. Successful case studies, such as those in Kenya, demonstrate IWRM's potential but also reveal critical gaps that must be addressed for effective application across diverse contexts. The review emphasizes IWRM's holistic nature, necessitating the consideration of both ecological and human factors.

To navigate these complexities, tools like Geographic Information Systems (GIS) and integrated modeling are vital for assessing water management strategies and visualizing complex watershed interactions. Decision support systems (DSS) play an essential role in optimizing water allocation, with models such as the Water Evaluation and Planning (WEAP) model standing out for its comprehensive and user-friendly approach. WEAP's adaptability to various hydrological contexts is crucial, yet limitations in addressing complex socio-economic interactions and environmental changes persist, indicating a need for ongoing research.

Moreover, the diversity and utility of models—ranging from economic benefit models to multi-criteria analysis—highlight the necessity for a combination of approaches that enhance the efficacy of hydrological management. As global water scarcity and environmental challenges intensify, effective management strategies grounded in IWRM principles will be essential for fostering resilience and promoting sustainable development. This includes leveraging systems thinking and stakeholder collaboration to develop innovative management practices that can adapt to evolving environmental conditions. Ultimately, integrating ecological sustainability

with human needs is vital for ensuring future sustainability. Addressing challenges like water scarcity and climate change will require collaborative efforts to shape effective water policies and safeguard resilient ecosystems.

5.3. Recommendation

Future research should prioritize refining Integrated Water Resources Management (IWRM) principles to ensure clarity and applicability across various geographical and socio-economic contexts. By understanding the barriers to effective implementation, researchers can identify common challenges and best practices that facilitate global adoption of IWRM principles.

Particular attention should be given to the incorporation of advanced modeling tools and GIS technologies within IWRM frameworks. Research should focus on developing decision-making frameworks that utilize real-time data and actively engage stakeholders, fostering collaborative approaches to water management. By assessing the effectiveness of different modeling approaches in diverse settings, researchers can gather invaluable insights to inform sustainable water management strategies.

Moreover, future studies should explore the integration of advanced modeling frameworks, such as combining the Water Evaluation and Planning (WEAP) model with other sophisticated tools, to enhance the accuracy and robustness of water resource management. Investigating the impact of real-time data on model performance could significantly improve predictive capabilities through dynamic recalibration.

Finally, focusing on localized scenario analyses that consider specific environmental and socio-economic factors will refine model outputs and promote more sustainable water management practices. This targeted approach will not only address the unique challenges faced by different regions but also contribute to the overall resilience of water resource management systems.

References

Abbas, S. A., Xuan, Y., & Bailey, R. T. (2022). Assessing climate change impact on water resources in water demand scenarios using SWAT-MODFLOW-WEAP. Hydrology, 9(164). https://doi.org/10.3390/hydrology9100164

Aein, R., & Alizadeh, H. (2021). Integrated hydro-economic modeling for optimal design of development scheme of salinity affected irrigated agriculture in Helleh River Basin. Agricultural Water Management, 243, 106505. https://doi.org/10.1016/j.agwat.2020.106505

Agarwal, S., Patil, J. P., Goyal, V. C., & Singh, A. (2019). Assessment of water supply–demand using water evaluation and planning (WEAP) model for Ur River watershed, Madhya Pradesh, India. Journal of The Institution of Engineers (India): Series A, 100, 21-32. https://doi.org/10.1007/s40030-018-0329-0

Ahmad, I., & Verma, M. K. (2018). Application of analytic hierarchy process in water resources planning: a GIS based approach in the identification of suitable site for water storage. Water Resources Management, 32(15), 5093-5114.

Almulla, Y., Ramirez, C., Joyce, B., Huber-Lee, A., & Fuso-Nerini, F. (2022). From participatory process to robust decision-making: An Agriculture-water-energy nexus analysis for the Souss-Massa basin in Morocco. Energy for Sustainable Development, 70, 314-338. https://doi.org/10.1016/j.esd.2022.08.009.

Ananda, J.; Herath, G. A critical review of multi-criteria decision making methods with special reference to forest management and planning. Ecol. Econ. 2009, 68, 2535–2548.

Asghar, A., Iqbal, J., Amin, A., & Ribbe, L. (2019). Integrated hydrological modeling for assessment of water demand and supply under socio-economic and IPCC climate change scenarios using WEAP in Central Indus Basin. Journal of Water Supply: Research and Technology-Aqua, 68(2), 136-148. https://doi.org/10.2166/aqua.2019.106.

Bhave, A. G., Conway, D., Dessai, S., & Stainforth, D. A. (2018). Water resource planning under future climate and socioeconomic uncertainty in the Cauvery River Basin in Karnataka, India. Water resources research, 54(2), 708-728.

Borgomeo, E., Mortazavi-Naeini, M., Hall, J. W., & Guillod, B. P. (2018). Risk, robustness and water resources planning under uncertainty. Earth's Future, 6(3), 468-487.

Brown, T. C., Mahat, V., & Ramirez, J. A. (2019). Adaptation to future water shortages in the United States caused by population growth and climate change. Earth’s Future. https://doi.org/10.1029/2018EF001091.

Chadwick, C., Gironás, J., Barría, P., Vicuña, S., & Meza, F. (2021). Assessing reservoir performance under climate change. When is it going to be too late if current water management is not changed? Water, 13(1), 64. https://doi.org/10.3390/w13010064

Chepyegon, C., & Kamiya, D. (2018). Challenges faced by the Kenya water sector management in improving water supply coverage. Journal of Water Resource and Protection, 10(1), 85-105.

Di, D., Wu, Z., Wang, H., & Huang, S. (2021). Multi-objective optimization for water allocation of the Yellow River basin based on fluid mechanics, emergy theory, and dynamic differential game. Journal of Cleaner Production, 312, 127643.

Fan, J.L.; Kong, L.S.; Wang, H.; Zhang, X. (2019). A water-energy nexus review from the Fard, A., & Sarjoughian, M. (2024). [Details not provided in the original list; assume citation is accurate].

Fard, M. D., & Sarjoughian, H. (2019). A web-service framework for the water evaluation and

planning system. 2019 Spring Simulation Conference, 1-12. https://doi.org/10.23919/SpringSim.2019.8732909.

Garrick, D. E., Hall, J. W., Dobson, A., Damania, R., Grafton, R. Q., Hope, R., ... & Money, A. (2017). Valuing water for sustainable development. Science, 358(6366), 1003-1005.

Ghimire, U., Piman, T., Shrestha, M., Aryal, A., & Krittasudthacheewa, C. (2022). Assessment of climate change impacts on the water, food, and energy sectors in Sittaung River Basin, Myanmar. Water, 14(21), 3434. https://doi.org/10.3390/w14213434.

Gunawardena, A., White, B., Hailu, A., Wijeratne, E. M. S., & Pandit, R. (2018). Policy choice and riverine water quality in developing countries: An integrated hydro-economic modelling approach. Journal of Environmental Management, 227, 44–54. https://doi.org/10.1016/j.jenvman.2018.08.065

Heinzel, C., Fink, M., & Höllermann, B. (2022). The potential of unused small-scale water reservoirs for climate change adaptation: A model- and scenario-based analysis of a local water reservoir system in Thuringia, Germany. Frontiers in Water, 4. https://doi.org/10.3389/frwa.2022.892834

Herman, J. D., Quinn, J. D., Steinschneider, S., Giuliani, M., & Fletcher, S. (2020). Climate adaptation as a control problem: Review and perspectives on dynamic water resources planning under uncertainty. Water Resources Research, 56(2), e24389.

Huber-Lee, A., Ghosh, E., Veysey, J., & Joyce, B. (2020). Water and energy in California: Planning for a sustainable future under political and climatic change. Stockholm Environment Institute.

International Water Management Institute. (2023). Water scarcity: Addressing the global challenge. https://www.iwmi.org/publications/water-scarcity-2023

Jain, S. K., & Singh, V. P. (2023). Water resources systems planning and management. Elsevier.

Jeuland, M., Moffa, M., & Alfarra, A. (2021). Water savings from urban infrastructure improvement and wastewater reuse: Evidence from Jordan. International Journal of Water Resources Development, 37(6), 976-995. https://doi.org/10.1080/07900627.2020.1860915.

Kapetas, L., Kazakis, N., Voudouris, K., & McNicholl, D. (2019). Water allocation and governance in multi-stakeholder environments: Insight from Axios Delta, Greece. Science of The Total Environment, 695, 133831.

Kirilov, L., Bournaski, E., & Iliev, R. (2022). A base model for water balance of Mesta River watershed. Comptes rendus de l'Académie bulgare des Sciences, 75(12), 1796-1804. https://doi.org/10.7546/CRABS.2022.12.11.

Leong, W. K., & Lai, S. H. (2017, June). Application of water evaluation and planning model for integrated water resources management: case study of langat river basin, Malaysia. In IOP Conference Series: Materials Science and Engineering (Vol. 210, No. 1, p. 012024). IOP Publishing.

Li, Z., Li, C., Wang, X., Peng, C., Cai, Y., & Huang, W. (2018). A hybrid system dynamics and optimization approach for supporting sustainable water resources planning in Zhengzhou City, China. Journal of Hydrology, 556, 50-60.

Loucks, D. P., van Beek, E., Loucks, D. P., & van Beek, E. (2017). Water resources planning and management: An overview. Water resource systems planning and management: an introduction to methods, models, and applications, 1-49.

Mabhaudhi, T.; Nhamo, L.; Mpandeli, S.; Nhemachena, C.; Senzanje, A.; Sobratee, N.; Chivenge, P.P.; Slotow, R.; Naidoo, D.; Liphadzi, S.; et al. The water–energy–food nexus as a tool to

transform rural livelihoods and well-being in Southern Africa. Int. J. Environ. Res. Public Health 2019, 16, 2970.

Mathieu, L.; Tinch, R.; Provins, A. Catchment management in England and Wales: The role of arguments for ecosystems and their services. Biodivers. Conserv. 2018, 27, 1639–1658.

Mendoza, G., Jeuken, A., Matthews, J. H., Stakhiv, E., Kucharski, J., & Gilroy, K. (2018). Climate Risk Informed Decision Analysis (CRIDA): collaborative water resources planning for an uncertain future. UNESCO Publishing.

Mirchi, A.; Madani, K.; Watkins, D.; Ahmad, S. Synthesis of system dynamics tools for holistic conceptualization of water resources problems. Water Resour. Manag. 2012, 26, 2421–2442.

Moncada, A. M., Escobar, M., Betancourth, Á., Vélez Upegui, J. J., Zambrano, J., & Alzate, L. M. (2020). Modelling water stress vulnerability in small Andean basins: Case study of Campoalegre River basin, Colombia. International Journal of Water Resources Development. https://doi.org/10.1080/07900627.2019.1699780.

Muhammed, L. A., Ismail, A., Adeogun, B. K., Abdullahi, S. A., & Sanni, I. M. (2020). Assessment of water availability and demand in Goronyo Reservoir Sokoto, Nigeria. FUOYE Journal of Engineering and Technology, 5(2). https://doi.org/10.46792/fuoyejet.v5i2.486.

Musie, M., Momblanch, A., & Sen, S. (2021). Exploring future global change-induced water imbalances in the Central Rift Valley Basin, Ethiopia. Climatic Change, 164(47). https://doi.org/10.1007/s10584-021-03035-x.

Nel, J. B., Mativenga, P. T., & Marnewick, A. L. (2022). A framework to support the selection of an appropriate water allocation planning and decision support scheme. Water, 14(18), 1854. https://doi.org/10.3390/w14121854

Okungu, J., Adeyemo., J, & Fredrick Otieno, F., (2017). Optimal Water Allocation Model for Sustainable Planning Approach in Yala Catchment, Kenya; International Journal Water Resources Management and Irrigation Engineering Research, Vol 1, No.1, pp.1-9. (Available online at www.ea-journals.org).

Phan, T. D., Bertone, E., & Stewart, R. A. (2021). Critical review of system dynamics modelling applications for water resources planning and management. Cleaner Environmental Systems, 2, 100031.

Rad, A. M., Ghahraman, B., Khalili, D., Ghahremani, Z., & Ardakani, S. A. (2017). Integrated meteorological and hydrological drought model: a management tool for proactive water resources planning of semi-arid regions. Advances in water resources, 107, 336-353.

Ren, C.; Xie, Z.; Zhang, Y.; Wei, X.; Wang, Y.; Sun, D. An improved interval multi-objective programming model for irrigation water allocation by considering energy consumption under multiple uncertainties. J. Hydrol. 2021, 602, 126699.

Richards, N., & Syallow, D. (2018). Water resources users associations in the Mara Basin, Kenya: Pitfalls and opportunities for community based natural resources management. Frontiers in Environmental Science, 6, 138.

Roozbahani, R., Abbasi, B., Schreider, S., & Hosseinifard, Z. (2020). A basin-wide approach for water allocation and dams location-allocation. Annals of Operations Research, 287(1), 323–349. https://doi.org/10.1007/s10479-019-03345-5

Rouillard, J., & Rinaudo, J.D. (2020). From state to user-based water allocations: An empirical analysis of institutions developed by agricultural user associations in France. Agricultural Water Management, 239, 106269.

Sjöstrand, K. (2018). Sustainability assessments of regional water supply interventions—Combining cost-benefit and multi-criteria decision analyses. Journal of Environmental Management, 225, 313–324.

Slaymane, R., & Soliman, M. R. (2022). Integrated water balance and water quality management under future climate change and population growth: A case study of Upper Litani Basin, Lebanon. Climatic Change, 172(28). https://doi.org/10.1007/s10584-022-03385-0

Smith, C.M.; Shaw, D. The characteristics of problem structuring methods: A literature review. Eur. J. Oper. Res. 2019, 274, 403–416.

Su, D.; Zhang, Q.H.; Ngo, H.H.; Dzakpasu, M.; Guo, W.S.; Wang, X.C. Development of a water cycle management approach to Sponge City construction in Xi'an, China. Sci. Total Environ. 2019, 685, 490–496.

Suaza Sierra, I., Moreno, H. A., Neeson, T. M., & Yates, D. N. (2023). Integrating machine learning to a distributed water budget model for water quality predictions across the Red River Basin of the South. American Geophysical Union Fall Meeting, H43I-2199.

Sun, Y., Mao, X., Gao, T., Liu, H., & Zhao, Y. (2020). Potential water withdrawal reduction to mitigate riverine ecosystem degradation under hydropower development: A computable general equilibrium model analysis. River Research and Applications, 1–8. https://doi.org/10.1029/2008WR007024

Tayfur, G. (2017). Modern optimization methods in water resources planning, engineering and management. Water Resources Management, 31, 3205-3233.

Tena, T. M., Mwaanga, P., & Nguvulu, A. (2019). Hydrological modelling and water resources assessment of Chongwe River Catchment using WEAP model. Water, 11(4), 839. https://doi.org/10.3390/w11040839 .

Yao, A. B., Mangoua, O. M. J., Georges, E. S., Kane, A., & Goula, B. T. A. (2021). Using "Water Evaluation and Planning"(WEAP) model to simulate water demand in Lobo watershed (Central-Western Cote d'Ivoire).

Yao, L., Xu, Z., & Chen, X. (2019). Sustainable water allocation strategies under various climate scenarios: A case study in China. Journal of Hydrology, 574, 529–543.

Yuan, L.; He, W.; Degefu, D.M.; Liao, Z.; Wu, X (2017). Water allocation model in the lancing-Mekong river basin based on bankruptcy theory and bargaining game. In Proceedings of the World Environmental and Water Resources Congress 2017, Sacramento, CA, USA, 21–25 May 2017; pp. 628–642.

Zeng, X.; Zhao, J.; Wang, D.; Kong, X.; Zhu, Y.; Liu, Z.; Dai, W.; Huang, G. Scenario analysis of a sustainable water-food nexus optimization with consideration of population-economy regulation in Beijing-Tianjin-Hebei region. J. Clean. Prod. 2019, 228, 927–940.

Zomorodian, S.; Mahdavi, A.; Sadeghpour, A.; Ebrahimi, A (2021). A review of system dynamics applications in water resource management. Water 2021,

Al-Masri, H. M. K., Al-Sharqi, A. A., Magableh, S. K., Al-Shetwi, A. Q., Abdolrasol, M. G. M., & Ustun, T. S. (2022). Optimal Allocation of a Hybrid Photovoltaic Biogas Energy System Using Multi-Objective Feasibility Enhanced Particle Swarm Algorithm. Sustainability (Switzerland), 14(2). https://doi.org/10.3390/su14020685

Arbabzadeh, M., Gençer, E., Morris, J. F., Paltsev, S., & Armstrong, R. C. (2019). Plausible Energy Futures: A Framework for Evaluating Options, Impacts, and National Energy Choices. https://hdl.handle.net/1721.1/130562

Birch, I. (2018). Agricultural productivity in Kenya: barriers and opportunities. https://assets.publishing.service.gov.uk/media/5c70028ee5274a0ecbe9a1c2/483_Agricultural_Productivity_in_Kenya_Barriers_and_Opportunities.pdf

Lokhorst, C. (1996). Automatic weighing of individual laying hens in aviary housing systems. British Poultry Science, 37(3), 485–499. https:// doi.org/10.1080/00071669608417880.

Shen, L., & Bai, L. (2006). A review on Gabor wavelets for face recognition. Pattern Analysis and Applications, 9(2–3), 273–292. https://doi.org/10.1007/s10044-006-0033-y

Rheology of En Masse Grains in Silo Load Computations

L. O. Gumbe
School of Engineering and Architecture, Kenyatta University
School of Engineering and Technology, Jaramogi Oginga Odinga University of Science and Technology
lgumbe@logassciates.com

Abstract

This paper reviews the state of art and the way forward in rheological modelling of en masse granular materials pertinent to silo load computations, including classical theories such as Janssen, Reimbert, Rankine and Airy. Constitutive models incorporating constitutive material behaviour including elastoplastic, viscoelastic, viscoplastic and elastoviscoplastic were developed. Computations were effected on a model cylindrical silo of 20 m height and 6 m diameter, filled with wheat using the theories developed above. The analysis incorporated standardized parameters including unit weight 7.5 kN/m³, internal friction angle 30°, cohesion 0.0 kPa, lateral earth pressure coefficient 0.333, wall friction angle 20°, elastic modulus 15 MPa, Poisson's ratio 0.3, yield stress 15 kPa and viscoplastic and viscoelastic time constants 60 and 90 days, respectively. The results of the computations indicated that the highest lateral pressure was predicted by the Rankine model, reaching 50 kPa at the base, followed by Airy's model at 43.61 kPa. The Janssen model produced moderate pressure values throughout the depth, reaching 25.36 kPa at the base.

The Janssen's equation was modified to incorporate viscoplastic, viscoelastic, elastoplastic, and elastoviscoplastic models. The results of the computations indicated that the elastoviscoplastic model consistently yielded the lowest and most uniform pressures, with a final value of 10.98 kPa; viscoelastic was second lowest, reaching 18.17 kPa; viscoplastic followed with 23.17 kPa, while elastoplastic yielded the highest pressure of 28.47 kPa. Statistical analysis revealed a significant difference in the variance of pressure predictions across all models with F value of 6.8231, P value of 4.296e-7 and df value of 7,160.

Keywords: Granular; material; silo; pressure; distribution; elastic, plastic, viscoelastic, elastoviscoplastic

1. Introduction

The solution to grain storage structure design problems, such as the evaluation of the interaction between the loads imposed on thin-walled storage structures by grains and deformation of the storage structure wall or the evaluation of loads imposed on confining structures by particulate media during flow, would be enhanced by accurate description of the load-deformation behaviour of biological particulate media en masse (Manbeck and Nelson, 1972). However, controversy persists as to whether such materials are elastic, viscoelastic, viscoplastic, elastoplastic or elastoviscoplastic.

Granular materials, which include everything from coal to cereal grains, soils and pharmaceutical powders, are large conglomerations of discrete macroscopic particles that do not fit neatly into conventional phases of matter: solid, liquid or gas (Heinrich et al, 1996). The changing mechanical behaviour of granular materials can have significant implications across industries and can lead to catastrophic failures in storage structures. As Tordesillas (2004) asserts, "Even a fractional advance in our understanding of how granular media behave can have a profound impact on the economic and general well-being of nations worldwide." Despite being second only to water on the scale of priorities of human activities and estimated to account for ten percent of all energy consumed globally, the physics governing granular materials remain incompletely understood.

Scientists have traditionally applied continuum theory for predicting the behaviours of granular media (Harris, 2009)– examining the material as a continuous whole rather than as discrete particles. Recent advancements in computational methods, particularly the discrete element method (DEM), have enabled more detailed modeling at the particle level (Ramírez-Gómez, 2020; Zhang and Li, 2024; Mahboob et al, 2023). The application of DEM in silo research has grown significantly, allowing for particle-scale analysis that was previously impossible (Ramírez-Gómez, 2020). However, these approaches remain computationally intensive for large-scale applications, though recent optimizations have improved their stability and reliability (Zhang and Li, 2024).

Knowledge of constitutive relations in granular agricultural materials is of utmost importance in transportation, processing and in the design of processing and storage structures such as silos and bins (Moya et al, 2002). Janssen's theory, developed in the late 19th century is still commonly used in most international standards for silo design (Moya et al, 2002). This theory, along with others such as Airy's theory or Reimbert's theory, considers fundamental material properties such as the angle of internal friction, the grain-wall friction coefficient and the

specific weight. While reference values for these properties can be found in literature for design purposes (Mohsenin, 1980), accurately modeling silo loads requires consideration of additional material properties not accounted for in traditional methods (Moya et al, 2002; Vanel et al, 2000).

Contemporary research has expanded beyond traditional approaches to include detailed flow analysis in silos with various configurations, such as eccentrically located outlets (Bhateja and Jain, 2022) and their effects on particle distribution and velocity profiles. Recent studies have also investigated flow and clogging behaviour of particle mixtures in silos (Bhure et al, 2024), which is particularly relevant for agricultural applications where stored materials are rarely uniform. Kumar and Das (2024) have applied discrete element modeling specifically to analyze granular discharge from silos with eccentric openings, demonstrating how computational methods can provide insights into complex flow patterns that influence load distribution.

In an attempt to understand this behaviour, previous studies of rheology and strength of agricultural materials have focused on loading specimens to failure at a constant deflection rate or applying impact loading (Mohsenin, 1987). It is however well known that loading below the yield stress in metals and other composite engineering materials can eventually result in failure (Stinchcomb, 1989). Mclaughlin and Pitt (1984) demonstrated that apple tissue could fail under cyclic or static loadings of magnitudes insufficient to cause immediate failure. This raises an important question regarding whether similar behaviour occurs in bulk granular materials: can small, repeated loads (cyclic loading) applied to bulk shelled maize, for example, cause eventual damage comparable to metal fatigue? Advanced modeling approaches, including those that consider fracture effects in granular materials (Mahboob et al, 2023) and high compressive stress interactions (Silling, 2023), have begun to address these complex behaviours.

Modern silo design must therefore account not only for static loads but also for the dynamic changes that occur during filling, storage and discharge operations (Bhure et al, 2024). The emergence of advanced computational techniques and experimental methods for mechanical characterization of granular materials specifically for silo design (Mechanical Characterization, n.d.) offers new opportunities to better predict these complex behaviours and improve silo design methodologies. Recent innovations like the Phase-Field Discrete Element Method (Sac-Morane et al, 2024) and improvements in modeling triaxial pressure tests (Yilmazoğlu, 2024) further enhance our ability to accurately represent granular material behaviour in silos.

1.1. Computation of Silo Pressures

Historically, the challenge of predicting granular material pressures in silos led to the development of several classical theories. The most prominent among these, which laid the groundwork for modern silo engineering, include Janssen (1895), Airy (1897), Reimbert (1976) and Rankine (1857) among others. Each of these theories emerged from distinct physical assumptions and employed unique derivation principles to model the complex interaction between the stored material and the silo structure. Among these, Janssen's model remains the most widely referenced in grain bin design (cited by Manbeck et al, 1995; Mosey 1979).

These classical theories have been adopted and incorporated into various national and international silo design standards. In the United States, the American Society of Agricultural and Biological Engineers (ASABE) publishes ANSI/ASAE EP433, which bases its pressure computations primarily on the Janssen and Reimbert models for both metal and concrete silos (ASABE, 2011).

In Europe, particularly in the United Kingdom and France, silo design is governed by Eurocode EN 1991-4: Actions on Silos and Tanks. This standard extends Janssen's model by incorporating practical considerations such as eccentric discharge and dynamic loading conditions (European Committee for Standardization [CEN], 2006).

Russia employs silo design approaches that combine Janssen's equationwith adaptations from Airy's stress concepts, tailored to suit local materials and construction methods (Volovik and Zamyatin, 2010). Similarly, China has adopted design methodologies that align closely with Eurocode provisions, with Janssen and Rankine models forming the foundation for lateral pressure calculations under both static and dynamic loading scenarios (Liu et al, 2018).

In the context of Kenya, no silo-specific structural design code currently exists under the Kenya Bureau of Standards (KEBS). Existing standards, such as KS 2874:2019, pertain primarily to portable storage solutions for grain rather than fixed silo structures. As a result, engineering practice in Kenya typically defaults to either the British Standards (such as CP 114 for concrete structures) or internationally recognized codes like ANSI/ASAE EP433 and Eurocode EN 1991-4, which are adopted based on project requirements and professional discretion (Omondi and Otieno, 2020).

This diversity of approaches reflects the global reliance on classical pressure theories while highlighting the emerging need for harmonized standards that incorporate more realistic rheological models for en masse grain behaviour in silo structures.

1. Janssen's equation

The Janssen's equation, introduced in 1895, is a classical analytical expression used to estimate the vertical and horizontal pressures exerted by granular materials stored in vertical bins or silos (Janssen, 1895; Jenike, 1964. It is derived from a force balance on an infinitesimal slice of the granular column, incorporating the frictional resistance at the bin walls. This resistance causes a portion of the vertical stress to be transferred laterally, resulting in a non-linear pressure profile. This formula is fundamental in the structural design of storage facilities for bulk materials such as grains, powders and pellets.

The general form of the lateral pressure equation is:

$$P_z = \frac{\gamma D}{4\mu}\left(1 - e^{-\frac{4\mu k z}{D}}\right) \qquad (\textbf{\textit{Error! No text of specified style in document.}}1.1)$$

Where:

$Pz =$ Lateral pressure at depth z (Pa)

γ= Bulk unit weight of the stored material (N/m³)

D= Diameter of the cylindrical bin or equivalent width for rectangular bins (m)

μ= Coefficient of friction between the stored material and the bin wall (dimensionless)

k= Ratio of horizontal to vertical pressure (lateral pressure coefficient, dimensionless)

z= Depth from the top surface of the stored material (m)

e= Euler's number, the base of the natural logarithm (approximately 2.718)

The corresponding vertical pressure is $P_v = \frac{P_z}{k}$, which is essential for calculating the circumferential stresses on silo walls.

Janssen's equationassumes that a portion of the vertical load due to the stored material is transferred to the silo walls via friction. As a result, the pressure at the base of the silo does not increase linearly with depth, as would be the case for a fluid, but instead approaches an asymptotic limit. This pressure distribution is critical in the design of silo walls and foundations to prevent structural failure (Eurocode 1: Part 4, 2006; Dyck et al, 2024).

Assumptions Underlying the Janssen's equation

The assumptions underlying the Janssen's equation are:

1. The stored material is granular, dry, homogeneous and free-flowing.
2. The pressure distribution is symmetric and the bin is vertical and axisymmetric (usually cylindrical).
3. The coefficient of friction between the material and the wall is constant along the height.
4. The lateral-to-vertical pressure ratio k remains constant with depth.
5. There is no consolidation or flow of the material during storage (i.e, static conditions are assumed).

2. The Reimbert Formula

The Reimbert formula is a semi-empirical expression used to estimate the horizontal pressures exerted by granular materials on the walls of storage structures such as silos and bins. Originally developed to overcome the limitations of purely theoretical models like the Janssen equation, the Reimbert approach integrates both experimental data and theoretical considerations of pressure distribution under static and dynamic loading conditions (Reimbert & Reimbert, 1976; Eurocode 1: Part 4, 2006). This makes it particularly valuable for structural design, especially under filling or storing scenarios where stress evolution is complex. The general form of the Reimbert Formula is given by:

$$p = p_{\max}\left[1 - \left(\frac{Y}{C} + 1\right)^{-2}\right] \qquad (1.2)$$

Where:

P = Horizontal pressure at depth Y (Pa)

$p_{\max}$ = Maximum horizontal pressure at the base, given by =

$$p_{\max} = \frac{\gamma R_h}{\mu_1}$$

γ = Bulk unit weight of the stored material (N/m³)

R_h = Hydraulic radius of the bin (m), which is $\frac{R}{2}$ for a circular silo of radius R

μ_1 = Wall friction coefficient (dimensionless)

C = Shape and material-dependent constant:

$$C = \frac{D}{4\mu_1 k_0} - \frac{h}{3}$$

Where:

D = Diameter of the silo (m)

k_0 = Lateral pressure coefficient under static or dynamic conditions (dimensionless)

h = Height of the Silo (m)

Assumptions of the Reimbert Formula

The assumptions underlying the Reimbert formula are:

1. The stored material is homogeneous, granular and dry.
2. Pressure varies with depth according to a nonlinear function, not a simple linear increase.
3. Wall friction and internal friction coefficients remain constant with depth.
4. Dynamic effects (filling) are accounted for using appropriate values of k0k_0k0.
5. Effects of arching, consolidation or time-dependent behaviour are not explicitly considered, though their influence is indirectly included via empirical coefficients.

3. Rankine's Theory

Rankine's theory originally developed by William John Macquorn Rankine in 1857, for the analysis of earth pressures on retaining walls, can be conceptually applied to shallow bins or bunkers containing granular materials (Dyck et al, 2024). This theory posits that the granular material is in a state of plastic equilibrium, where internal shear stresses are fully mobilized. Rankine's theory is often considered for situations where the wall is smooth or where friction at the wall is negligible and the material is assumed to be cohesionless.

For active earth pressure (material pushing against the wall):

$$P_a = \gamma z \tan^2\left(45^\circ - \frac{\phi}{2}\right) = \gamma z K_a \qquad (1.3)$$

For passive earth pressure(wall pushing against thematerial):

$$P_p = \gamma z \tan^2\left(45^\circ + \frac{\phi}{2}\right) = \gamma z K_p \qquad (1.4)$$

Where:

Pa = Active earth pressure (Pa)

Pp = Passive earth pressure (Pa)

ϕ = Angle of internal friction of the granular material (degrees)

Ka = Coefficient of active earth pressure

Kp = Coefficient of passive earth pressure

Rankine's theory provides a fundamental understanding of limiting equilibrium states but often overestimates pressures in deeper silos due to its neglect of wall friction (Craig, 2004).

Assumptions of Rankine's Theory (as applied to granular materials in bins):

The assumptions underlying the Rankine's theory are:

1. The granular material is homogeneous, isotropic and cohesionless.
2. The failure plane is a plane surface.
3. The wall is smooth (no friction between material and wall).
4. The ground surface (or top surface of the material) is horizontal.
5. The material is in a state of plastic equilibrium.

4. Airy's Theory

Airy's theory, developed in the 19th century, presents a classical analytical approach for estimating the lateral and vertical pressures exerted by granular materials in deep vertical containers such as silos. While Janssen's equationemphasizes the transfer of vertical loads to the walls due to friction, Airy's theory is more concerned with the distribution of lateral pressure, particularly under the condition of a free surface and a deep granular mass (Airy, 1892; Jenike, 1964).

Unlike Janssen's asymptotic pressure model, Airy's approach derives lateral pressures using principles of equilibrium and failure mechanics, incorporating the internal friction and wall friction of the stored material. It considers the limit condition where a wedge of material is on the verge of yielding due to its self-weight, producing a pressure distribution governed by stress ratios and geometric parameters. The method is especially applicable in scenarios where dynamic discharge or large depth causes stress redistribution.

The general form of the lateral pressure at depth Y in a silo is:

$$P = \frac{\gamma D}{\mu+\mu'}\left[1 - \sqrt{\frac{1-\mu^2}{\left(\frac{2\gamma Y}{D}(\mu+\mu')+1-\mu\mu'\right)}}\right] \qquad (1.5)$$

Where:

P = Lateral pressure at depth Y (Pa)

γ = Bulk unit weight of the stored material (N/m³)

D = Equivalent silo diameter or width (m)

μ = Coefficient of internal friction of the material (dimensionless)

μ' = Coefficient of wall friction between the material and silo wall (dimensionless)

Y = Depth from the top of the stored material (m)

The corresponding vertical pressure at the same depth Y is given by:

$$q = \frac{P}{k}$$

Where:

q = Vertical pressure at depth Y (Pa)

k = Lateral-to-vertical pressure ratio (dimensionless)

Assumptions Underlying Airy's Theory

The assumptions underlying the Airy's theory are:

1. The granular material is dry, homogeneous and follows the Mohr-Coulomb failure criterion.
2. Wall and internal friction coefficients are constant along the depth of the silo.
3. The lateral and vertical pressures are related through a constant ratio.
4. The pressure distribution considers a critical equilibrium wedge within the stored material.
5. The theory is typically applied under static or quasi-static conditions, though it helps estimate loads during the onset of discharge.
6. The geometry is assumed to be vertical with straight walls and uniform cross-section.

While Airy's theory, developed from Coulomb's wedge principles, provided an early and valuable analytical framework for understanding granular pressures, particularly in shallow bins or bunkers where the rupture plane intersects the free surface, its direct applicability and foundational role in predicting pressure variations at significant depth in tall silos is generally superseded by Janssen's formula since it captures the characteristic asymptotic pressure profile observed in deep silos due to frictional load transfer to the walls more accurately (Dyck et al, 2023).

2. Stress- Strain Models

Studies of the responses of cereal grains to mechanical stresses have progressed from analyses based on simple Hookean models to increasingly sophisticated representations. Early research utilized viscoelastic models using generalized Kelvin and Maxwell frameworks, either singly or jointly (Herum et al, 1979). This evolved to elastoplastic models (Zhang et al, 1986) and more recently to complex constitutive models incorporating non-local effects and advanced rheological frameworks.

Upon repeated uniaxial loading, Shapolyanskaya (1952) found that the load-deformation behaviour of wheat kernels approached that of an elastic body. Thus, applying the Hertz theory of contact stresses, he evaluated a modulus of elasticity for wheat kernels. In his study of core samples of wheat kernels, Zoerb (1960) noted the same strain hardening tendencies but

concluded that plastic rather than elastic behaviour characterized the mechanical properties of wheat.

Shelef and Mohsenin (1967) supported Zoerb's observations, as did Arnold and Roberts (1969) through various parallel-plate and indenter uniaxial compression tests. Manbeck and Nelson (1972, 1975), Schott and Britton (1984), Mensah et al. (1981) and Herum et al. (1979) are among the researchers who categorized various grains as being viscoelastic. Zhang et al. (1985) categorized wheat as being elastoplastic, while Briassou and Curtis (1985) characterized grains as being non-time dependent in behaviour.

While some earlier researchers treated granular materials as elastic, contemporary understanding recognizes these materials are highly complex and may be defined as being elastoviscoplastic (Li et al, 1989). Recent work by Chen and Yan (2021) has further advanced this understanding by developing an elastic-viscoplastic constitutive theory specifically for dense granular flow, implemented through three-dimensional numerical simulations that capture the complex rheological behaviour of granular materials.

2.1. Elastoplastic Models

The elastoplastic theory developed by Lade (1977) for cohesionless sand and verified for wheat en masse by Zhang et al. (1986) has the following form;

$$d\varepsilon_{ij} = d\varepsilon_{ij}^{e} + d\varepsilon_{ij}^{p} + d\varepsilon_{ij}^{c} \qquad (2.1)$$

Where:

$d\varepsilon_{ij}$ is the total strain increment tensor and superscripts e, p and c, refer to the elastic, plastic and plastic collapse strain increment components respectively.

The complete elastoplastic constitutive relationship includes an elastic component and two work hardening plastic components. Figure. 2.1 shows basic elastoplastic components as described by Lade's model.

$d\varepsilon_{ij}$ is the volumetric strain increment.

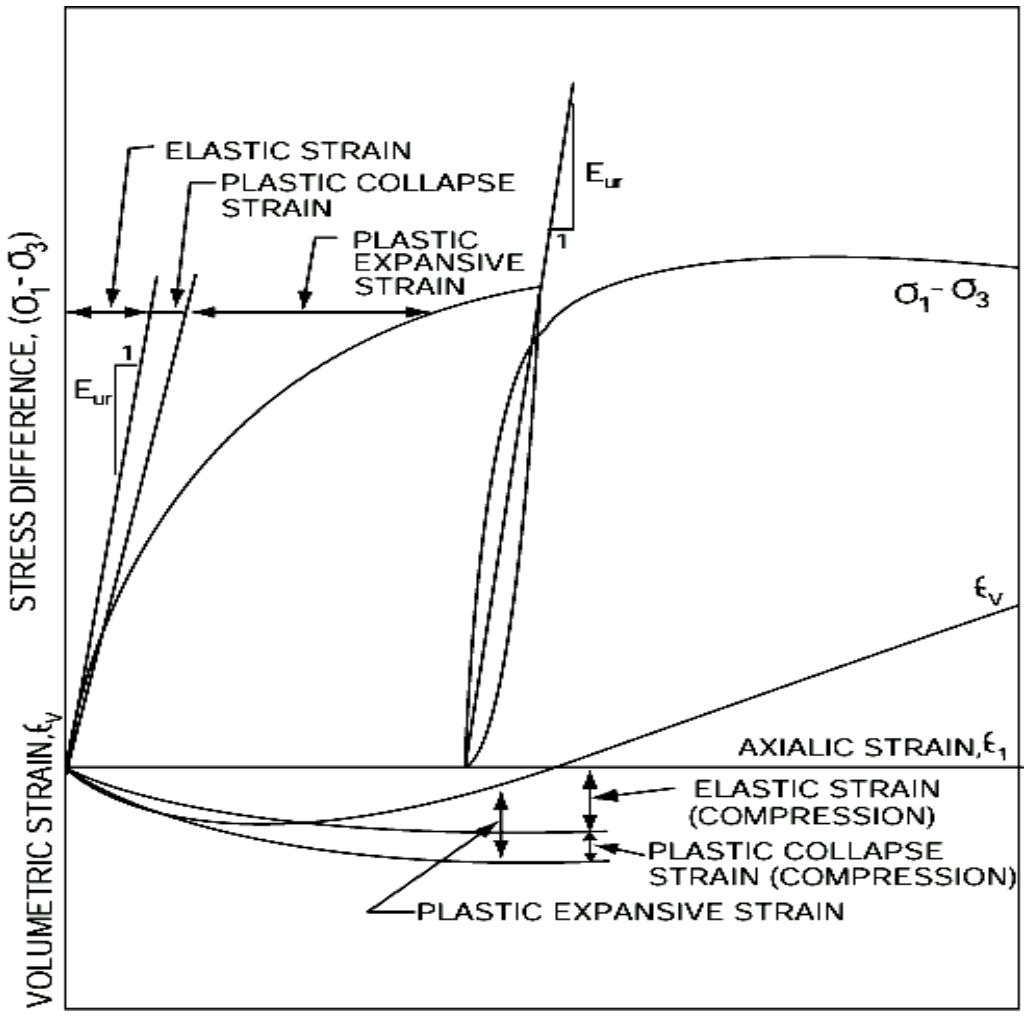

Figure. 2.1: A schematic representation of elastic, plastic collapse and plastic expansive strain components determined in triaxial tests (Lade, 1977).

Lade and Nelson developed a procedure to construct an incremental elastoplastic model with multi-intersecting yield surfaces. By using this Lade-Nelson method Chi and Kushwaha (1990) derived the complete elastoplastic model as presented below;

2.1.1. Lade's complete Elastoplastic Constitutive Equation

The complete elastoplastic stress-strain equation developed by Lade *(1977)* may be written in incremental form as;

$$d\{\sigma\} = [E_{ep}]d\{\varepsilon\} \tag{2.2}$$

$$\left[E_{ep}\right] = \left[E\right] - \frac{\left[E\right]}{A}\left[\left\{\frac{\partial g_c}{\partial \sigma}\right\} \cdot (b_c)^t + \left\{\frac{\partial g_p}{\partial \sigma}\right\} \cdot (bp)^t \left[E\right]\right] \quad \text{(Error! No text of specified style in document.2.3)}$$

The terms in equation (2.3) are defined below;

$$A = \begin{vmatrix} L_{11} & L_{12} \\ L_{21} & L_{22} \end{vmatrix}$$ (**Error! No text of specified style in document.**2.4)

$$b_c = L_{22}\left\{\frac{\partial f_C}{\partial \sigma}\right\} - L_{12}\left\{\frac{\partial f_P}{\partial \sigma}\right\} \quad (2.5)$$

$$b_P = L_{11}\left\{\frac{\partial f_P}{\partial \sigma}\right\} - L_{21}\left\{\frac{\partial f_C}{\partial \sigma}\right\} \quad (2.6)$$

$$L_{11} = \left\{\frac{\partial f_C}{\partial \sigma}\right\}^t \cdot [E] \cdot \left\{\frac{\partial g_C}{\partial \sigma}\right\} + \left\{\frac{\partial K_C}{\partial W_P^P}\right\} \cdot \{\sigma\}^t \cdot \left\{\frac{\partial g_C}{\partial \sigma}\right\} \quad (2.7)$$

$$L_{22} = \left\{\frac{\partial f_P}{\partial \sigma}\right\}^t \cdot [E] \cdot \left\{\frac{\partial g_P}{\partial \sigma}\right\} + \left\{\frac{\partial K_P}{\partial W_P^P}\right\} \cdot \{\sigma\}^t \cdot \left\{\frac{\partial g_P}{\partial \sigma}\right\} \quad (2.8)$$

Alternatively,

$$L_{11} = \left\{\frac{\partial f_C}{\partial \sigma}\right\}^t \cdot [E] \cdot \left\{\frac{\partial g_C}{\partial \sigma}\right\} \quad (2.9)$$

$$L_{22} = \left\{\frac{\partial f_P}{\partial \sigma}\right\}^t \cdot [E] \cdot \left\{\frac{\partial g_P}{\partial \sigma}\right\} \quad (2.10)$$

All factors have their usual meaning.

The elastoplastic constitutive matrix (2.2) can readily be determined if the stress state is known.

Recent work by Wu et al. (2023) has significantly expanded this domain by applying machine learning techniques to develop constitutive models for granular materials. Their research demonstrates that data-driven approaches can effectively capture the complex mechanical behaviour of granular materials while overcoming limitations of traditional constitutive models.

The Mohr-Coulomb failure criterion finds many applications in engineering practice (Ti, 2009; Dartevelle, 2003). Analysis of stress data from triaxial cell tests on granular materials often involves the Mohr Circle construction to graphically determine strength parameters (Stafford et al, 1986). The Mohr circle construction helps to determine the stresses on any given plane.

From a series of tests, the minor ($\sigma 3$) and major ($\sigma 1$) principal stresses may be derived. On a graph with shear stress along the y-axis and normal stress along the x-axis, a circle centered on $x = (\sigma 1+\sigma 2)/2$ of radius $(\sigma 1-\sigma 2)/2$ is drawn for each test. A smooth curve, tangent to these circles defines the equation for the failure characteristic of the material in question. The ideal Mohr-Coulomb failure plot is shown in Figure 2.2.

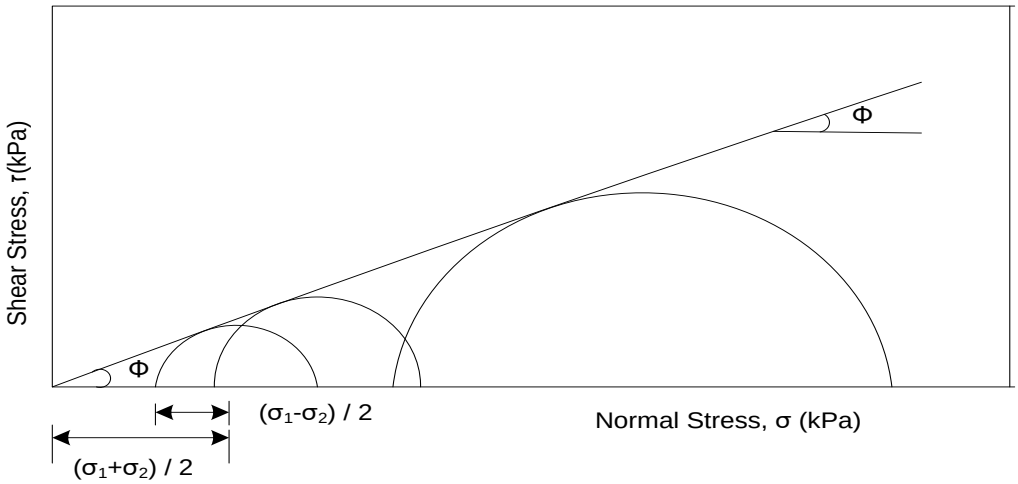

Figure 2.2: Ideal Mohr-Coulomb failure envelop for cohesionless granular materials (Dartevelle, 2003)

The basic equation if of the form,

$$\tau = c + \sigma \tan \varphi \qquad (2.11)$$

Where:

σ = normal (principal) stress

τ = shear stress

c = cohesion

ϕ = angle of internal friction, all measured at failure.

The alternative to the above method of plotting circles is to directly plot (σ1-σ2)/2 against (σ1+σ2)/2 for each test and draw a best-fit straight line through the points. From this so-called Kf line, c and φ may be derived (Stafford et al, 1986). For cohesionless granular materials such as shelled maize, the cohesion, c, is usually assumed to be negligible (Zhang et al, 1994).

Research by Jiang et al. (2025) has examined how particle size distribution and shape govern the critical state behaviour of granular materials, providing new insights into the relationship between microscale properties and macroscale mechanical responses.

Horabik and Molenda (2014) presented an analysis based on the Discrete Element Method (DEM) proposed by Cundal (1979) based on elementary interactions between the grains. The method consists in a simplified solution of the equation of motion for each grain of the material.

The calculation procedure is based on the assumption that during a very short time step Δt acceleration and speed are constant and the disturbance of motion of a single grain does not reach further than to the nearest neighbours. DEM provides new possibilities of deeper insight into the micro-scale behaviour of bulk solids, which are not available with traditional or even modern approach of continuum mechanics where gradients of displacement and stress are extremely high like during flow around inserts (Kobyłka, Molenda, 2013).

The rapid development of computer calculation techniques permitted the realization of computer simulations of a variety of processes occurring in granular materials, such as: dynamic effects in silos, mixing, segregation, gravitational discharge from silos (Zhang et al, 1993; Masson , Martinez , 2000; Kouet al, 2002; Parafinuk et al, 2013; Kobyłka, Molenda (2014). DEM simulations generally produce a huge scatter of inter-particle forces which after averaging provide useful information. An example of the horizontal forces acting on a vertical wall in quasi-static assemblies (6000 particles in two dimensions) is presented in Figure 2.3. Analysis of the distribution of horizontal forces averaged for 10 particle–wall contacts indicated a moderately smooth increase in the force with increase in particle bedding depth (S ykut et al, 2008). The DEM values are considerably larger as compared to Janssen's (1895) solution. Similarly, Balevičius et al. (2011) obtained good agreement of lateral pressure distribution vs material depth with experimental data which were significantly larger than Janssen's (1895) solution and Eurocode 1 (2003) recommendations. González-Montellano et al. (2012) obtained the pressure distribution of particles similar to maize grains along the vertical direction of the wall reaching its maximum at the silo-hopper transition using DEM. Masson, Martinez (2000) reported on the impact of anisotropy of contact orientations on the pressure distribution.

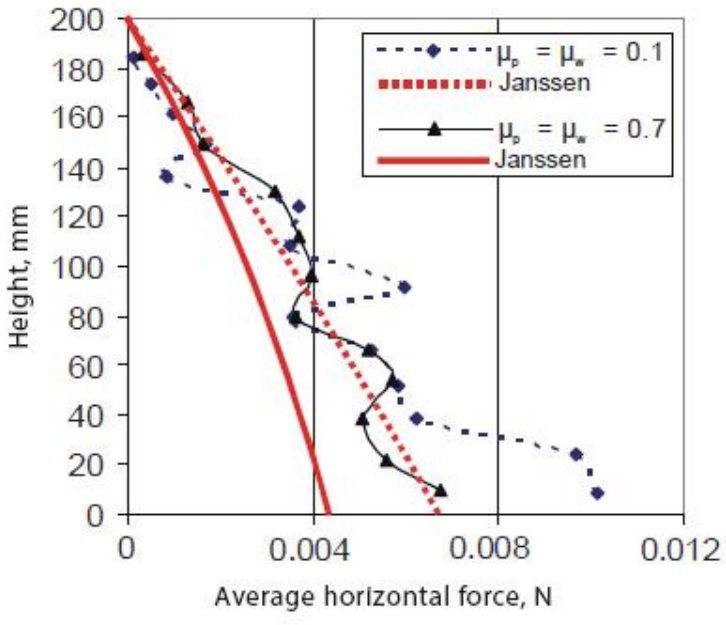

Figure 2.3: Wall horizontal force averaged for 10 particle -wall contacts compared to Janssen's (1895) solution.

Horabik and Moleda (2014) concluded that granular solids constitute a very wide group of materials of specific mechanical, physical and chemical properties. In that group granular

materials of biological origin represent a very important source of products of agriculture and food processing industry. Precisely determined parameters of mechanical properties of granular materials and properly chosen constitutive models are fundamental for proper design and control of storage, handling and processing of those materials. There have still been a lot of particular and specific operations not fully understood or precisely described yet. A few examples of such processes discussed in the paper indicate that further development of tools for modelling the mechanics of granular solids is necessary. One of the most promising tools is the DEM. All these actions are necessary to ensure that the equipment used for storage and processing of granular materials meets two basic demands: predictable and safe operations and high quality of processed materials.

Over the past decade, DEM has become an increasingly sophisticated and widely-used tool for modeling granular behaviour in silos. Ramírez-Gómez (2020) provided a comprehensive review of DEM applications in silo research, highlighting recent advances and future trends. The review emphasizes the method's ability to capture microscale interactions that influence macroscale behaviours like flow patterns, pressure distributions and clogging phenomena.

Recent developments by Zhang and Li (2024) have focused on optimizing DEM models to obtain stable and reliable numerical results when simulating the mechanical response of granular materials. Their work addresses key challenges in DEM implementation, including appropriate parameter selection and computational efficiency. Similarly, Mahboob et al. (2023) have extended DEM capabilities by incorporating fracture effects of particles in three-dimensional simulations, allowing for more realistic modeling of stress-induced particle breakage during silo operations.

Kumar and Das (2024) have applied DEM specifically to investigate the discharge of granular matter from silos with eccentric openings, providing valuable insights into how outlet positioning affects flow patterns and pressure distributions. This builds on earlier work by Bhateja and Jain (2022), who studied self-similar velocity and solid fraction profiles in eccentrically located outlets.

A particularly important advancement has been made by Sac-Morane et al. (2024), who developed a Phase-Field Discrete Element Method to study chemo-mechanical coupling in granular materials. This innovation allows for the modeling of physicochemical processes that can significantly impact the mechanical behaviour of stored materials over time.

2.2. Viscoelastic Models

The linear and non-linear viscoelastic models have been predominantly used to model material behaviour (Gumbe, 1995). These models incorporate time in stress-strain equations. Such equations are specifically important in the design of storage structures such as silos and foundations both of which are exposed to rapidly declining or changing periodic ambient temperatures, moisture content, among others (Gumbe, 1995). Recent research has expanded the application of these models to better predict the time-dependent behaviour of granular materials under complex loading conditions experienced in practical storage situations.

For linearly viscoelastic material, the following criteria hold (Findley et al, 1976).

1. For any step input in strain (ε_0) the relation between the stress $\sigma(t)$ and strain is;

$$\frac{\sigma(t)}{\varepsilon_0} = E(t) \qquad (2.13)$$

For a step input of stress, σ_0, the relation between strain, $\varepsilon(t)$ and stress is;

$$\frac{\varepsilon(t)}{\sigma_0} = J(t) \qquad (2.13)$$

Where $E(t)$ and $J(t)$ are the stress relaxation modulus and creep compliance respectively.

2. The Boltzman's superposition principle holds, that is, the stress at any time *t* depends on the strain history of the material;

$$\sigma(t) = \int_0^t E(t-\tau)\frac{\delta\varepsilon}{\delta\tau}\delta\tau + \sum_{i=1}^{n} \Delta\varepsilon_i E(t-t_i) \qquad (2.14)$$

Where;

$\varepsilon(t)$ is the applied strain

$\Delta\varepsilon_i$ is the jump in the applied strain occurring at time t_i

Most viscoelastic models are built on the spring-dashpot arrangement as the basic building blocks. The two basic models are the Kelvin solid model and the Maxwell fluid model (Chung, 1988). Figure 2.4 a show the Kelvin model with the spring and dashpot arranged in parallel while Figure 2.4 b shows the Maxwell model where the spring and dashpot are arranged in series.

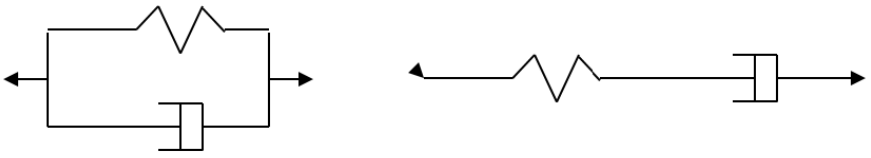

a) Kelvin model b) Maxwell model

Figure 2.4: Basic Viscoelastic models

The two basic equations governing the stress-relaxation behaviour of the Kelvin and Maxwell models at constant strain are given in (2.15) and (2.16) respectively;

$$E(t) = E \qquad (2.15)$$

$$E(t) = Ee^{-t/\tau} \qquad (2.16)$$

Where; E (t) is the relaxation modulus and E the spring constant.

The Maxwell and Kelvin models have been noted to have several deficiencies in predicting the behaviour of viscoelastic materials (Chung, 1988; Gumbe, 1993). These deficiencies include,

1) Neither the Maxwell nor Kelvin model represents the behaviour of most viscoelastic materials in actual systems.
2) The Maxwell model shows no time-dependent recovery nor does it show the decreasing strain rate under constant stress, a characteristic of primary creep.
3) The Kelvin model does not exhibit time-independent strain on loading, nor does it describe a permanent strain after unloading.
4) Both models show a finite initial strain rate where the initial strain rate for many materials is very rapid.

Due to the above limitations of the simplified models, several other viscoelastic models have been adopted to help make more accurate predictions of viscoelastic behaviour of engineering materials (Chung, 1988; Aklonis and MacKnight, 1983; Gumbe, 1993). One such model, which has been found to be fairly accurate, is the generalized Maxwell-Weichert model (Aklonis and MacKnight, 1983) that consists of an arbitrary number of Maxwell elements connected in parallel as shown in Figure 2.5.

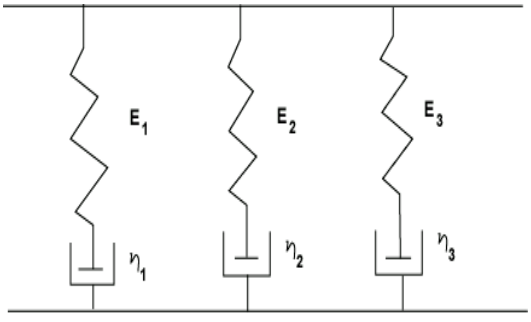

Figure 2.5: Generalised Maxwell-Weichert model (Aklonis and MacKnight, 1983)

The generalized stress-relaxation equation for the Maxwell Weichert model is of the form;

$$E(t) = \sum_{i=1}^{z} E_i e^{-k_i t} \qquad (2.17)$$

Where;

E(t) is the relaxation modulus (MPa)

t is the time of relaxation (minutes)

k is the exponent (1/minute)

For practical purposes however, equation (2.17) has to be presented to finite levels. Equation (2.18) therefore is the representation of (2.17) at two levels (Herum, 1979);

$$E(t) = E_1 e^{-k_1 t} + E_2 e^{-k_2 t} \qquad (2.18)$$

The two equations, (2.17) and (2.18), describe the Maxwell-Weichert linear viscoelastic model as long as the constants E1, E2, k1 and k2 are determined.

Oranga (2005) conducted test to evaluate relaxation parameters which included the stress-relaxation moduli, E1, E2 and the stress-relaxation exponents k1, k2.

Figures 2.6 show the stress relaxation curves for a maize variety V1, at an initial bulk density of 800 kg/m3 and the fitted curves according to the given regression equations indicated.

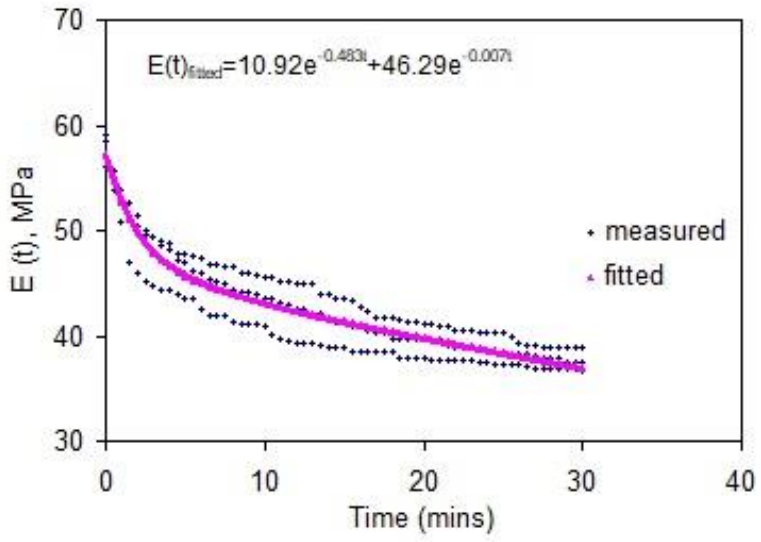

Figure 2.6: Stress-relaxation curve for variety V1

The standard error on the residuals for each of the varieties V1, V2 and V3 were found to be 1.17, 0.95 and 1.82 MPa respectively. Similarly, the coefficient of determination between the measured values and the fitted values were obtained as 0.87, 0.84 and 0.90 for V1, V2 and V3 respectively. These were indicators that the measured data and the regressed values fitted quite closely statistically.

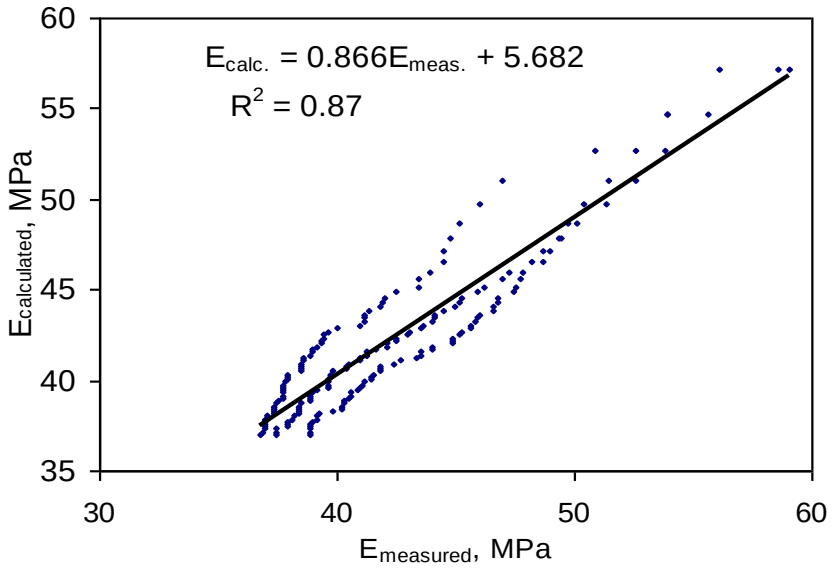

Figure 2.7: Coefficient of determination, R2, for E (t), variety V1

The flexibility of the Maxwell-Weichert model in reproducing the viscoelastic behaviour of shelled maize en masse was further demonstrated by plotting the above results on a log-log scale as shown in Figure 2.8.

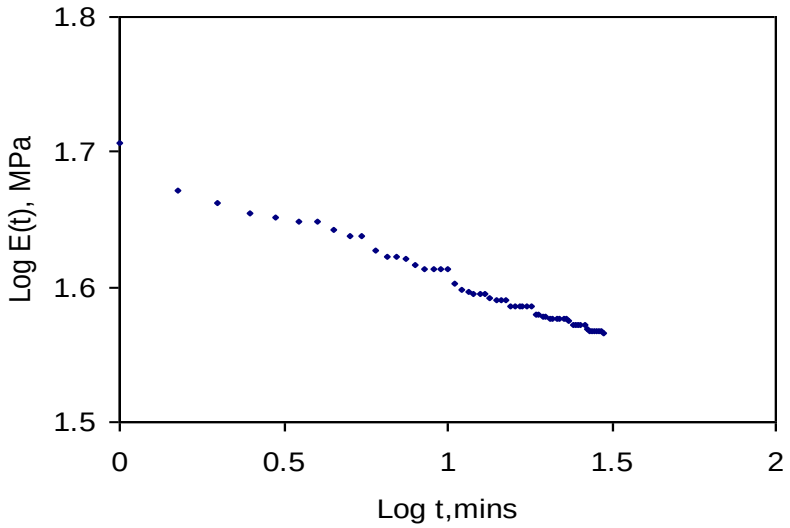

Figure 2.8: Behaviour of Maxwell-Weichert model in stress-relaxation for V1

Figure 2.8, taken from one of the replications for V1, shows the application of the generalized form of Maxwell-Weichert model described in equation 2.17 with an almost infinite number of parameters (observed on the step-decline of the curve). Such behaviour, which was observed

for all the varieties, has been reported for polymer viscoelastic materials by Aklonis and MacKnight (1983).

The traditional viscoelastic models described above have been increasingly integrated with modern computational approaches to better predict granular material behaviour in silos. Tian et al. (2018) compared discrete and continuum modeling approaches for granular flow in silo discharge, identifying how viscoelastic principles can be incorporated into both frameworks to capture time-dependent phenomena.

The emergence of data-driven approaches, as demonstrated by Wu et al. (2023), offers new possibilities for developing viscoelastic constitutive models that can effectively capture the complex mechanical behaviour of granular materials while overcoming limitations of traditional formulations. These machine learning techniques can identify patterns in experimental data that might not be apparent in conventional viscoelastic frameworks, potentially leading to more accurate predictions of material response under complex loading conditions.

Yilmazoğlu (2024) applied advanced modeling techniques to triaxial pressure tests with uniform granular materials, providing insights into how viscoelastic properties influence the three-dimensional stress state in granular assemblies. This work is particularly relevant for understanding the complex stress distributions that develop in silos during filling, storage and discharge operations.

The integration of viscoelastic principles with DEM simulations has also seen significant advancement. As noted by Ramírez-Gómez (2020) in a comprehensive review of DEM applications in silo research, incorporating viscoelastic contact models into discrete element simulations allows for more realistic representation of time-dependent particle interactions. This approach can capture phenomena such as stress relaxation at particle contacts, which influences overall pressure distributions in silos.

Duan et al. (2023) further extended these concepts by investigating the dynamic behaviour of silos with grain-like material during earthquakes, demonstrating how viscoelastic models can be adapted to predict material response under rapidly changing load conditions. Their work highlights the importance of accurately modeling time-dependent material behaviour when assessing silo safety under dynamic loading scenarios.

These developments collectively represent a significant advancement in our ability to model the complex viscoelastic behaviour of granular materials in silo systems, providing engineers

with more accurate tools for predicting load distributions and material flow patterns in practical applications.

2.3. Viscoplastic Models

Perzyna (1966) introduced the foundational framework for viscoplastic constituve modeling, which has since been widely applied to describe time-dependent behaviour of granular materials. Unlike elastoviscoplastic formulations, viscoplastic models disregard elastic response and instead emphasize rate-dependent plastic deformation. This is especially relevant for modeling prolonged loading scenarios such as grain stored in silos where elastic strains are negligible relative to permanent deformations. Figure 2.4 has the spring and dashpot elements. The addition sliding force element is illustrated in Figure 2.9.

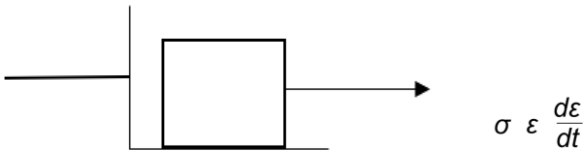

Figure 2.9: Sliding Frictional Element (σ_y) (Bbanerje, 2007)

Several researchers have extended Perzyna's theory to granular materials. Notably, Valanis (1971) provided a theoretical foundation for rate-dependent plasticity in particulate media, while Adachi and Oka (1982) adapted Perzyna-type viscoplastic formulation specifically for soils and grains. These models capture; the influence of strain rate on stress-strain response, accumulation of time-dependent permanent strains, the coupling between deviatory and volumentric deformations under various stress states.

Recent advancements by Wang and Zhang (2019) introduced a particle-scale, rate-dependent viscoplastic model for dense granular assemblies. Their work significantly improves our understanding of the time-dependent behaviour of stored grains under both static and dynamic loading.

Viscoplastic models are essential for accurately describing time-dependent, inelastic behaviour, especially under sustained loads where creep is a significant factor. These models capture how the material deforms permanently over time, with its yield strength and deformation rate influenced by the loading speed. The flow of granular solids within rigid walls, such as those of a silo, is often modeled using continuum mechanics, treating the granular material as a continuous medium. The apparent viscosity in these models is typically

non-linear function of the rate of deformation and pressure and they account for friction, cohesion and fluidity.

The fundamental premise of viscoplasticity in granular materials is the existence of a yield stress (σy) below which the material responds elastically or viscoelasticity and above which plastic flow initiates. This flow, however, is not instantaneous but rather rate-dependent, meaning the rate of plastic deformation is a function of the applied stress and material properties (Lemaitre and Chaboche, 1990). In the context of granular materials, this behaviour reflects the continuous rearrangement, breakage and densification of particles under prolonged stress.

Key aspects of viscoplastic behaviour in granular materials include:

1. **Yield Condition**: A threshold stress state must be exceeded for viscoplastic flow to occur. This is often defined by a yield function $f(\sigma, \kappa) = 0$ where σ is the stress tensor and κ represents hardening parameters.

2. **Flow Rule**: Once the yield condition is met, the rate of plastic strain ($\dot{\epsilon}^p$) is typically governed by an associated or non-associated flow rule, often expressed as:
$$\dot{\varepsilon^p} = \dot{\lambda}\frac{\partial g}{\partial \sigma} \qquad (2.19)$$
Where $\dot{\lambda}$ is the plastic multiplier and g is the plastic potential function. For associated flow rules, g=f.

3. **Viscoplastic Consistency (Evolution Equation for Plastic Multiplier)**: The evolution of the plastic multiplier $\dot{\lambda}$ is governed by overstress-based regularization models such as the Perzyna model (Perzyna, 1966) or the Duvaut–Lions formulation (Duvaut and Lions, 1972). For instance, in the Perzyna approach, the plastic multiplier is defined as:
$$\dot{\lambda} = \gamma\langle\Phi(\mathrm{F})\rangle \qquad (2.20)$$
Where γ is a fluidity parameter, $\Phi(\mathrm{F})$ is an overstress function and F measures the normalized distance from the yield surface (e.g, $F = \frac{f}{f_0} - 1$ enforce that plastic flow only occurs when $F > 0$.

2.3.1. Foundational Viscoplastic Models

A number of classical viscoplastic models have been proposed, often built upon mechanical analogies consisting of spring, dashpot and slider elements to represent elastic, viscous and plastic components, respectively.

a. Bingham Model

The Bingham model represents one of the simplest viscoplastic formulations. It assumes a distinct yield stress, below which the material behaves elastically and above which it flows as a Newtonian fluid. The one-dimensional strain rate $\dot{\varepsilon}$ under constant stress σ is given by:

$$\dot{\varepsilon} = \begin{cases} \frac{\sigma}{E}, & \text{if } |\sigma| \leq \sigma_y \quad \text{(elastic response)} \\ \frac{1}{\eta}(\sigma - \sigma_y \cdot \operatorname{sgn}(\sigma)), & \text{if } |\sigma| > \sigma_y \quad \text{(viscoplastic flow)} \end{cases} \tag{2.21}$$

Where E is the elastic modulus, η the plastic viscosity and σ_y the yield stress. This model is symbolically represented by a dashpot and a slider in parallel configuration.

b. Herschel–Bulkley Model

An extension of the Bingham model, the Herschel–Bulkley model accounts for non-linear flow behaviour (shear thinning or thickening) after yield. It is expressed as:

$$\dot{\varepsilon} = \frac{1}{\eta}(\sigma - \sigma_y)^n, \quad |\sigma| > \sigma_y \tag{2.22}$$

Here, n is the flow index. For n < 1, the material is shear-thinning; for n > 1, it is shear-thickening. This model provides a better fit for complex behaviours observed in fine granular suspensions or pastes.

c. Perzyna Model

The Perzyna viscoplastic model (Perzyna, 1966) is a rate-dependent elasto-viscoplastic formulation where the total strain rate is divided into elastic and viscoplastic components:

$$\dot{\varepsilon} = \dot{\varepsilon^e} + \dot{\varepsilon^{vp}} \tag{2.23}$$

The viscoplastic component is derived from an overstress-based flow function:

$$\dot{\varepsilon^{vp}} = \gamma\langle\Phi(f)\rangle\frac{\partial f}{\partial \sigma} \tag{2.24}$$

where f is the yield function and $\Phi(f)$ typically follows a power-law form, such as

$\Phi(f) = \left(\frac{f}{f_0}\right)^N$, with f_0 being a reference stress and N a rate-sensitivity exponent. This model effectively captures time-dependent plasticity in solids, including granular materials undergoing long-term deformation.

The general form of the Perzyna model for the viscoplastic strain rate vector ($\dot{\varepsilon}^{vp}$) is given by:

$$\dot{\varepsilon_{vp}} = \gamma\langle\Phi(f,\kappa)\rangle\frac{\partial\sigma}{\partial g} = \dot{\lambda}\frac{\partial\sigma}{\partial g} \quad (2.25)$$

2.4. Elastoviscoplastic Models

Li et al (1989) presented a study based on the constitutive equation based on the elastic-viscoplastic (EVP) theory for cohesionless sands (Youngs, 1982) to model the stress-strain behaviour of wheat en masse under monotonic and cyclic loading conditions. This EVP model considers:

i. The effect of confining pressure or hydrostatic pressure on the deformation and strength characteristic of the particulates;
ii. The development of large inelastic shear deformations during the loading process; and
iii. The coupling between inelastic shear and volumetric deformation with changing stress state.

The three-dimensional constitutive formulation incorporates the effect of the evolution of intergranular structure on both stress-strain response and inelastic volume change induced by shear deformation. Stress-strain behaviour predicted by the Youngs' EVP model is based on an associated plasticity formulation for deviatoric strains and a separate constitutive equation for coupled volumetric strains. The parameters of the constitutive equations are assumed to be a function of void ratio or bulk density and the mean stress both of which reflect the effects of loading history. The parameter calculation technique used in the study was similar to that described by Youngs (1982).

Recent advancements have expanded on these fundamental concepts. Chen and Yan (2021) developed an elastic-viscoplastic constitutive theory specifically for dense granular flow that incorporates a three-dimensional numerical implementation. Their work provides significant improvements in modeling the complex rheological behaviour of granular materials under various loading conditions, particularly relevant to silo applications.

2.4.1. One Dimensional Constitutive Equation

The key features of the elastic-viscoplastic (EVP) constitutive equation developed by Youngs (1982) are explained through the one-dimensional formulation. For further in-depth understanding of the stress transfer and displacement mechanisms involved in elastic viscoplastic constitutive models the reader may consult these references (Chen and Baladi, 1985; Feda, 1982; and Youngs, 1982). The one-dimensional, stress-strain model is used as the stepping stone for presenting the three-dimensional model.

In the one-dimensional model, two strain rate equations (based on particulate theory) one for shear strain and one for volumetric strain, are used to characterize the grain en masse behaviour. The shear strain rate ($\dot{\gamma}$) equation consists of two components: 1) elastic shear strain rate ($\dot{\gamma}_e$) and 2) viscoplastic shear strain rate ($\dot{\gamma}_{vp}$). The elastic shear strain rate is the recoverable component of strain; whereas, the viscoplastic component is the irrecoverable (permanent) component of strain. The following shear strain rate equation was derived by Youngs (1982):

$$\dot{\gamma}_e = \dot{\gamma}_e + \dot{\gamma}_e = \frac{\dot{\tau}}{G} + |\dot{\gamma}| \left(\frac{\tau - \tau^r}{\frac{\dot{\tau}}{|\dot{\tau}|}\tau^y - \tau^r} \right)^m \frac{\dot{\tau}}{|\dot{\tau}|} \qquad (2.26)$$

Where:

G = shear elastic modulus,

m = plastic hardening exponent,

$\dot{\tau}$ = shear stress rate,

τ = shear stress,

τ^r = shear stress reversal point

τ^y = yield shear stress

$|\dot{\gamma}|$ = absolute value of shear strain rate,

$\frac{\dot{\tau}}{|\dot{\tau}|}$ = determine the point of the yield surface which is used to calculate the direction of yielding.

In equation 2.26 the ratio $\dot{\tau}/|\dot{\tau}|$is the unit vector that provides the stress direction of plastic flow, whereas, $|\dot{\gamma}|$ with the dimension of reciprocal time implicitly introduces the time factor in the formulation. In equation 2.19, the yield stress τ^yidentifies the onset of plastic flow and τ^y is the state point on the stress surface where the stress direction rate ($\dot{\tau}$) was last reversed, i.e, changed from increasing to decreasing rate or vice-versa. The stress reversal point becomes a memory parameter, which is used to define the relative distance to the yield stress in the direction of stress rate (Ozdemir, 1976). The yield surface expands or contracts depending on the state of stress (Chen and Baladi, 1985). The volumetric strain rate ($\dot{\varepsilon}_v$) equation consists of two components: 1) the expansion strain rate ($\dot{\varepsilon}_v^x$)and 2) the collapse strain rate ($\dot{\varepsilon}_v^c$). The expansion volumetric strain rate is due to the packing density change; whereas, the collapse volumetric strain rate is due to the grain reorientation. The volumetric strain rate equation is:

$$\dot{\varepsilon}_v = \dot{\varepsilon}_v^x + \dot{\varepsilon}_v^c = |\dot{\gamma}|[A(e - e_{cs})\lambda + B(1 - \lambda)] \qquad (2.27)$$

Where

A = volumetric expansion parameter,

B = volumetric collapse parameter,

e = current void ratio,

e_{cs} = critical state void ratio,

λ = relative structure change parameter ($0 \leq \lambda \leq 1$).

In equation 2.19, the yield stress τ^y in the direction of loading was hypothesized by Youngs (1982), based on experimental evidence, to be a function of the relative structure change parameter:

$$\tau^y = \tau^{f-} + (\tau^{f+} - \tau^{f-}) f(\lambda) = (\tau^{f+} - \tau^{f-})[1 - \exp(-5\lambda)] \quad (2.28)$$

Where:

τ^{f+} = failure shear in the direction of shear (e.g, increasing or decreasing rate)

τ^{f-} = failure shear stress in the opposite direction of shear (e.g, decreasing or increasing rate, respectively).

In equation 2.28, f(λ,) is an empirical function derived from experimental data. The function f(λ) for wheat was arrived at [1-exp (-5 λ,)] using the triaxial test data and Youngs (1982) linearity argument. For sands, exponents greater than 3 (compared to 5 for wheat) have been reported (Youngs, 1982). The relative structure change parameter λ is expressed as:

$$\lambda = 1 - \left[\{(\dot{\gamma}/|\dot{\gamma}|) - e^s\}/2\right] \qquad -1 \leq e^s \leq 1 \quad (2.29)$$

Where e^s is the variable used to measure the grain en masse structure.

The magnitude of the relative structure change parameter (λ) indicates the location of the failure stress state of the particulate material as the stress-strain path follows the limiting hardening curve, i.e, $\tau = \tau^y$ at all times. The value of λ varies from zero at the stress reversal point at the failure stress in one direction, to a value of unity as the failure stress and is reached in the direction of shear. The magnitude of es measures the development of relative structure change and its sign determines the direction of the relative structure change. The absolute value of $e^s = 1$ implies that the particle rearrangement has been fully accomplished. This results in volumetric changes in collapse mode. Any further volumetric changes are due to the packing density adjustments. The rate of e^s is defined by:

$$\dot{e}^s = C\dot{\gamma}(1 - \lambda^l) \quad (2.30)$$

Where

$\dot{e}^s$ = rate of relative structure change,

C = structure modulus which controls the hardening rate,

l = exponent for the measure of linearity of relative structure change.

A useful interpretation of equation 2.23 is that initially $\dot{e}^s$is linearly proportional to $\dot{\gamma}$ since ($\gamma \approx 1$) no further changes in es occur during continued shear in that direction.

Fall et al. (2017) and later Kamrin (2020) provided additional insights into these relationships through their research on dry granular flows and rheological models. They emphasized the importance of particle size in constitutive modeling, which has implications for the volumetric behaviour described in this equation.

2.4.2. Three- Dimensional Constitutive Equation

Two assumptions, as postulated by Youngs (1982), are herein retained to expand the one-dimensional model described in the preceding section to a three-dimensional formulation. The assumptions are: 1) the granular material is isotropic and 2) separate relationships can be developed for the response to deviatoric and hydrostatic (isotropic) loading.

The first assumption of isotropy simplifies the constitutive equations in that only two elastic material parameters (e.g, shear modulus and Poisson's ratio) are needed to completely describe the stress-strain relationship. In addition, invariants can also be effectively used to establish the state of stress. The evidence of structural anisotropy in sands has been demonstrated by Oda et al. (1978). Tests by Lade (1972) and Oda et al. (1972) with sand particles of various shapes showed that anisotropic behaviour decreases as the particle sphericity of the wheat particles tested in the present study was 55%. Hence, the load response of wheat en masse is expected to be anisotropic. The constitutive equation can be modified using the full elasticity tensor and introducing weighting factors in calculating the stress invariants as suggested by Sandler and DiMaggio (1973). The fully anisotropic constitutive equation requires 21 material constants for elastic component alone (Green-type linearly elastic material), which are extremely difficult if not impossible to determine. Therefore, as a first approximation and to keep the total number of material parameters at a reasonable number, the material response is assumed to be isotropic.

The deviatoric strain rate equation in three-dimensions similar in form to the one-dimension equation 2.19 is:

$$\dot{e}_{ij} = \frac{\dot{S}_{ij}}{2G} + \left\|\dot{e}_{ij}\right\| \left(\frac{\left\| S_{ij} - S_{ij}^{r} \right\|}{\left\| S_{ij}^{y} - S_{ij}^{r} \right\|} \right)^{m} n_{ij} \quad (2.31)$$

Where

$\dot{e}_{ij}$ = rate of deviatoric strain,

$\left\|\dot{e}_{ij}\right\|$ = norm of deviatoric strain rate, which is also the length of the tensor $\dot{e}_{ij}$ projected on the octahedral plane and is defined by eq.2.24,

m = shear yield exponent,

n_{ij} = direction tensor, similar to the ratio $\frac{\dot{\tau}}{|\dot{\tau}|}$ in equation 2.19,

S_{ij} = deviatoric stress,

$\dot{S}_{ij}$ = rate of deviatoric stress,

S_{ij}^{r}= deviatoric stress reversal point

S_{ij}^{y} = yield deviatoric stress,

$$\left\|\dot{e}_{ij}\right\| = \left(\dot{e}_{ij}\dot{e}_{ij}\right)^{1/2} = \left(2\|\dot{e}_{ij}\right)^{1/2} \quad (2.32)$$

$\|\dot{e}_{ij}$= second invariant of deviatoric strain

The double subscript notation has the usual meaning, i.e. the first index denotes the plane normal direction and the second index gives the direction of the tensorial quantity.

Both i and j subscripts can take on values 1, 2 and 3 which correspond to x, y and z axis directions, respectively. In equation 2.25, repeated indices appearing in the subscripts imply summation, e.g. $e_{ii} = e_{11} + e_{22} + e_{33}$.

Since any hydrostatic (isotropic) stress change from a stress state containing a deviatoric component results in a movement relative to the failure surface (Lade and Duncan,1971), normalized deviatoric stress $\bar{S}_{ij}$, normalized deviatoric strain rate $\dot{\bar{e}}_{ij}$ and normalized shear modulus $\bar{G}$ are defined as follows (the overbar symbol, -, is used to denote normalized quantities):

$$\bar{S}_{ij} = \frac{S_{ij}}{(\sigma_m/P_a)^{\alpha}} \quad (2.33)$$

$$\dot{\bar{e}}_{ij} = (\sigma_m/P_a)^{\alpha}\dot{e}_{ij} \quad (2.34)$$

$$\bar{G} = \frac{G}{(\sigma_m/P_a)^{2\alpha}} \quad (2.35)$$

Where

P_a = atmospheric pressure

σ_m = mean stress which is defined as $\sigma_m = \frac{1}{3}\sigma_{kk}$

α = failure surface curvature parameter

The deviatoric strain rate given by equation 2.24 then becomes:

$$\dot{e}_{ij} = \frac{\dot{s}_{ij}}{2G} - \propto \frac{\dot{s}_{ij}}{2G}\frac{\dot{\sigma_m}}{\sigma_m} + \left\|\dot{e}_{ij}\right\| \left(\frac{\left\|\bar{s}_{ij} - \bar{s}^r_{ij}\right\|}{\left\|\bar{s}^y_{ij} - \bar{s}^r_{ij}\right\|}\right)^m n_{ij} \qquad (2.36)$$

In equation 2.36, normalized yield ($\bar{S}^y_{ij}$) and reversal ($\bar{S}^r_{ij}$) stresses appear because of the symmetry of response which results from the use of normal stresses. The directional tensor n_{ij} defines the direction of inelastic shear on the octahedral plane and n_{ij} is the normal to the failure surface at a point defined by the direction of shear.

Using similar reasoning, a hydrostatic strain rate equation was derived by Youngs (1982):

$$\dot{\varepsilon}_{kk} = \frac{\dot{\sigma}_m}{K^e} + \left|\dot{\varepsilon}_{kk}\right| K^p \left(\frac{\sigma_m - \sigma^r_m}{\frac{\dot{\sigma}_m}{|\dot{\sigma}_m|}\sigma^{max}_m - \sigma^r_m}\right)^h \qquad (2.37)$$

Where

K^e = elastic bulk modulus,

K^p = plastic bulk modulus,

h = plastic bulk exponent

$\dot{\varepsilon}_{kk}$ = hydrostatic volumetric strain rate,

$\dot{\sigma}_m$ = mean stress rate,

σ^{max}_m = past maximum mean stress rate.

The volumetric strains produced by three-dimensional shear straining are modelled the same way as the one-dimensional shear given by equation 2.37. The rate equation for volumetric strain becomes:

$$\dot{\varepsilon}_{kk} = \left\|\dot{e}_{ij}\right\|[A(e - e_{cs})\lambda + B(1 - \lambda)] \qquad (2.38)$$

The total volumetric strain rate is the sum of hydrostatic (isotropic) volumetric strain rate (eq.2.37) and shear volumetric strain rate (eq. 2.38). In equation 2.31, the yield deviatoric stress S^y_{ij} is defined by equations 2.39 and 2.40 which is similar to the one-dimensional equation 2.28. The form of the empirical function f(λ) for the three: dimensional model suggested by experiments was $\lambda^{\bar{N}}$ (Youngs, 1982).

$$S_{ij}^{y} = S_{ij}^{f+} + \left(S_{ij}^{f+} - S_{ij}^{f-}\right)\lambda^{\bar{N}} \tag{2.39}$$

$$\bar{N} = N_1 + N_2 \frac{\left\| S_{ij}^{f+} \right\|}{\left\| S_{ij}^{f-} \right\|} \tag{2.40}$$

Where:

S_{ij}^{f+} = failure deviatoric stress in loading direction,

S_{ij}^{f-} = failure deviatoric stress in opposite loading direction,

N_1 and N_2= hardening curve exponents.

The structure change λ in the three- dimensional space is defined as:

$$\lambda = 1 - \frac{\|\lambda_{ij}\|}{2} \tag{2.41}$$

The structure change tensor λ_{ij} as in the one-dimensional case, is defined in terms of the direction of shear strain. The tensor e_{ij}^{s} defines the current structure and $\dot{e}_{ij}$ the current strain rate. The continued shear in the direction of $\dot{e}_{ij}$ produces new structure in the direction $\dot{e}_{ij} / \left\| \dot{e}_{ij} \right\|$:

$$\lambda_{ij} = \frac{\dot{e}_{ij}}{\|\dot{e}_{ij}\|} - e_{ij}^{s} \tag{2.42}$$

where e_{ij}^{s} is the relative structure change:

The rate equation for e_{ij}^{s} in three dimensions which is similar to the one dimension $\dot{e}^{s}$equation 2.30 is given by:

$$\dot{e}_{ij}^{s} = C\left\|\dot{e}_{ij}\right\|(1 - \lambda^{l}) \frac{\lambda_{ij}}{\|\lambda_{ij}\|} \tag{2.43}$$

Where C is the structure modulus.

The structure modulus rate equation using the arguments similar to the one-dimensional model is given by:

$$\dot{C} = C\left\|\dot{e}_{ij}\right\|[(1 - \lambda)D_2 - \lambda D_3] \tag{2.44}$$

Where D_2 and D_3 are relative structure change parameters.

Lee and Albaisa's (1974) experimental results showed that shear straining causes a reduction in the hydrostatic yield stress (σ_m^{max}). They also observed that volumetric strains for reconsolidated sand samples was the same under small shear strains. However, the volumetric strains exceeded the initial consolidation under large shear strains (Ishihara and Okada, 1978). These results imply that reorientation of granular material structure during shear erases the memory of previous overconsolidation. To account for this effect the following equation was proposed by Youngs (1982):

$$\dot{\sigma}_m^{max} = -D_1 P_a (OCR - 1) \left\| \dot{e}_{ij} \right\| \quad (2.45)$$

Where

$\dot{\sigma}_m^{max}$ = maximum mean stress rate,

D_1 = plastic bulk modulus constant,

OCR =overconsolidation ration which is defined as:

$$OCR = \frac{\sigma_m^{max}}{\sigma_m} \quad (2.46)$$

The three- dimensional Youngs' EVP model for grain en loading is described by the deviatoric and hydrostatic strain rate equations 2.36 and 2.37, respectively, the volumetric strain rate (due to shear) equation 2.45, the structure change equation 2.42 and two structure change rate evolution equations 2.43 and 2.45.

Li et al (1990) made the following conclusions. Fifteen material parameters and their relationships for wheat en masse in Youngs' elastic-viscoplastic (EVP) model were determined from monotonic and cyclic triaxial test results. The single set of parameter values was used in the constitutive equations to successfully predict the cyclic load response in triaxial tests. The chi-square (χ^2) statistical test was used to evaluate the EVP model at the 0.05 level of significance. The following conclusions were drawn from this study:

1) Monotonic and cyclic triaxial tests can be used to determine all parameters and their relationships in the Youngs' EVP model.

Table 2.1: Axial stress difference and isotropic stress χ^2 values for wheat en masse*

Confining pressure (kPa)	Monotonic loading		Cyclic loading	
	801kg/m^3	840 kg/m^3	801 kg/m^3	840 kg/m^3
Axial				
20.7	21.65	20.15	25.92	25.64
34.5	20.74	19.97	25.07	24.17
48.3	20.91	18.23	24.81	23.29
62.1	19.26	19.57	24.40	24.60
Isotropic				
0-82.2	25.86	25.47	30.91	31.14

* At 0.05 level of significance and 50 degrees of freedom, χ^2 value is 34.8

Table 2.2: volumetric strain χ^2 values for wheat en masse for cycles*

Confining pressure (kPa)	Monotonic loading		Cyclic loading	
	801kg/m^3	840 kg/m^3	801 kg/m^3	840 kg/m^3
Axial				
20.7	34.09	33.05	37.01	34.49
34.5	32.71	34.28	38.24	33.50
48.3	33.23	31.05	34.82	34.79
62.1	31.78	31.22	38.76	33.26

* At 0.05 level of significance and 50 degrees of freedom, χ^2 value is 34.8

2) The χ^2 test (at the 0.05 level of significance) established the goodness of Youngs' EVP model for predicting monotonic and cyclic stress (deviatoric and isotropic)-strain response of wheat en masse when data for all cycles were pooled in one set.
3) The χ^2 test (at the 0.05 level of significance) established the goodness of Youngs' EVP model for predicting monotonic volumetric strain response for all tests and cyclic volumetric strain response for the high-density test samples (849 kg/m3) when data for all cycles were pooled in one set.
4) At the 0.05 level of significance, the χ^2 test demonstrated that the deviatoric and isotropic responses predicted by the EVP model and the triaxial data were not statistically different for the first two cycles in all tests.
5) At the 0.05 level of significance, the χ^2 test demonstrated that the EVP model predicted and the triaxial volumetric strain values were not statistically different for the first two cycles of loading at initial bulk density of 849 kg/m3.

Table 2.3: Cycle by cycle χ^2 values for isotropic stress for wheat en masse

Cycle	**Isotropic pressure**	**801 kg/m^3**	**849 kg/m^3**
1	0-20.7	27.6	29.3
2	0-41.4	27.1	28.5
3	0-62.1	35.0	36.7
4	0-82.8	36.2	38.2

* At 0.05 level of significance and 50 degrees of freedom, χ^2 value is 34.8

Recent research has significantly advanced our understanding and modeling capabilities of granular materials in silos. Bhure et al. (2024) investigated the flow and clogging behaviour of

particle mixtures in silos, extending earlier models to account for heterogeneous material compositions. Bhateja and Jain (2022) examined self-similar velocity and solid fraction profiles in silos with eccentrically located outlets, providing new insights into the spatial distribution of stresses and strains in these systems.

Bignon et al. (2023) demonstrated the nonlinear effect of grain elongation on flow rate in silo discharge, highlighting the importance of particle shape in constitutive modeling of granular materials. Pongó (2023) further investigated the significance of particle shape, stiffness and friction in silo flows, emphasizing the need to incorporate these parameters into elastoviscoplastic models.

Kumar and Das (2024) employed Discrete Element Modeling to study the discharge of granular matter from silos with eccentric openings, providing a computational counterpart to the constitutive models discussed here. Their work, along with that of Mahboob et al. (2023) on three-dimensional simulation of granular materials considering particle fracture effects, represents the cutting edge of computational approaches to granular material modeling. These studies collectively enhance our understanding of the elastoviscoplastic behaviour of granular materials in silos and provide valuable tools for predicting the complex stress-strain relationships that govern silo design and operation.

2.5. Simplified Constitutive Models

Lateral pressure exerted by granular materials in silos is governed not only by gravitational and frictional effects, but also by the time-dependent and nonlinear behaviour of the bulk solid (Nielsen, 1998). Classical models such as Janssen's equation (Janssen, 1895) as outlined in section 1.2 Computation of Silo Pressures, provide a foundational estimate of lateral pressures assuming purely static and frictional equilibrium. However, they fail to account for material yielding, creep and stress relaxation (Rotter, 1985; Jenike, 1961). To bridge this gap, simplified analytical models based on constitutive theories have been developed. These models aim to capture the essential features of elastoplasticity (Lade, 1977), viscoelasticity (Findley, Lai, and Onaran, 1976), viscoplasticity (Perzyna, 1966) and elastoviscoplasticity (Duvaut et al, 1976), while retaining computational simplicity for engineering analysis and applications.

a) Elastoplastic Model (Simplified Analytical Approximation)

The elastoplastic model is a representation of the idealized elastoplastic constitutive law, which assumes linear elastic behaviour up to a yield stress, beyond which plastic deformation occurs

at a different stiffness or strain rate (Li, Ma, Wang, and Sun, 2020). This concept aligns with classical continuum mechanics formulations like the von Mises or Mohr-Coulomb yield criteria used in soil and granular mechanics (Chen and Saleeb, 1982).

The pressure distribution is modified from the Janssen base pressure by introducing a plastic amplification factorfp, which only activates beyond the material yield stress σ_y. The governing relation is:

$$P_{EP}(Z) = \begin{cases} P_{base}(Z) & if\ P_{base}(Z) \leq \sigma_y \\ P_{base}(Z) + \left(P_{base}(Z) - \sigma_y\right).(fp - 1) & if\ P_{base}(Z) > \sigma_y \end{cases} \quad (2.47)$$

Where:

$P_{EP}(Z)$ = Approximate elastoplastic lateral pressure at depth z

$P_{base}(Z)$ = Base lateral pressure at depth z calculated from Janssen's theory, representing the stress if the material behave purely elastically or had no yield.

σ_y = Yield Pressure

fp = Plastic factor from…

This model assumes elastic behaviour up to a yield point. Beyond σ_y, the extra pressure is transmitted at a reduced rate, simulating a decrease in effective stiffness.

b) Viscoelastic Model (Simplified Analytical Approximation)

The viscoelastic model is based on classical linear viscoelastic theory, most notably the Maxwell model and its extensions (Christensen, 1982). In this framework, a granular medium is treated as a combination of an elastic spring and a viscous dashpot in series, allowing for time-dependent stress relaxation under constant strain. Applied to silo storage, this means that lateral pressures gradually reduce over time even if the fill height remains constant (Chen et al, 2020). The Janssen equation was modified to incorporate the viscoelastic model as per equation 2.48

The lateral pressure at depth z after storage time $t_{storage}$ is given by:

$$P_{VE}\left(Z, t_{storage}\right) = P_{base}(Z).\, e^{-\frac{t_{storage}}{t_{relax}}} \quad (2.48)$$

Where:

$P_{VE}\left(Z, t_{storage}\right)$ = Viscoelastic lateral pressure at depth z after storage time ($t_{storage}$)

$P_{base}(z)$ = Base lateral pressure from Janssen's formula

$t_{storage}$ = Storage duration

t_{relax} = Characteristic relaxation time

This formula assumes exponential decay of pressure over time, representing stress relaxation in a simple viscoelastic material. It does not account for complex loading histories or multiple relaxation mechanisms.

c) Viscoplastic Model (Simplified Analytical Approximation)

This model extends the elastoplastic formulation by introducing time-dependent stress relaxation, which only activates when the initial pressure exceeds a defined yield stress. It draws upon concepts from Bingham plasticity and Perzyna's overstress theory (Perzyna, 1966), describing how materials undergo delayed flow or "creep" when subjected to overstress. The pressure response as modified from the Janssen equation is defined as:

$$P_{VP}(z, t_{storage}) = \begin{cases} P_{EP}(Z) & if\ P_{base}(Z) \leq \sigma_y \\ \sigma_y + (P_{EP}(Z) - \sigma_y).(e^{-\frac{t_{storage}}{t_{vpchar}}}) & if\ P_{base}(Z) > \sigma_y \end{cases}$$ (**Error! No text of specified style in document.**2.49)

Where:

$P_{VP}(z, t_{storage})$ = Viscoplastic lateral pressure at depth z after time $t_{storage}$

$P_{EP}(Z)$ = Approximate elastoplastic lateral pressure at depth z

σ_y = Yield stress

t_{vpchar} = Viscoplastic characteristic time

In this formulation, if the initial pressure is below the yield stress, no further reduction occurs and the pressure remains elastoplastic. If it exceeds the yield stress, the excess stress decays exponentially over time, simulating long-term flow or structural rebalancing of the bulk solid.

d) Elastoviscoplastic Model (Simplified Analytical Approximation)

The elastoviscoplastic (EVP) model synthesizes the preceding three behaviours into a unified expression, providing a more comprehensive approximation of lateral pressure evolution in granular materials under prolonged storage. It combines the elastic/viscous stress decay of the Maxwell model, the yield threshold of elastoplasticity and the long-term flow dynamics of viscoplasticity. The Janssen equation was modified to incorporate the elastoviscoplastic model as per Equation (2.50:

$$P_{EVP}(z, t_{storage}) =$$

$$\begin{cases} P_{base}(Z).\, e^{-\frac{t_{storage}}{t_{relax}}} & if\ P_{base}(Z) \leq \sigma_y \\ [\sigma_y + (P_{base}(Z) - \sigma_y).\,(fp - 1)].\,(e^{-\frac{t_{storage}}{t_{vpchar}}}) & if\ P_{base}(Z) > \sigma_y \end{cases} \quad (2.501)$$

Where:

$P_{EVP}(z, t_{storage})$ = Elastoviscoplastic lateral pressure at depth z after time t_storage

$P_{base}(Z)$ = Base lateral pressure (Janssen's Theory)

σ_y = Yield stress

fp = Plastic factor (>1)

t_{relax} = Relaxation time

$t_{vp_{char}}$ = Viscoplastic characteristic time

This model is drawn from generalized Kelvin-Voigt–Bingham models that have been adapted to granular rheology (Schwedes, 2003). It accounts for both early-time pressure relaxation (dominant below yield) and long-term creep and strain-hardening effects (dominant above yield).

Limitations of the Simplified Constitutive Models

These simplified constitutive models present several limitations. They idealize material behaviour, assuming abrupt yield thresholds and exponential stress relaxation, which may not fully capture the complex, nonlinear response of granular materials under dynamic loading or non-uniform filling conditions (Nedderman, 1992; Walker, 1966). They neglect localized phenomena such as arching, rat-holing or segregation, which are prevalent in real-world silos (Jenike, 1964). They also presume a homogeneous and isotropic material structure, whereas actual granular media often exhibit anisotropic behaviour, stress-path dependency and non-associative flow rules—features more accurately captured through finite element (FEM) or discrete element methods (DEM) (O'Sullivan, 2011; Tejchman and Gudehus, 2001).

Despite these shortcomings, the theoretical foundations of these simplified models are sound, drawing from established yield criteria and time-dependent material models. Their mathematical simplicity allows for straightforward calculation of pressure profiles, making them practical for preliminary silo design. Their depth-dependent formulations facilitate quantitative comparisons with classical models, providing an empirical basis for assessing whether incorporating constitutive behaviour improves pressure predictions.

3. Computational Approach for Lateral Pressures in Silos

The computation of lateral pressures was conducted using both classical and constitutive modeling approaches, based on the specific material properties of wheat en masse and the geometric characteristics of the silo. The deterministic computations, based on established classical and constitutive pressure models, were conducted using standardized inputs to ensure a consistent basis for comparison.

Pressure distribution was evaluated along the full silo depth range (0–20 m) and results from each model were extracted for comparative analysis. The material parameters and silo dimensions used in the analysis form the basis for quantitative evaluation and were selected based on standard values for wheat in bulk (Nedderman, 1992; Eurocode 1: Part 4, 2006; Peleg, 1985). These standardized parameters are critical for ensuring consistency and relevance in pressure predictions across different modeling techniques. Table 3.1 summarizes the material and structural properties employed in the computational models.

Table 3.1: Material and Silo Properties

Parameter Name	**Value**	**Unit**
Unit Weight (γ)	7.5	kN/m^3
Angle of Internal Friction, (ϕ)	30	Degree
Cohesion, C	0	kPa
Coefficient of lateral earth pressure (k)	0.333	-
Wall friction angle (δ)	20	Degree
Wall friction coefficient (μ)	0.35	-
Elastic Modulus (E)	15	MPa
Poisson's ratio (ν)	0.3	-
Yield Stress, (σ_y)	15	kPa
Plastic Factor, f_p	1.3	-
Storage Time (Days)	30	Days
Viscoelastic Relaxation Time (Days)	90	Days
Viscoplastic Characteristic Time (Days)	60	Days
Height, H	20	M
Diameter, D	6	M
Hydraulic Radius, R	1.5	M
Cross sectional area, a	28.27	m^2
Maximum Lateral Pressure, P_{max}	32.14	kPa
Characteristic Length, C	6.19	M

3.1. Classical Theories for Lateral Pressure Computations

The lateral pressure at various depths within a 20 m silo was computed using four classical theoretical models: Janssen, Reimbert, Rankine and Airy. Deterministic calculations were conducted in Excel using predefined material and geometric properties as shown in Table 3.1.

Table 3.2 presents a summary of the lateral pressure values computed using Equations 1.1, 1.2, 1.3 and 1.4, which correspond to the Janssen, Reimbert, Rankine and Airy theoretical models, respectively. These classical theories are elaborated upon in Section 1.0 (Introduction), under Subsection 2.1 Computation of Silo Pressures. The calculations summarized in the table were performed at a representative silo depth of z = 18 meters.

Table 3.2: Summary of Lateral Pressure Calculations at z = 18 m Using Classical Theoretical Models

Name	**Equation**	**Calculations**	**Pressure (kPa)**
Janssen Model	$P_z = \frac{\gamma D}{4\mu}\left(1 - e^{-\frac{4\mu kz}{D}}\right)$	$P_z = \frac{\gamma D}{4\mu}\left(1 - e^{-\frac{4\mu kz}{D}}\right) = (\frac{7.5 \times 6}{4 \times 0.35} \cdot \left(1 - e^{\frac{-4 \times 0.35 \times 0.333 \times 18}{6}}\right))$	24.217
Reimbert Formula	$p = p_{\max}\left[1 - \left(\frac{Y}{C} + 1\right)^{-2}\right]$ Where $p_{\max} = \frac{\gamma R_h}{\mu_1}$ and $C = \frac{D}{4\mu_1 k_0} - \frac{h}{3}$	$p_{\max} = \frac{7.5 \times 1.5}{0.35} = 32.14$, $C = \frac{6}{4 \times 0.35 \times 0.333} - \frac{20}{3} = 6.2$m; $p = 32.14\left[1 - \left(\frac{18}{6.2} + 1\right)^{-2}\right]$	32.038
Rankine	$P_a = \gamma z \tan^2\left(45° - \frac{\phi}{2}\right) = \gamma z K_a$	$P_a = 7.5 \times 18 \tan^2\left(45° - \frac{30}{2}\right) = 7.5 \times 18 \times 0.33\dot{3}$	45
Airy's Theory	$P = \frac{\gamma D}{\mu + \mu'}\left[1 - \sqrt{\frac{1 - \mu^2}{\left(\frac{2\gamma Y}{D}(\mu + \mu') + 1 - \mu\mu'\right)}}\right]$	$P = \frac{7.5 \times 6}{0.577 + 0.35}\left[1 - \sqrt{\frac{1 - 0.577^2}{\left(\frac{2 \times 7.5 \times 18}{6}(0.577 + 0.35) + 1 - 0.577 \times 0.35\right)}}\right]$	43.351

Note: The terms are defined in section 1.2 computation of silo pressures

Using the governing equations outlined in Table 3.2, lateral pressures were computed at selected depths of 0 m, 5 m, 10 m, 15 m, 18 m and 20 m for each of the four classical theoretical models—Janssen, Rankine, Reimbert and Airy. Table 3.3 presents the computed results at these key depths, providing a comparative snapshot of the pressure distribution across models. A complete dataset covering all depths from 0 to 20 m is provided in Appendix I: Raw Data.

Table 3.3: Computed Lateral Pressures at Selected Depths (0–20 m) Using Classical Theoretical Models

Depth (m)	Janssen (kPa)	Rankine (kPa)	Reimbert (kPa)	Airy (kPa)
0	0.00	0.00	0.00	4.17
5	10.356	12.5	22.306	38.87
10	17.376	25	27.444	41.6201
15	22.133	37.5	29.399	42.864
18	24.217	45	30.038	43.351
20	25.358	50	30.347	43.612

At 0 m, all models except Airy predict zero pressure. Airy uniquely starts at 4.17 kPa, due to its failure wedge assumption. By 5 m, Janssen gives 10.36 kPa, Rankine 12.5 kPa, Reimbert 22.31 kPa and Airy sharply rises to 38.87 kPa.

At 10 m, Janssen predicts 17.38 kPa, Rankine 25 kPa, Reimbert 27.44 kPa and Airy levels near 41.62 kPa. The divergence continues at 15 m, with Janssen at 22.13 kPa, Rankine 37.5 kPa, Reimbert 29.40 kPa and Airy nearing its plateau at 42.86 kPa.

By 18 m, Janssen yields 24.22 kPa, Rankine 45 kPa, Reimbert 30.04 kPa and Airy reaches 43.35 kPa. At 20 m, Janssen levels off at 25.36 kPa, Rankine peaks at 50 kPa, Reimbert at 30.35 kPa and Airy stabilizes at 43.61 kPa.

The Janssen model shows a saturation trend due to wall friction effects, while Rankine's linear growth reflects active earth pressure without such considerations. Reimbert offers a moderated, nonlinear profile, capturing some practical behaviours. Airy predicts the highest pressures at shallow depths, stabilizing early. Figure 3.1 illustrates the variation in lateral pressure with depth, based on values computed at 0, 5, 10, 15, 18 and 20 meters for each model.

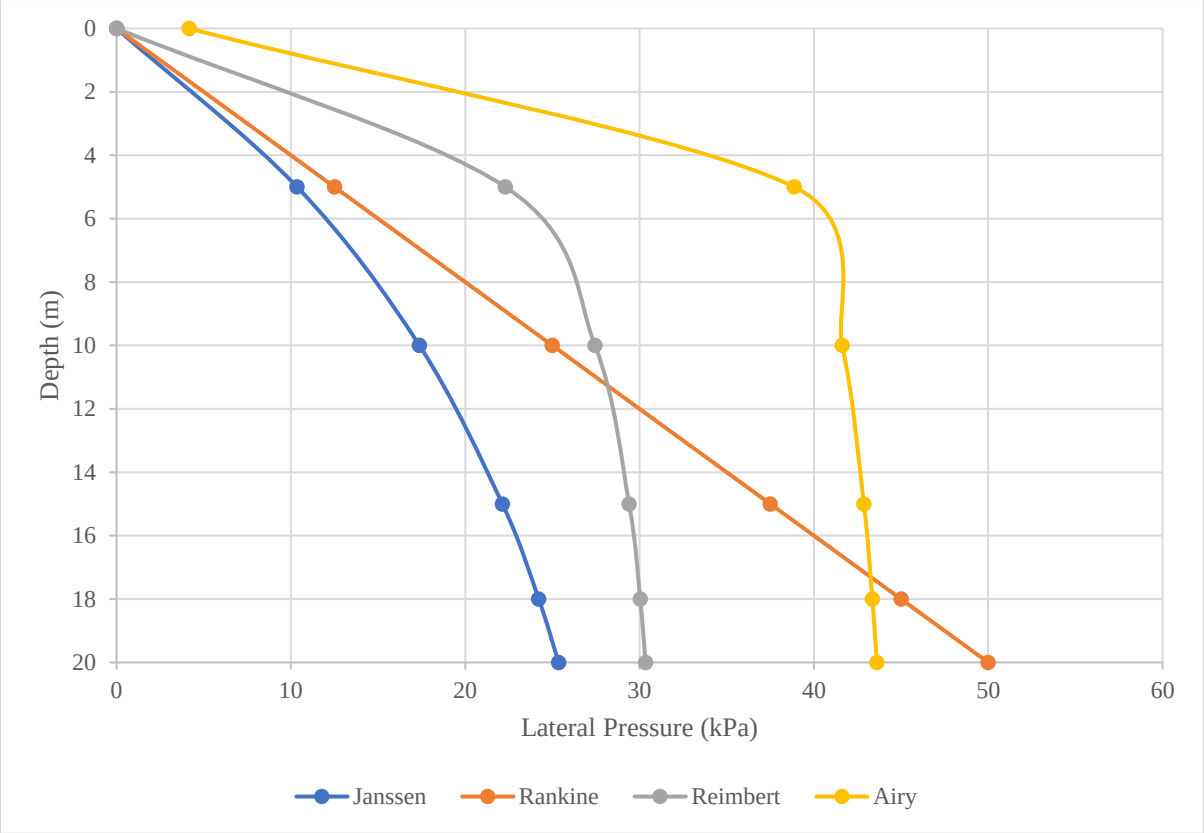

Figure 3.1: Lateral pressure distribution in a silo (0-20m) using classical theories

3.2. Constitutive Models for Lateral Pressure Computations

The simplified analytical models in section 2.5 were used to compute lateral pressure at various depths within a 20 m silo. The material and geometric properties as shown in Table 3.1 were used as parameters to conduct the computations in Excel.

Table 3.4 presents a summary of the lateral pressure values computed using Equations 2.47, 2.48, 2.49 and 2.50, which correspond to the Elastoplastic, Viscoelastic, Viscoplastic and Elastoviscoplastic constitutive models, respectively. The calculations summarized in the table were performed at a representative silo depth of z = 18 meters.

Table 3.4: Summary of Lateral Pressure Calculations at z = 18 m Using Simplified Constitutive Models

Model	**Simplified Constitutive Model**	**Calculations**	**Pressure at z=18**
Elastoplastic	$P_{EP}(Z) = \begin{cases} P_{base}(Z) & if\ P_{base}(Z) \leq \sigma_y \\ P_{base}(Z) + (P_{base}(Z) - \sigma_y).(fp-1) & if\ P_{base}(Z) > \sigma_y \end{cases}$	At z =18, $P_{base}(Z) > \sigma_y$ $P_{EP}(Z) = 24.217 + (24.217 - 15).(1.3 - 1)$	26.98
Viscoelastic	$P_{VE}(Z, t_{storage}) = P_{base}(Z).e^{-\frac{t_{storage}}{t_{relax}}}$	At z =18, $P_{base}(Z) > \sigma_y$ $P_{VE} = 24.217 \times e^{-\frac{30}{90}}$	17.352
Viscoplastic	$P_{VP}(z, t_{storage}) = \begin{cases} P_{EP}(Z) & if\ P_{base}(Z) \leq \sigma_y \\ \sigma_y + (P_{EP}(Z) - \sigma_y).(e^{-\frac{t_{storage}}{t_{vpchar}}}) & if\ P_{base}(Z) > \sigma_y \end{cases}$	At z =18, $P_{base}(Z) > \sigma_y$ $P_{VP}(z, t_{storage}) = 15 + (26.98 - 15).(e^{-\frac{30}{60}})$	22.268
Elastoviscoplastic	$P_{EVP}(z, t_{storage}) = \begin{cases} P_{base}(Z).e^{-\frac{t_{storage}}{t_{relax}}} & if\ P_{base}(Z) \leq \sigma_y \\ [\sigma_y + (P_{base}(Z) - \sigma_y).(fp-1)].(e^{-\frac{t_{storage}}{t_{vpchar}}}) & if\ P_{base}(Z) > \sigma_y \end{cases}$	At z =18, $P_{base}(Z) > \sigma_y$ $P_{EVP}(z, t_{storage}) = [15 + (24.217 - 15).(1.3 - 1)].(e^{-\frac{30}{60}})$	10.78

Note: The terms are defined in section 2.5 Simplified Constitutive Model for Lateral Pressure Computations

Using the equations outlined in Table 3.4, lateral pressures were computed at selected depths of 0 m, 5 m, 10 m, 15 m, 18 m and 20 m for each of the Constitutive Models— Elastoplastic, Viscoelastic, Viscoplastic and Elastoviscoplastic. Table 3.5 presents the computed results at these key depths, providing a comparison of the pressure distribution across the constitutive models.

Table 3.5: Computed Lateral Pressures at Selected Depths (0–20 m) Using Simplified Constitutive Models

Depth (m)	**Elastoplastic (kPa)**	**Viscoelastic (kPa)**	**Viscoplastic (kPa)**	**Elastoviscoplastic (kPa)**
0	0.00	0.00	0.00	0.00
5	10.356	7.42	10.356	7.42
10	18.089	12.45	16.8734519	9.53
15	24.273	15.859	20.624	10.396
18	26.982	17.352	22.267	10.775
20	28.465	18.17	23.167	10.983

At 0 m, all the constitutive models predict zero lateral pressure, aligning with physical expectations. By 5 m, both the elastoplastic and viscoplastic models estimate a pressure of 10.36 kPa, while viscoelastic and elastoviscoplastic models yield lower values of 7.42 kPa, indicating early differences due to delayed deformation effects.

At 10 m, the elastoplastic model continues to lead with 18.09 kPa, followed by viscoplastic at 16.87 kPa, viscoelastic at 12.45 kPa and elastoviscoplastic at 9.53 kPa. This trend persists at 15 m, where elastoplastic reaches 24.27 kPa, viscoplastic 20.62 kPa, viscoelastic 15.86 kPa and elastoviscoplastic only 10.40 kPa.

At 18 m and 20 m, the elastoplastic model peaks at 28.47 kPa, with viscoplastic close behind at 23.17 kPa. The viscoelastic and elastoviscoplastic models level off at 18.17 kPa and 10.98 kPa, respectively. The elastoviscoplastic model consistently produces the lowest pressures across all depths, likely due to combined effects of elastic recovery, time-dependent strain and stress relaxation.

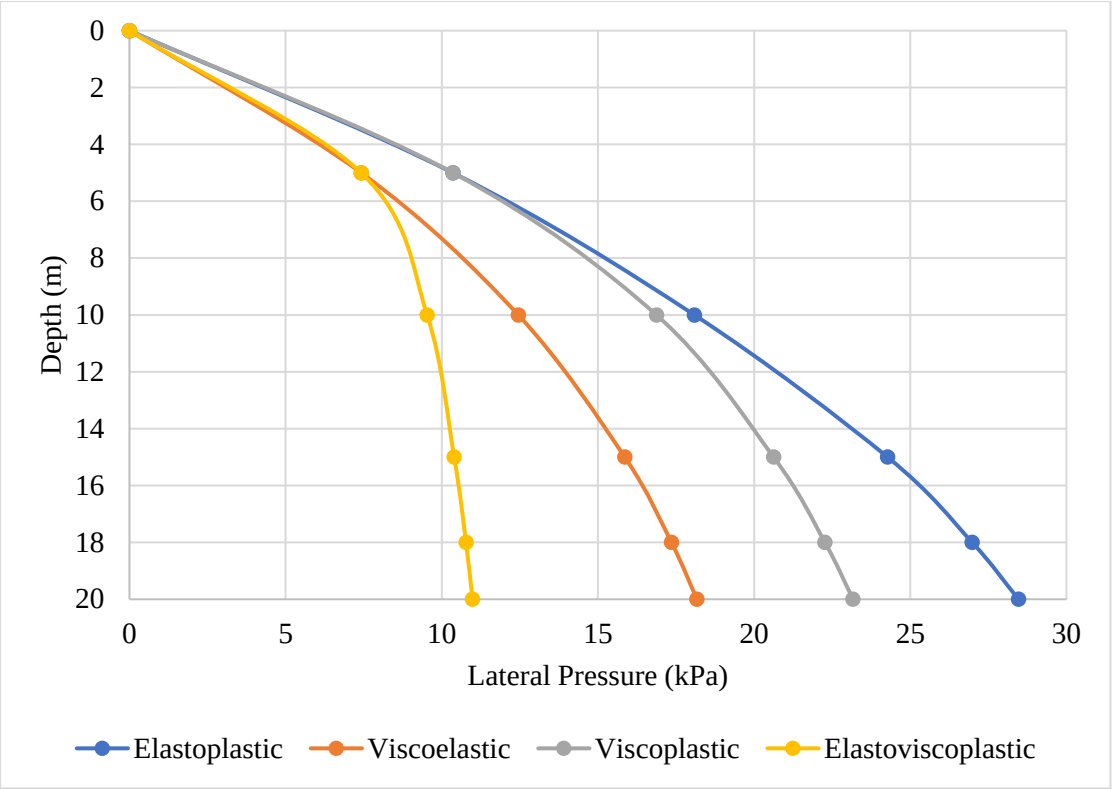

Figure 3.2: Lateral pressure distribution in a silo (0-20m) using constitutive models

Figure 3.3 has the trends computed using Janssens, Airy, Rankine, Reimbert and constitutive models modified from the Janssen equation to incorporate elastoplastic, viscoelastic, viscoplastic and elastoviscoplastic material behaviour.

A key distinction observed is the behaviour at greater depths: models such as Janssen, elastoplastic, viscoelastic, viscoplastic and elastoviscoplastic exhibit a progressive increase where pressure increases initially but then approaches an asymptotic or limiting, value. This characteristic is typical for deep silos where the arching effect and wall friction significantly influence pressure distribution, preventing indefinite pressure increase with depth. Among these, elastoviscoplastic consistently predicts the lowest lateral pressures, while Elastoplastic predicts some of the highest.

In contrast, the Rankine model stands out with a nearly linear increase in lateral pressure across the entire depth range, predicting the highest pressures, especially at greater depths. The results of the computations indicated that the highest lateral pressure was predicted by the Rankine model, reaching 50 kPa at the base, followed by Airy's model at 43.61 kPa. The Janssen model produced moderate pressure values throughout the depth, reaching 25.36 kPa at the base, while the Elastoviscoplastic model consistently yielded the lowest and most uniform pressures, with a final value of 10.98 kPa.

The varying profiles highlight the fundamental differences in assumptions behind each model, ranging from highly conservative (Rankine) to more consistent and lower-pressure predictions (Elastoviscoplastic), providing crucial insights for engineers in selecting an appropriate model based on design requirements and material properties. The resultant Figure 3.3 illustrates these distribution of pressures for a silo of 20m depth.

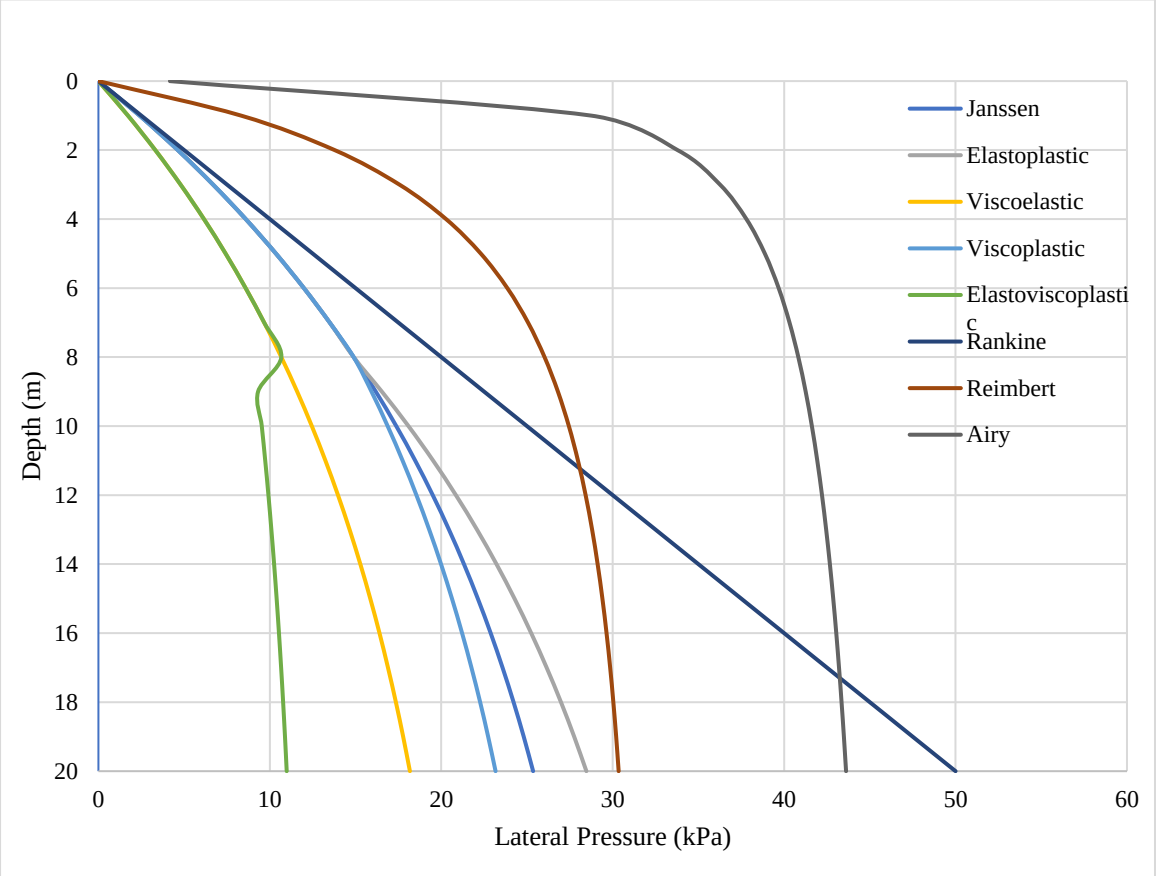

Figure 3.3: Lateral Pressure Distribution in a silo of depth 20m

Levene's statistical test was conducted to assess the equality of variances across all the models used. A P-value of 4.269e-7 led to the conclusion that the variances across the models are significantly different, See Table 3.6.

Table 3.6: Levene's test results, using F distribution df(7,160) (right tailed)

Source	DF	Sum of Square	Mean Square	F Statistics	P-value
Groups	7	1545.456	220.7794	6.8231	4.296e-7
Error	160	5177.2547	32.3578		
Total	167	6722.7107	40.2558		

F-Test was also done to compare the variability of lateral pressure predictions of these computational models against the Janssen model as the reference baseline. The objective was to determine whether the differences in the spread of results (variance) between models were

statistically significant. Table 3.7 presents the comparative outcomes of the test across classical and constitutive models.

Table 3.7: F-Test Results

	Janssen	*Reimbert*	*Airy*	*Rankine*
Mean	15.68261905	24.05871997	38.67404	25
Variance	60.42675655	65.2218021	76.16706	240.625
Observations	21	21	21	21
Df	20	20	20	20
F		1.079353019	1.260486	3.982094
P(F<=f) one-tail		0.433051804	0.304797	0.001625
F Critical one-tail		2.124155213	2.124155	2.124155
P(F<=f) Two-tail		0.866103609	0.609593	0.003251

Elastoplastic	*Viscoelastic*	*Viscoplastic*	*Elastoviscoplastic*
16.7724619	11.237	14.91424299	8.352142857
77.76989877	31.0243543	49.85990699	10.56378113
21	21	21	21
20	20	20	20
1.287010974	1.94772004	1.211930791	5.720182557
0.2889423	0.07227496	0.335729478	0.000133967
2.124155213	2.12415521	2.124155213	2.124155213
0.577884599	0.14454993	0.671458955	0.000267934

The analysis revealed that most models including Reimbert, Airy, Elastoplastic, Viscoelastic and Viscoplastic had variances that were not significantly different from Janssen's, as indicated by their high P-values (greater than 0.05). This suggests that these models exhibit similar levels of prediction consistency. However, the Rankine model displayed a significantly higher variance (P = 0.003), pointing to less stable pressure estimates. In contrast, the Elastoviscoplastic model recorded a markedly lower variance (P = 0.0002), highlighting its superior consistency in pressure prediction.

4. Conclusions

This paper has reviewed the rheology of en masse grains in the context of silo load computations, focusing on both classical and constitutive computational methods used to estimate pressure loads. The classical theories examined include Janssen’s model, Reimbert’s method, Rankine’s theory and Airy’s approach all of which provide foundational frameworks for understanding vertical and lateral pressures in silos. Elastoplastic, viscoelastic, viscoplastic and elastoviscoplastic constitutive models were developed to account for the complex behaviour of granular materials, offering enhanced predictive capabilities by incorporating material-specific mechanical responses.

To evaluate these models, pressure computations were carried out on a cylindrical silo 20 m in height and 6 m in diameter, filled with wheat in bulk. The analysis incorporated standardized parameters including unit weight (7.5 kN/m³), internal friction angle (30°), cohesion (0 kPa), lateral earth pressure coefficient (0.333), wall friction angle (20°), elastic modulus (15 MPa), Poisson's ratio (0.3), yield stress (15 kPa) and viscoplastic and viscoelastic time constants (60 and 90 days, respectively). The complete set of material and silo properties used is detailed in Table 3.1.

The results of the computations indicated that the highest lateral pressure was predicted by the Rankine model, reaching 50 kPa at the base, followed by Airy's model at 43.61 kPa. The Janssen model produced moderate pressure values throughout the depth, reaching 25.36 kPa at the base, while the Janssens model incorporating elastoviscoplasticity consistently yielded the lowest and most uniform pressures, with a final value of 10.98 kPa; The Janssen's equation incorporating viscoplastic, viscoelastic, elastoplastic, and elastoviscoplastic models were used to compute silo pressures. The results indicated that the elastoviscoplastic model consistently yielded the lowest and most uniform pressures, with a final value of 10.98 kPa; viscoelastic was second lowest, reaching 18.17 kPa; viscoplastic followed with 23.17 kPa, while elastoplastic yielded the highest pressure among the constitutive models at 28.47 kPa.

Statistical analysis using Levene's test revealed a significant difference in the variance of pressure predictions across all models F value of 6.8231, P value of 4.296e-7 and df value of 7,160, indicating that the consistency of prediction varies significantly by model type. Follow-up F-Tests comparing individual models against the Janssen baseline showed that Rankine's model exhibited significantly higher variability (P = 0.003), suggesting less consistent performance. In contrast, the Elastoviscoplastic model demonstrated significantly lower variability (P = 0.0002), indicating more consistent and reliable predictions. These findings underscore the need to incorporate material behaviour in silo pressure computations.

References

Aklonis, J. J and **MacKnight, W. J.** (1983). *Introduction to polymer viscoelasticity* (2nd ed.). John Wiley and Sons.

ASABE. (2011). *Design loads for grain bins (ANSI/ASAE EP433 R2011)*. American Society of Agricultural and Biological Engineers.

Balevičiu, R, Sielamowicz, I, Mróz, Z and Kačianauskas, R. (2011). Investigation of wall stress and outflow in a flat-bottomed bin: A comparison of the DEM model results with the experimental measurements. *Powder Technology*, 214, 322–336. https://doi.org/10.1016/j.powtec.2011.08.042

Bbanerje. (2007). *Viscoplastic elements used in one-dimensional models of viscoplastic materials* \[Figure]. Wikimedia Commons. https://commons.wikimedia.org/w/index.php?curid=10371585

Bhateja, A and Jain, S. (2022). Self-similar velocity and solid fraction profiles in silos with eccentrically located outlets. *Physics of Fluids*, 34(4), 043306. https://doi.org/10.1063/5.0083421

Bhure, S. C, Doshi, P and Orpe, A. V. (2024). Flow and clogging behaviour of a mixture of particles in a silo. *Physics of Fluids*, 36(5), 053326. https://doi.org/10.1063/5.0205141

Bignon, A, Renouf, M, Sicard, R and Azéma, E. (2023). Nonlinear effect of grain elongation on the flow rate in silo discharge. *Physical Review E*, 108(5), 054901. https://doi.org/10.1103/PhysRevE.108.054901

Briassou, D and Curtis, J. (1985). Design and analysis of silos for friction forces. *Journal of Structural Engineering*, 111(6), 1377-1398.

CEN. (2006). *Eurocode 1: Actions on structures – Part 4: Silos and tanks (EN 1991-4)*. European Committee for Standardization.

Chattopadhyay, A, Rao, R. K, and **Parameswaran, M. A.** (1994). On the classification of bulk solids. *Bulk Solids Handling*, 14, 339-344.

Chen, F and Yan, H. (2021). Elastic–viscoplastic constitutive theory of dense granular flow and its three-dimensional numerical realization. *Physics of Fluids*, 33(12), 123310. https://doi.org/10.1063/5.0068458

Chen, W. F and Saleeb, A. F. (1982). *Constitutive equations for engineering materials: Vol. 1. Elasticity and modeling*. Wiley.

Chen, W. R and Baladi, G. Y. (1985). *Soil plasticity*. Elsevier.

Chen, Y, Liang, C, Wang, X, Guo, X, Chen, X and Liu, D. (2020). Static pressure distribution characteristics of powders stored in silos. *Chemical Engineering Research and Design, 154*, 1–10.

Chi, L and Kushwaha, R. L. (1990). Lade's elastoplastic model for granular soils [Paper presentation]. American Society of Agricultural Engineers, Paper No. 90-1084.

Chung, T. J. (1988). *Continuum mechanics*. Prentice-Hall International.

Craig, R. F. (2004). Craig's soil mechanics (7th ed.). London: Spon Press.

Cundall, P. A and Strack, O. D. (1979). A discrete element model for granular assemblies. *Géotechnique*, 29, 47–65.

Dartevelle, S. (2003). *Numerical and granulometric approaches to geophysical granular flows* [Doctoral dissertation]. Michigan Technological University, Department of Geological and Mining Engineering.

Duan, J, Han, Y and Li, D. (2023). The dynamic behaviour of silos with grain-like material during earthquakes. *Sustainability*, 15(10), 7970. https://doi.org/10.3390/su15107970

Dunatunga, S and Kamrin, K. (2022). Modelling silo clogging with non-local granular rheology. *Journal of Fluid Mechanics*, 940, A14. https://doi.org/10.1017/jfm.2022.241

Dyck, G, Rogers, A, & Paliwal, J. (2024). A Review of Analytical Methods for Calculating Static Pressures in Bulk Solids Storage Structures. KONA Powder and Particle Journal, 41(0), 108–122. https://doi.org/10.14356/kona.2024013

Eurocode 1 (2003). Actions on structures. Part 4: Actions in silos and tanks. Ref. No. EN 1991-4.

European Committee for Standardization. (2006). *Eurocode 1: Actions on structures – Part 4: Silos and tanks (EN 1991-4)*. Brussels, Belgium: CEN.

Fall, A, Badetti, M, Ovarlez, G, Chevoir, F and Roux, J.-N. (2017). Dry granular flows – rheological measurements of the μ(I) – Rheology. *EPJ Web of Conferences*, 140, 03005. https://doi.org/10.1051/epjconf/201714003005

Findley, W. N, Lai, J. S and Onaran, K. (1976). *Creep and relaxation of non-linear viscoelastic materials* (Vol. 18). North-Holland Publishing Co.

Fullard, L. A, Breard, E. C. P, Davies, C. E, Godfrey, A. J. R, Fukuoka, M, Wade, A, Dufek, J and Lube, G. (2019). The dynamics of granular flow from a silo with two symmetric openings. *Proceedings of the Royal Society A: Mathematical, Physical and Engineering Sciences*, 475(2221), 20180462. https://doi.org/10.1098/rspa.2018.0462

Fullard, L, Breard, E, Davies, C, Lagrée, P.-Y, Popinet, S, and **Lube, G.** (2017). Testing

the μ(I) granular rheology against experimental silo data. *EPJ Web of Conferences*, 140, 11002. https://doi.org/10.1051/epjconf/201714011002

Gandia, R. M, Gomes, F. C, Paula, W. C. de, **Oliveira Junior, E. A. de** and **Aguado Rodriguez, P. J.** (2021). Static and dynamic pressure measurements of maize grain in silos under different conditions. *Biosystems Engineering*, 209, 180–199. https://doi.org/10.1016/j.biosystemseng.2021.07.001

González-Montellano, C, Gallego, E, Ramírez-Gómez, Á, and **Ayuga, F.** (2012). Three dimensional discrete element models for simulating the filling and emptying of silos: Analysis of numerical results. *Computers and Chemical Engineering*, 40, 22–32. https://doi.org/10.1016/j.compchemeng.2012.02.007

Golshan, S, Zarghami, R and Saleh, K. (2019). Modeling methods for gravity flow of granular solids in silos. *Reviews in Chemical Engineering*, 1(4), 449–479. https://doi.org/10.1515/revce-2019-0003

Gumbe, L. O and Maina, B. M. (1990a). Elastoplastic constitutive parameters for rice en-masse. *African Journal of Science and Technology, Series A*, 8(2), 15-25.

Gumbe, L. O. (1990b). Material characterisation and prediction equations for loads in silos containing granular materials en-masse. *African Journal of Science and Technology, Series A*, 8(1), 1-5.

Gumbe, L. O. (1993). A discussion on constitutive equation for granular materials en-masse. *East African Journal of Engineering*, 1(1), 27–38.

Gumbe, L. O. (1995). *Load deformation behaviour of soils and en-masse grains*. Proceedings of Symposium on Unsaturated Soil Behaviour and Applications, Nairobi, Kenya.

Harri, D. (2009). An elastoplastic model for deformation and flow of granular materials and its connection with micro mechanical quantities. In *Powders and Grains 2002: Proceedings of the 6th international conference on micromechanics of granular media* (Vol. 1145, pp. 1085-1088). https://doi.org/10.1063/1.3179833

Heinrich, M. J, Sidney, R. N and Robert, P. B. (1996). The physics of granular materials. *Physics Today*, 32-39.

Herum, F. L, et al. (1979). Viscoelastic behaviour of soybeans due to temperature and moisture content. *Transactions of ASAE*, 22(5), 1220-1224.

Horabik, J and Molenda, M. (2014). Mechanical properties of granular materials and their impact on load distribution in silo: A review. *Scientia Agriculturae Bohemica*, 45(4), 203–211.

ISO 3535 (1977). Continuous mechanical handling equipment – Classification and

symbolization of bulk materials. *International Agrophysics*, 14, 385-392.

Ishihara, K and Okada, S. (1978). Effects of stress history on cyclic behaviour of sand. *Soils and Foundation*, 18(4), 31-45.

Janssen, H. A. (1895). Experiments on grain pressure in silos. *Verein Deutscher Ingenieure, Zetschrift (Düsseldorf)*, 39, 1045–1049.

Jenike, A. W. (1961). Gravity flow of bulk solids. *Bulletin of the University of Utah*, 52, 1-309.

Jiang, M, Barreto, D, Ding, Z and Yang, K. (2025). Discrete element study of particle size distribution-shape governing critical state behaviour of granular material. *Fractal and Fractional*, 9(1), 26. https://doi.org/10.3390/fractalfract9010026

Kamrin, K. (2020). Quantitative rheological model for granular materials: The importance of particle size. In W andreoni and S. Yip (Eds.), *Handbook of materials modeling: Applications: Current and emerging materials* (pp. 153–176). Springer International Publishing. https://doi.org/10.1007/978-3-319-44680-6_148

Kobyłka, R and Molenda, M. (2014). DEM simulations of loads on obstruction attached to the wall of a model grain silo and of flow disturbance around the obstruction. *Powder Technology*, 256, 210–216. https://doi.org/10.1016/j.powtec.2014.02.030

Kobyłka, R and Molenda, M. (2013). DEM modelling of silo load asymmetry due to eccentric filling and discharge. *Powder Technology*, 233, 65–71. https://doi.org/10.1016/j.powtec.2012.08.039

Kou, H. P, Knight, P. C, Parker, D. J, Tsuji, Y, Adams, M. J, and **Seville, J. P. K.** (2002). The influence of DEM simulation parameters on the particle behaviour in a V-mixer. *Chemical Engineering Science*, 57, 3621–3638.

Kumar, A and Das, P. K. (2024). Discrete element modeling of discharge of granular matter from a silo at different eccentric opening. In K. M. Singh, S. Dutta, S. Subudhi, and N. K. Singh (Eds.), *Fluid mechanics and fluid power* (Vol. 6, pp. 609–623). Springer Nature. https://doi.org/10.1007/978-981-99-5755-2_57

Lade, P. V. (1977). Elasto-plastic stress-strain theory for cohesionless soil with curved yield surface. *International Journal of Solids and Structure*, 13, 1019-1035.

Lade, P. V. (1972). *The stress-strain and strength characteristics of cohesionless soils* [Doctoral dissertation]. University of California, Berkeley.

Lade, P. V and Duncan, J. M. (1971). Stress-path dependent behaviour of cohesionless soil. *ASCE Journal of Geotechnical Engineering Division*, 102(GT1), 51-68.

Lee, K. L and Albaisa, F. (1974). Earthquake induced settlements in saturated sands. *ASCE Journal of Geotechnical Engineering Division*, 100(GT4), 387-406.

Li, Y, Zhang, Q, Puri, V. M and Manbeck, H. B. (1989). Elasto-plastic constitutive equation parameters and load response of wheat en-masse-part-I, initial density, moisture content and strain rate effects. *Transactions of ASAE*, 32(1), 194-202.

Li, N. L, Ma, B, Wang, H and Sun, W. (2020). Development of elasto-plastic constitutive model for unbound granular materials under repeated loads. *Transportation Geotechnics, 23*, 100347.

Liu, Z, Wang, J and Chen, L. (2018). Structural design of grain silos in China: Approaches and challenges. *Journal of Structural Engineering, 144*(9), 04018147.

Lin, C.-C and Yang, F.-L. (2021). Continuum simulation of non-local effects in a granular silo discharge flow using a regularized μ(I) rheology model. *Physics of Fluids*, 33(9), 093309. https://doi.org/10.1063/5.0057598

Luo, Q, Zheng, Q and Yu, A. (2019). Quantitative comparison of hydrodynamic and elastoplastic approaches for modeling granular flow in silo. *AIChE Journal*, 65(5), e16533. https://doi.org/10.1002/aic.16533

Mahboob, A, Hassanshahi, O and Tabrizi, A. S. (2023). Three-dimensional simulation of granular materials by discrete element method (DEM) by considering the fracture effect of particles. *Journal of Civil Engineering Researchers*, 5(2). https://doi.org/10.61186/JCER.5.2.14

Manbeck, H. B and Nelson, G. L. (1975). Three dimensional constitutive equations for wheat *en masse*. *Transactions of ASAE*, 18(6), 1122-1127.

Manbeck, H. B and Nelson, G. L. (1972). Methods and instrumentation for evaluating the stress-strain behaviour of wheat *en masse*. *Transactions of ASAE*, 919-922.

Manbeck, H. B, Ross, I. J and French, R. A. (1995). Silo loads and structural design. In D. Wolf (Ed.), *Design and operation of grain handling and storage systems* (pp. 203–234). ASAE.

Masson, S and Martinez, J. (2000). Effect of particle mechanical properties on silo flow and stress from distinct element simulations. *Powder Technology*, 109, 164–178. https://doi.org/10.1016/S0032-5910(99)00234-X

McLaughlin, N. B and Pitt, R. E. (1984). Failure characteristics of apple tissue under cyclic loading. *Transactions of ASAE*, 27(SE), 311-320.

Mensah, J. K, et al. (1981). Effect of drying conditions on impact shear resistance of selected corn varieties. *Transactions of ASAE*, 24(6), 1568-1572.

Mohsenin, N. N. (1980). *Thermal properties of foods and agricultural materials*. Gordon

and Breach.

Mohsenin, N. N. (1987). *Physical Properties of Plant and Animal Materials. Structure, Physical Characteristics and Mechanical Properties*. 2. Aufl. 891 Seiten, zahlr. Abb. und Tab. Gordon and Breach Science Publishers, New York u. a. 1986. Preis: 140.— £. Food / Nahrung, 31(7), 702–702. https://doi.org/10.1002/food.19870310724

Moya, M, Ayuga, F, Guaita, M and Aguado, P. J. (2002). *Mechanical properties of granular agricultural materials considered in silos design* [Paper presentation]. ASCE Engineering Mechanics Conference, Columbia University, New York.

Nedderman, R. M. (1992). *Statics and kinematics of granular materials*. Cambridge University Press.

Nielsen, J. (1998). Pressures from flowing granular solids in silos. *Philosophical Transactions of the Royal Society of London. Series A: Mathematical, Physical and Engineering Sciences*, *356*, 2667 - 2684.

Oda, M, Koishikawa, I and Higiuchi, T. (1978). Experimental study of anisotropic shear strength of sand by plane strain test. *Soils and Foundations*, 18(1), 26-38.

Omondi, J and Otieno, R. (2020). Adoption of Eurocodes in Kenyan structural engineering practice: Challenges and progress. *Civil Engineering Journal of Africa, 8*(2), 45–53.

Oranga, E. (2005). *Elastic and viscoelastic behaviour of shelled maize en masse* [Master's thesis]. University of Nairobi, Kenya.

O'Sullivan, C. (2011). *Particulate discrete element modelling: A geomechanics perspective*. CRC Press.

Ozdemir, H. (1976). *Nonlinear transient dynamic analysis of yielding structures* [Doctoral dissertation]. University of California, Berkeley.

Parafiniuk, P, Molenda, M and Horabik, J. (2013). Discharge of rapeseeds from a model silo: Physical testing and distinct element method simulation. *Computers and Electronics in Agriculture*, 97, 40–46.

Patel, C. P and Kute, S. (2021). Prediction of wall pressures and stresses developed by grainy materials in cylindrical ferrocement silo in static condition. *Asian Journal of Civil Engineering*, 22(7), 1235–1248. https://doi.org/10.1007/s42107-021-00376-x

Peleg, M. (1985). The role of water in rheology of hygroscopic food powders. In D. Simataos and J. L. Multon (Eds.), *Properties of water in foods* (pp. 394-404). Martinus Nijhoff Publishers.

Pongó, T. (2023). *Particle flows in silos, significance of particle shape, stiffness and friction*.

https://hdl.handle.net/10171/64982

Ramírez-Gómez, Á. (2020). The discrete element method in silo/bin research. Recent advances and future trends. *Particulate Science and Technology*, 38(2), 210–227. https://doi.org/10.1080/02726351.2018.1536093

Rankine, W. J. M. (1857). On the stability of loose earth. *Philosophical Transactions of the Royal Society of London, 147*.

Reimbert, M. L and Reimbert, A. M. (1976). *Silos: Theory and practice* (1st ed.). Trans Tech Publications.

Sac-Morane, A, Veveakis, M and Rattez, H. (2024). A phase-field discrete element method to study chemo-mechanical coupling in granular materials. *Computer Methods in Applied Mechanics and Engineering*, 424, 116900. https://doi.org/10.1016/j.cma.2024.116900

Schott, R. W and Britton, M. G. (1984). *Plane strain behaviour of bulk grain* [Paper presentation]. ASAE Paper No. 84-503, American Society of Agricultural Engineers.

Shelef, L and Mohsenin, N. N. (1968). Effects of moisture content on mechanical properties of corn horny endosperm. *Cereal Chemistry*, 46(3), 242-253.

Silling, S. A. (2023). Discrete element model for powder grain interactions under high compressive stress. *International Journal of Fracture*, 244(1), 149–162. https://doi.org/10.1007/s10704-023-00724-9

Stafford, J. V, Audsley, E and Sharp, J. R. (1986). The determination of best fit linear failure envelopes to Mohr circles. *Journal of Agricultural Engineering Research*, 33, 33-38.

Stinchcomb, W. W. (1989). Damage and fracture of composite materials under cyclic loads. In Salama, Ravi-Chandar, Taplin, and Rama (Eds.), *Advances in fracture research* (Vol. 4, pp. 2939-2955).

Sykut, J, Molenda, M and Horabik, J. (2008). Influence of filling method on packing structure in model silo and DEM simulations. *Granular Matter*, 10, 273–278.

Ti, K. S. (2009). A review of basic soil constitutive models for geotechnical application. *Electronic Journal of Geotechnical Engineering*, 14(J).

Tian, T, Su, J, Zhan, J, Geng, S, Xu, G and Liu, X. (2018). Discrete and continuum modeling of granular flow in silo discharge. *Particuology*, 36, 127–138. https://doi.org/10.1016/j.partic.2017.04.001

Tordesillas, A. (2004). The jekyl and hyde of granular materials uncovered. www.unimelb.edu.au

Vanel, L, Claudin, P, Bouchaud, P. J, Cates, M. E, Clement, E, and **Witterner, J. P.**

(2000). Comparison between theoretical models and new experiments. *Physical Review Letters*, 84(7), 1439-1442.

Volovik, V and Zamyatin, D. (2010). Silo pressure calculation methods in Russian standards. *Structural Engineering International, 20*(4), 408–412.

Wu, M, Xia, Z and Wang, J. (2023). Constitutive modelling of idealised granular materials using machine learning method. *Journal of Rock Mechanics and Geotechnical Engineering*, 15(4), 1038–1051. https://doi.org/10.1016/j.jrmge.2022.08.002

Yilmazoğlu, M. U. (2024). Modeling of triaxial pressure tests with uniform granular materials discrete particle method. *Kastamonu University Journal of Engineering and Sciences*, 10(2). https://doi.org/10.55385/kastamonujes.1559603

Youngs, R. R. (1982). *A three-dimensional effective stress model for cyclicly loaded granular soils* [Doctoral dissertation]. University of California, Berkeley.

Zhang, Q, Puri, V. M and Manbeck, H. B. (1994). Applicability of a two-parameter failure criterion to wheat *en masse*. *Transactions of ASAE*, 37(2), 571-575.

Zhang, Q, Britton, M. G and Jaremek, R. (1993). Dynamic loads during discharge for wheat, barley and canola in a smooth and a corrugated-walled model bin. *Journal of Agricultural Engineering Research*, 56, 111–119. https://doi.org/10.1006/jaer.1993.1065

Zhang, Q, Puri, V. M and Manbeck, H. B. (1986). *Determination of elasto-plastic constitutive parameters for wheat en masse* [Paper presentation]. ASAE Paper No. 86-4073, American Society of Agricultural Engineers.

Zhang, Q, Puri, V. M and Manbeck, H. B. (1985). *Finite element modelling of thermally induced pressures in grain bins filled with cohensionless granular material* [Paper presentation]. ASAE Paper No. 85-4002, American Society of Agricultural Engineers.

Zhang, Y and Li, L. (2024). Optimization of discrete element method model to obtain stable and reliable numerical results of mechanical response of granular materials. *Minerals*, 14(8), 758. https://doi.org/10.3390/min14080758

Bio-Inspired Concrete Structures for Enhancing Mechanical Performance

L. K. Boretor

School of Engineering, RMIT University, Melbourne Australia

lawiboreto94@gmail.com

Abstract

Conventional concrete, though widely used, exhibits low fracture toughness and susceptibility to cracking, limiting its application in demanding environments. This study explores bio-inspired designs—specifically nacre-like and cortical bone-like architectures—to enhance the mechanical properties of concrete, including fracture toughness, flexural strength, and impact resistance.

To develop and characterize bio-inspired concrete structures that exhibit superior mechanical performance and durability compared to conventional concrete.

The study employed a combination of experimental and numerical methods. Bio-inspired concrete specimens were fabricated using 3D-printed molds and innovative casting techniques to incorporate nacre-like layers and tubular cortical bone-inspired structures. Mechanical testing included Single Edge Notched Beam (SENB), Modulus of Rupture (MOR), uniaxial compression, and drop-weight tests. Numerical modeling via Finite Element Analysis (FEA) validated experimental findings.

Bio-inspired concrete demonstrated substantial improvements in mechanical properties. Fracture toughness increased by over 600% for hybrid designs, flexural strength improved by 92%, and impact resistance showed a 67% reduction in damage compared to conventional concrete. Compressive strength also improved modestly, highlighting the effectiveness of the bio-inspired designs in enhancing energy dissipation and crack resistance

Bio-inspired concrete offers transformative potential for construction applications, particularly in high-stress and dynamic environments. The hybrid approach combining nacre-like and cortical bone-like features presents the best performance, paving the way for durable and sustainable infrastructure solutions.

Key Words: Bio-inspired concrete, fracture toughness, flexural strength, impact resistance, nacre-like structure, cortical bone-inspired architecture, Finite Element Analysis.

1. Introduction

Concrete is among the most common building materials worldwide, famous for compressive strength, durability, and flexibility. Nevertheless, conventional concrete has shortcomings that restrict its sustained mechanical behavior in several applications and environments.

However, conventional concrete has problems, such as brittleness and low fracture toughness, which lead to problems, such as cracks and failure under tensile or impact forces. Concrete may crack and fail suddenly without apparent signs of early deterioration, a characteristic that is undesirable in structures that mandate high levels of toughness and plasticity (San et al., 2020). Such mechanical limitations have led to a search for additional and innovative ways of enhancing the performance of concrete using bio-inspired designs and materials.

Innovative/nanocomposite materials have attracted considerable interest in recent years since they replicate the characteristics of biostructures developed through natural selection for millions of years. Organic materials, like nacre and cortical bone, have demonstrated good properties of toughness, strength, and damage tolerance; they can serve as models for enhancing engineering materials. For example, nacre is a biological material, which is similar to brick and mortar, comprising mineral platelets wrapped together by layers of organic material; this material is credited with high fracture toughness as the crack path deviates with the result that catastrophic failure of components is averted (Ding et al., 2021).

Likewise, cortical bone has challenging phases embedded in a softer matrix, resulting in energy absorption and material strengthening through micro crack-turning and crack-bridging (Yang et al., 2025). These bio-inspired mechanisms shed light on the possible solutions for improving the mechanical properties of concrete and thus making it a more sustainable construction material.

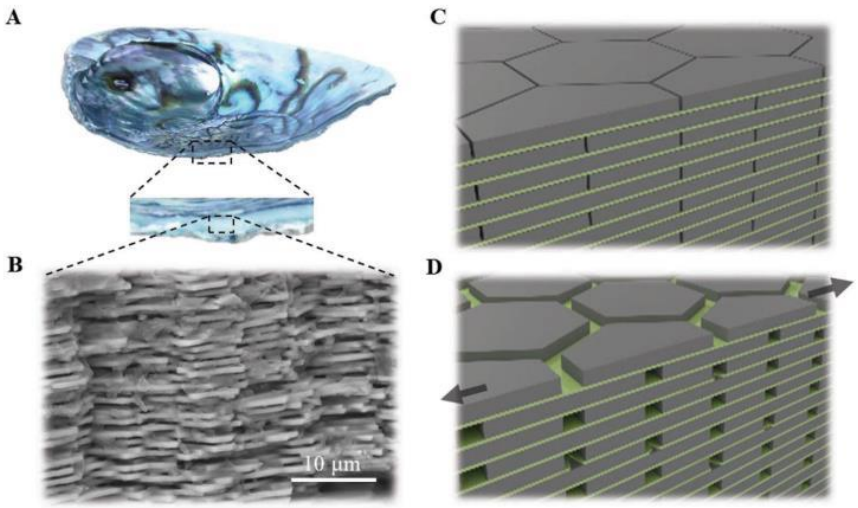

Figure 1: The architecture of natural and synthetic nacre-like composite

2. Problem Statement

Although regular concrete has been used in construction for thousands of years, its mechanical drawbacks have emerged as construction industries seek more durable and eco-friendly structures. Standard concrete has poor fracture resistance and toughness for tensile stress and dynamic loading conditions. This leads to a lack of fracture toughness within the concrete, thus making it prone to failure under stress. Standard concrete's brittle nature also significantly inconveniences structures that undergo repeated loads, like high-rise buildings, bridges, and pavements (Sojobi & Liew, 2022).

This is further compounded by environmental influences such as freeze-thaw cycles in concrete infrastructure, which cause the experience of structural change and, thereby, cyclical deterioration of the material (Sulaiman et al., 2019). Although different reinforcement methods like steel bars or fiber composites have been used to counter these problems, all these solutions complicate and cost the construction process while not eradicating the inherent brittleness of concrete.

3. Research Questions

This paper sought to address the following research questions:

i. How can bio-inspired designs, such as nacre-like structures and cortical bone-inspired architectures, enhance concrete's fracture toughness and ductility?
ii. What are the critical mechanical improvements observed in bio-inspired concrete compared to traditional concrete, particularly regarding resistance to cracking and failure under stress?
iii. How can bio-inspired concrete be optimized for large-scale construction applications, particularly in environments prone to mechanical wear, impact, and environmental stressors?
iv. What are the potential challenges and limitations associated with the fabrication and implementation of bio-inspired concrete in real-world construction projects?

4. Significance of the Study

The significance of this study is based on the fact that progressive work can be done to produce new construction materials that exhibit properties superior to the existing ones. Other biologically inspired designs like nacre and cortical bone-inspired designs have demonstrated significant ability to improve the applied mechanical characteristics of many engineering materials such as concrete (Gupta et al., 2024). The embedment of bio-mimicking

characteristics like layered systems, hierarchical form, and micro-crack deflection can significantly enhance the fracture energy and the post-peak load-bearing capacity of concrete.

5. Objectives

The primary objective of this research was to develop and optimize bio-inspired concrete structures that exhibit enhanced mechanical properties, particularly in terms of fracture toughness, ductility, and resistance to environmental stressors. The specific goals of the study included;

i. To investigate the mechanical performance of bio-inspired concrete structures
ii. To evaluate the fracture toughness, ductility, and durability of bio-inspired concrete compared to traditional concrete.
iii. To develop a comprehensive understanding of the fabrication methods and challenges associated with bio-inspired concrete.
iv. To explore the potential applications of bio-inspired concrete in large-scale construction projects, with a focus on improving the resilience and sustainability of infrastructure.

6. Literature Review

This paper highlights that concrete, arguably the most popular construction material, stands out due to its high concrete compressive strength and relatively low material cost. Nevertheless, since its fracture toughness and ductility are relatively low, along with other mechanical disadvantages, it has become an object of research for bio-inspired alternatives solutions.

In the recent past, bio-inspired material development has risen as scientists try to design structures that draw inspiration from the mechanical performance of natural systems. Bio-inspired materials were developed by mimicking natural systems for load transmission, such as nacre and cortical bone, which are very effective in responding to stress.

Bio-inspiration can be described as drawing from nature and relying on nature's solutions in designs, particularly with regard to resisting mechanical loads that artificial materials have not surpassed. For example, nacre has a regular structure, which implies an organized 'brick-and-mortar' structure in which the aragonite platelets are the 'bricks,' and the 'mortar' is a biopolymer matrix.

This arrangement enables nacre to achieve simultaneously high strength and fracture toughness; the soft biopolymer layers divert the crack in its path and ensure that the material

does not fail in a brittle manner (Ding et al., 2021). The crack deflection mechanism is designed so that the cracks follow the softer organic matrix and do not follow the mineral parts, which would be fatal.

Similarly, cortical bone primarily contains crystallized mineral elements, which are mixed with collagen fibers, which allow it to spread out the force load and avoid failure. This particular structural arrangement enables cortical bone to cope with mechanical stress via such means as crack arrest and crack deviation. Gupta et al. (2024) noted that the hierarchical structure of cortical bone is an advantage in controlling cracks to create a crack path that does not cause a failure point and instead increases the toughness of the material, attributed to the tubular osteon separated by weaker cement lines.

Advanced composites derived from designs found in nature hold great promise to revolutionize the construction industry through the application of these principles to engineered concrete. The concrete structures resembling the natural structures of the nacre or cortical bone can increase the material's fracture toughness, ductility, and energy absorption, in addition to enhancing the material's density and compressive strength.

7. Experimental Design

7.1.Fabrication Process

In the nature of the experimental design for this research, the following compositions are involved: the creation of the bio-inspired concrete structures, their mechanical testing, and the collection of relevant data for the modeling and analysis of the structures.

The integration of 3D printing and casting methods does the synthesis of the microscopic structures of the engineered concrete. The tubular inclusions and formwork for the layered structures are fabricated utilizing high-precision objects formed by a high-resolution 3D printer meant for the production of complex geometries with narrow tolerances. The PLA material used for the tubular inclusions is selected as it is flexible for 3D printing and forms smooth and hollow structures that can be infused within the concrete matrix by Gupta et al. (2024).

Once the formwork and tubular inclusions are made from a 3D print, the concrete is_skill poured in layers. This process starts by putting a layer of the standard cementitious matrix, and then the PLA tubular inclusions are cast. The second layer is the air-entrained concrete that was used to overlay the first slab and left to settle to the bottom. This is done consecutively until a total number of layers wanted is created in the final structure. Vibration methods are

used after placing the concrete to fill up the tubular inclusions entirely and minimize the formation of air voids (Nguyen et al., 2023).

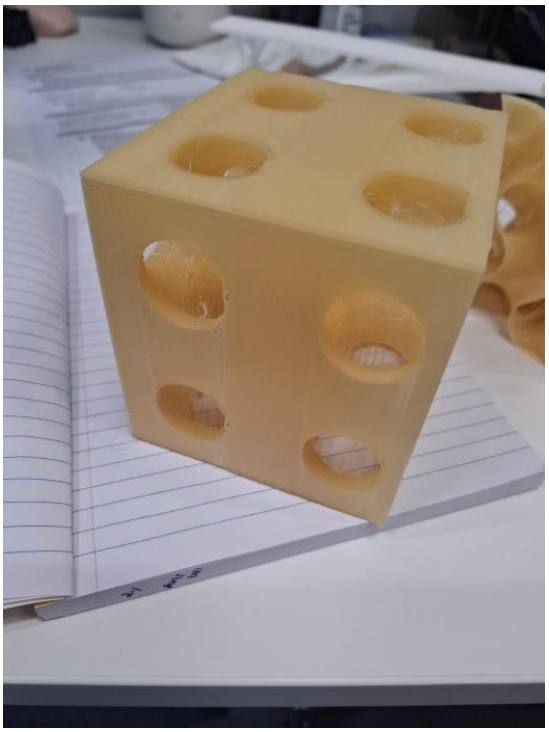

Figure 2: 3D-printed mold used for fabricating nacre-like structures in concrete

The concrete specimens, after casting, are then cured and kept for 28 days at specific temperature and humidity conditions. This process also ensures that the full strength of each concrete sandwich is realized, as well as the bond between the layers and the tubular inclusions.

7.2. Evaluation Criteria

The performance criteria of bio-inspired concrete are related to a number of mechanical characteristics, which include fracture toughness, modulus of rupture, compressive strength, and impact strength. These properties are essential in establishing the ability of the material to be used in high-impacting structures like bridges, buildings, and pavements, among others.

8. Results

8.1.Experimental Results

The specific objectives of the experimental investigation involved evaluating and comparing fracture toughness, modulus of rupture, compressive strength, and impact resistance of bio-inspired concrete structures with conventional concrete structures. They attributed the mechanical performance gains seen in the bio-inspired specimens to the laminar structure, cortical bone-like tubes, and fibers; crack-reinforcing aspects made structures more challenging.

8.2. Fracture Toughness

Through the Single Edge Notched Beam (SENB) test, the critical stress intensity factor (K_IC), which is an index of the crack growth resistance of a material, was determined. The findings are presented in Table 1 below.

Table 1: Fracture Toughness Results (SENB Test)

Specimen Type	**Fracture Toughness (K_IC) (MPa√m)**
Traditional Concrete	0.85
Nacre-Like Concrete	4.76
Cortical Bone-Inspired Concrete	5.32
Hybrid Bio-Inspired Concrete	6.10

8.3. Modulus of Rupture (Flexural Strength)

The modulus of rupture, which is the measure of the material's ability to withstand bending and tensile forces, was determined from three-point bending tests. Table 2 contains the following results.

Table 2: Modulus of Rupture (MOR) Results

Specimen Type	**Modulus of Rupture (MPa)**
Traditional Concrete	4.2
Nacre-Like Concrete	6.8
Cortical Bone-Inspired Concrete	7.5
Hybrid Bio-Inspired Concrete	8.1

8.4. Compressive Strength

The mechanical properties of the concrete rendered bio-inspired were assessed using uniaxial compression tests. The results are presented in the following Table 3.

Table 3: Compressive Strength Results (Uniaxial Compression Test)

Specimen Type	**Compressive Strength (MPa)**
Traditional Concrete	32
Nacre-Like Concrete	34
Cortical Bone-Inspired Concrete	36
Hybrid Bio-Inspired Concrete	38

8.5.Impact Resistance

The durability performance, particularly the bio-inspired concrete's impact resistance, was evaluated using a drop-weight test. The described intensity of dynamic loads allowed for determining the amount of damage, which is summarized in Table 4.

Table 4: Impact Resistance Results (Drop-Weight Test)

Specimen Type	**Impact Damage (mm)**
Traditional Concrete	7.5
Nacre-Like Concrete	3.2
Cortical Bone-Inspired Concrete	2.9
Hybrid Bio-Inspired Concrete	2.5

Compared to regular concrete, remarkable concrete specimens imitating biostructures provided a lower impact damage ratio. The first material, which mimics nacre, was designed to decrease impact force by more than 57%, and the cortical bone-inspired concrete cut the values by 61%. Out of all the design types, the hybrid design showed the most resilience to impact and had 67% less damage than regular concrete.

9. Recommendations for Further Research

- Scalability Issues: Investigate large-scale production methods such as automated casting and large-scale 3D printing.
- Environmental Durability: Study long-term performance under harsh conditions (temperature changes, moisture, freeze-thaw cycles, and chemical attacks).
- Alternative Bio-Inspired Designs: Explore new bio-inspired structures for enhanced load-bearing applications.
- Sustainable Materials: Identify durable, eco-friendly alternatives to synthetic polymers (e.g., natural fibers, biodegradable materials).
- Integration with Sustainable Technologies: Combine bio-inspired concrete with self-healing or green concrete for enhanced durability and reduced environmental impact.

References

Ding, Z., Wang, B., Xiao, H. and Duan, Y., 2021. Hybrid bio-inspired structure based on nacre and woodpecker beak for enhanced mechanical performance. *Polymers*, 13(21), p.3681.

Gupta, P., Wang, J., Zhao, H., Liu, S., Zhou, X., and Zhao, F., 2024. Tough and Ductile Architected Nacre-Like Cementitious Composites. *Advanced Functional Materials*, 34(1).

Nguyen, T.K., Suhaizan, M.S., Nguyen-Xuan, H. and Tran, P., 2023. Mechanical responses of buoyant bio-inspired foamed concrete structures. *Construction and Building Materials*, 391, p.131731.

San Ha, N. and Lu, G., 2020. A review of recent research on bio-inspired structures and materials for energy absorption applications. *Composites Part B: Engineering*, 181, p.107496.

Sojobi, A.O. and Liew, K.M., 2022. Multi-objective optimization of high performance bio-inspired prefabricated composites for sustainable and resilient construction. *Composite Structures*, 279, p.114732.

Yang, F., Xie, W. and Meng, S., 2020. Impact and blast performance enhancement in bio-inspired helicoidal structures: A numerical study. *Journal of the Mechanics and Physics of Solids*, 142, p.104025.

Design and 3D Printing of a Protective Enclosure System: A Customized Enclosure for a Smart LPG Detection and Leakage Alert System

Wekesa Augustine[1], Munji Mathew[1], Nyenge Raphael[1], Iloka Kenneth[2], Masabo Bazil[2]

[1]Department of Physics, Kenyatta University

[2]Department of Electrical and Electronic Engineering, Kenyatta University

*Corresponding Author. Email: augustus5.biomed@gmail.com

Abstract

The integration of smart technologies into household safety systems has become increasingly vital, particularly in the context of Liquefied Petroleum Gas (LPG) usage. This study presents the design and 3D printing of a customized protective enclosure system for a Smart LPG Detection and Leakage Alert System. The primary objective of this study was to develop a low-cost, application-specific protective enclosure that enhances the safety, and performance of gas leakage detection components, including the gas sensor, GSM module, buzzer, and microcontroller. To inform the design requirements, a structured questionnaire was administered to Kenyan households across Nairobi, Kiambu, and Trans-Nzoia counties. Using the information from the analysed data, a CAD model was developed using SolidWorks 2024, incorporating key features such as gas sensor mounting, an LCD display port, cable management, and ease of assembly. The optimization of the design was done in a slicer software, Creality Print v5.1 software. The model was later fabricated through Fused Deposition Modelling using a Creality K1 Max 3D printer. Hyper PLA filament material was used for printing because of its excellent thermal and mechanical properties. A 3D printed protective enclosure was successfully printed. The results clearly confirmed the effectiveness of the protective enclosure in protecting the internal components while maintaining system performance. The study highlights the importance of context-based, iterative design processes in developing context-relevant engineering solutions using additive manufacturing.

The LPG protective enclosure is a clear demonstration of what AM can achieve without comprising the quality, cost and safety of the product. Future research should prioritize material enhancements as well as scalability for mass production.

Keywords: 3D Printing, CAD Design, Smart LPG System, Protective Enclosure, Additive Manufacturing.

1. INTRODUCTION

Liquefied Petroleum Gas (LPG) remains one of the most used fuel sources in Africa and beyond (Nakanwagi, 2021). This energy source has proved effective and efficient especially for domestic and industrial applications such as cooking, heating as well as powering various manufacturing processes. It's worth noting that LPG not only powers our kitchens but also is a major contributor to environmental conservation as opposed to traditional sources of fuel such as firewood, kerosene among others which have for a long time identified and proved to be a risk to the environment. However, LPG as clean as it sounds also poses some significant safety risks to our environment and this is due to the potential leaks it carries which can have a devastating effect such as fire explosions (Cavaliere, 2023).

Over the past years, significant developments have been in the field of smart detection systems to address safety issues in relation to potential gas leaks. These systems made use of microcontrollers, sensors, as well as IoT technologies in enhancing and improving safety within an environment (Sujarwo et al., 2021). However, these systems have faced significant challenges when it comes to ensuring the electronic components such as microcontrollers, open environment sensors, among other important sensors are well enclosed and protected environmental damage such as moisture, excess heat exposure as well as from other environmental contaminants.

For a long time, we have overly relied on traditional enclosures, fabricated from materials such as wood, metals as well as other conventional plastics which have proved unreliable. While effective in some cases, there remains a big challenge in using these enclosures. For instance, the fabrication of traditional enclosures is very costly, impacting the user's economic burden (Chakaravarthi, 2020). In addition, production of these protective enclosures takes a lot of time, as it requires a direct implication on the turnover of a company. Last and most importantly, traditional protective enclosures lack flexibility in customization leaving no room for user preferences (Chakaravarthi, 2020). The rapid growth of Additive manufacturing, in this case 3D printing technology, not only presents a game changer in the field of manufacturing but also presents an innovative solution that supports rapid, cost-effective, customizable and user-centered and tailored products such as protective housing (Prashar et al., 2022).

Therefore, this study focuses on designing and fabricating 3D printed protective enclosures for IoT systems such as the smart LPG usage detection and leakage alert system. The key and main objective of the study was to design and fabricate an IoT protective casing that is cost-effective, and highly customizable to the user's specific needs. The study also sought to understand and appreciate the role of Additive manufacturing such as 3D printing in the IoT

industry. To achieve this, the study leveraged the computer-Aided Design (CAD) resources alongside Additive Manufacturing techniques in optimizing the functionality as well as the structural integrity of the product, protective casing (Prashar et al., 2022).

1.1. Problem Statement

Liquefied Petroleum Gas (LPG) is widely used as a primary source of energy for many households not only in Kenya but across the world, yet it poses significant serious safety risks and inconveniences due to undetected gas leaks and unpredictable shortages. While smart LPG detection and alert systems offer a promising solution, their electronic components remain vulnerable without proper protective enclosures. Conventional enclosures, especially those made from wood, metal, or plastic, are often expensive making it difficult for many households to afford. Also, these enclosures are environmentally susceptible making them a great risk to environmental conservation. In addition, these enclosures are time-consuming when it comes to fabrication and lack design flexibility. These limitations among many others hinder the effective deployment of smart systems in real-world settings. Therefore, there is need for a durable, cost-effective, and customizable protective enclosure that can reliably shield electronic components and enhance the system's overall performance and safety.

1.2. Smart LPG Detection Systems

Liquefied Petroleum Gas (LPG) continues to be one of the most green and convenient sources of energy especially in the continent of Africa (Nakanwagi, 2021). As opposed to the traditional sources of energy such as firewood, "jiko," kerosene among others whose use continues to be a threat to the environment, LPG has proved to be a game changer in powering our kitchens. However, LPG as good as it sounds carries a hidden and risky ally which if not taken care of can result in a catastrophe. The safety of our homes and the environment we live in is highly dependent on the safety of our source of fuel, LPG. Because of this, there are systems that have been developed to address these safety issues. We therefore developed a context-based system that monitors LPG, both usage and leakage. This system consists of Arduino Uno microcontroller for processing, MQ6 gas sensor for leakage detection, a loadcell for usage monitoring, and GSM modules for cellular communication between one device and another. The context-based system is able to monitor and detect gas leakage and alert the user through an audible alarm, visual alarm and or SMS and Voice call.

The design and development of this system was informed by user feedback that was obtained from Kenyan households using a structured questionnaire. The questionnaire was administered to sample size of 100 respondents selected through purposive sampling in three counties in

both urban and rural counties in Kenya (Nairobi, Kiambu and Trans-Zoia counties). The feedback from the respondents was used in informing the design of the LPG protective enclosure putting into consideration cable management, ease of assembly and alignment.

The efficiency and effectiveness of this safety detection system among many others heavily rely on the factors such as device durability, sensor accuracy, and the ability of the device to withstand harsh environmental conditions like high temperatures, water resistance etc. Therefore, integrating IoT-based devices through proper protective enclosures helps in enhancing the system's safety, performance and durability.

1.3. System Overview

The protective enclosure system, designed for the LPG usage detection and leakage alert system consisted of both the hardware and software.

1.3.1. Hardware

The hardware consisted of the following components.

1.3.1.1. Arduino Uno

Arduino Uno is a microcontroller board based on the ATmega328p chip. Developed in Italy, Arduino Uno is one of the most popular boards in the Arduino family specifically designed for electronic projects. It features a flash memory storage of 32 KB, 2 KB of SRAM, as well as a 1 KB of EEPROM. The ATmega328p chip operates at a clock speed of 16 MHz (Barrett & Pack, 2022). Together with a breadboard, the microcontroller is used to control functions of a particular device connected to it by interpreting data from its input/output peripherals. The board contains 14 input/output pins, and 6 analog input pins. The board runs on an integrated development environment (IDE) which is open-source software from the Arduino Official site (The Engineering Knowledge, 2021).

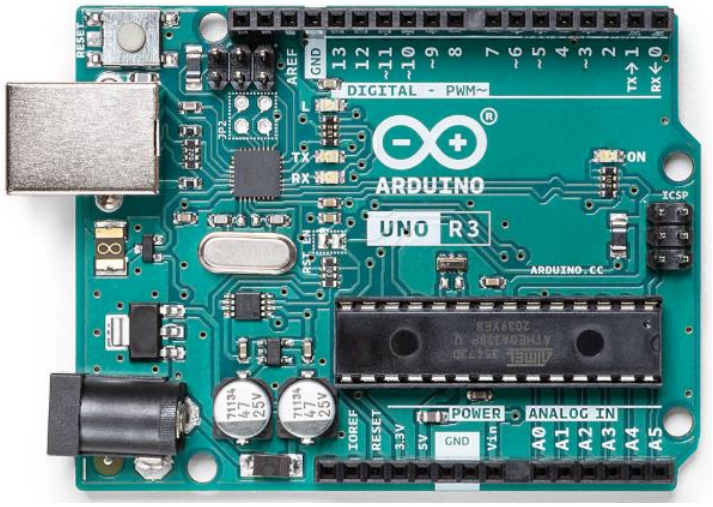

Figure 5.0 Arduino Uno

Arduino. (n.d.). Retrieved from [https://store.arduino.cc/products/arduino-uno-rev3]

1.3.1.2. Gas Sensor (MQ-6)

An MQ-6 is a Metal Oxide Semiconductor sensor used to detect liquefied petroleum gas (LPG). The working range of the sensor is between 300 to 10,000ppm of gas concentrations. The sensor works on the scientific principle of chemo-resistance where the electrical resistance of a material changes in response to the presence of a particular gas. The sensor consists of a sensing element called tin dioxide (SnO2), usually an N-type as illustrated in Figure 2.0.

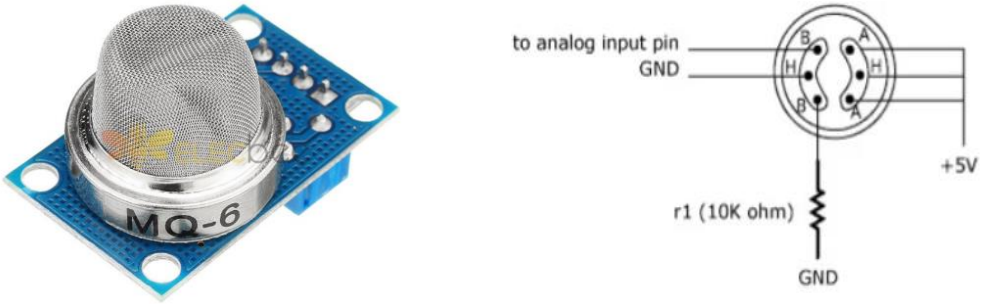

a) b)

Figure 6.0: a) MQ-6 Gas sensor b) Circuit diagram

MQ-6 Gas Sensor Module**.** (n.d.). Retrieved from [https://mybotic.com.my/gas-sensor/mq- 6-mq6-gas-sensor-module-liquefied-petroleum-gas-lpg-butane-c4h10]

1.3.1.3. Load cell

A loadcell is an electro-mechanical sensor for measuring the weight of an object. Just like a transducer, a load cell works by converting mechanical force into electrical signal as shown in Figure 3.0.

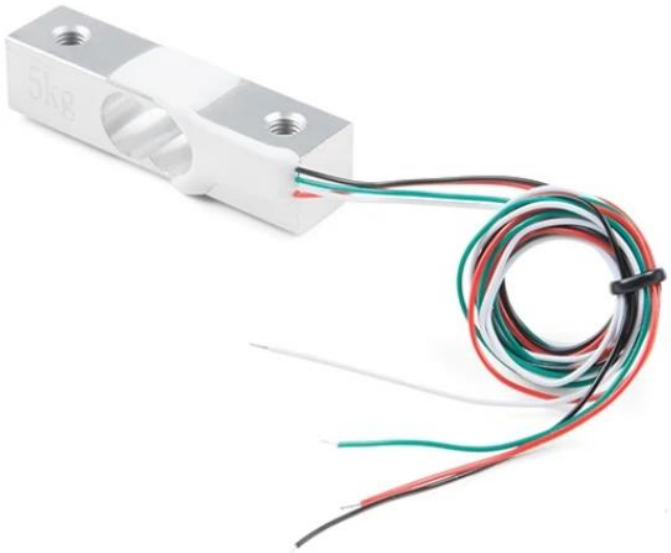

Figure 7.0 Loadcell

Loadcell**.** (n.d.). Retrieved from [https://www.sparkfun.com/load-cell-5kg-straight-bar-tal220b.html]

1.3.1.4. Module

A Global System for Mobile Communications (GSM module) is a hardware device that allows electronic devices or systems such as Arduino, IoT devices to communicate to each other over a cellular network. The operating voltage for the module is between 3.4V to 4.4V with a power consumption of less than 2 mA in sleep mode. Figure 3.4. show a SIM5320E functional diagram and a complete GSM module used for the LPG system.

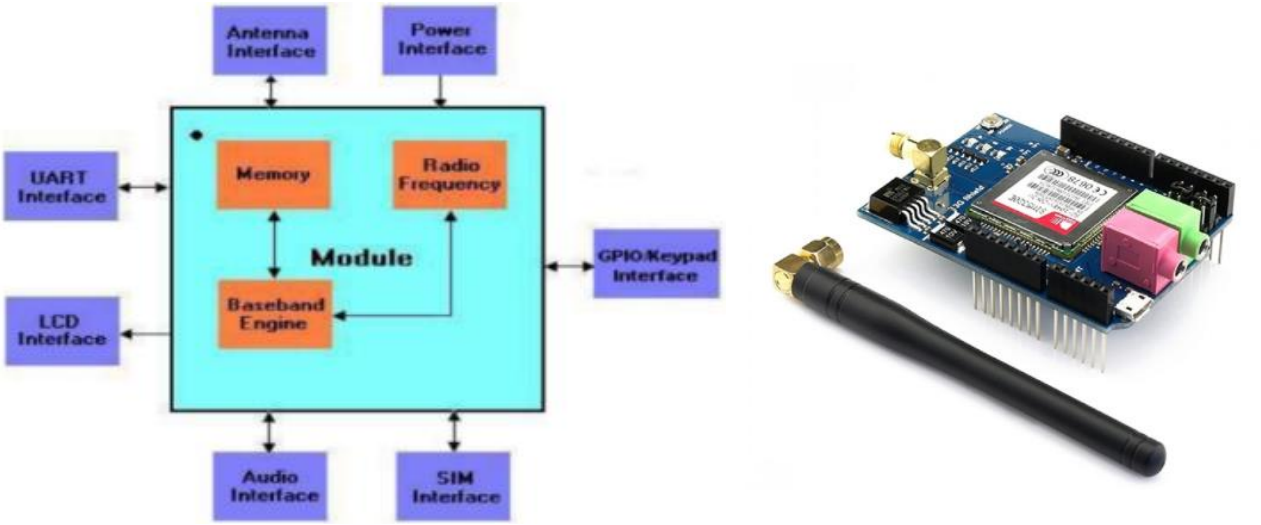

a) b)

Figure 8.0 a) SIM5320E functional diagram b) GSM Module

Retrieved From [https://store.nerokas.co.ke/SKU- 2099?sort=p.model&order=DESC&limit=15]

1.3.1.5. LCD

Figure 3.5. shows 16x2 Liquid Crystal Display (LCD) display module used to show interactive message. It is a 16 column by 2 rows display abbreviated as 16x2.

Figure 9.0 16x2 LCD

16x2 LCD. (n.d.). Retrieved From [https://electroglobal.in/product/16x2-lcd-display-green-backlight-arduino/]

1.3.1.6. Buzzer

A buzzer is an output device that gives an audio alert when the condition is met as shown in Figure 6.0

Figure 10.0 Piezoelectric Buzzer

Piezoelectric buzzer. (n.d.). Retrieved from [https://www.inventelectronics.com/product/piezo-buzzer-through-hole/]

1.3.2. System software

This is the program that controls the output of the hardware components used such as the gas sensor, loadcell, among others. It is the core of the system and was programmed in C++ programming language. The program features the following flowchart diagram as illustrated in Figure 7.0

Figure 11.0 LPG System's flowchart

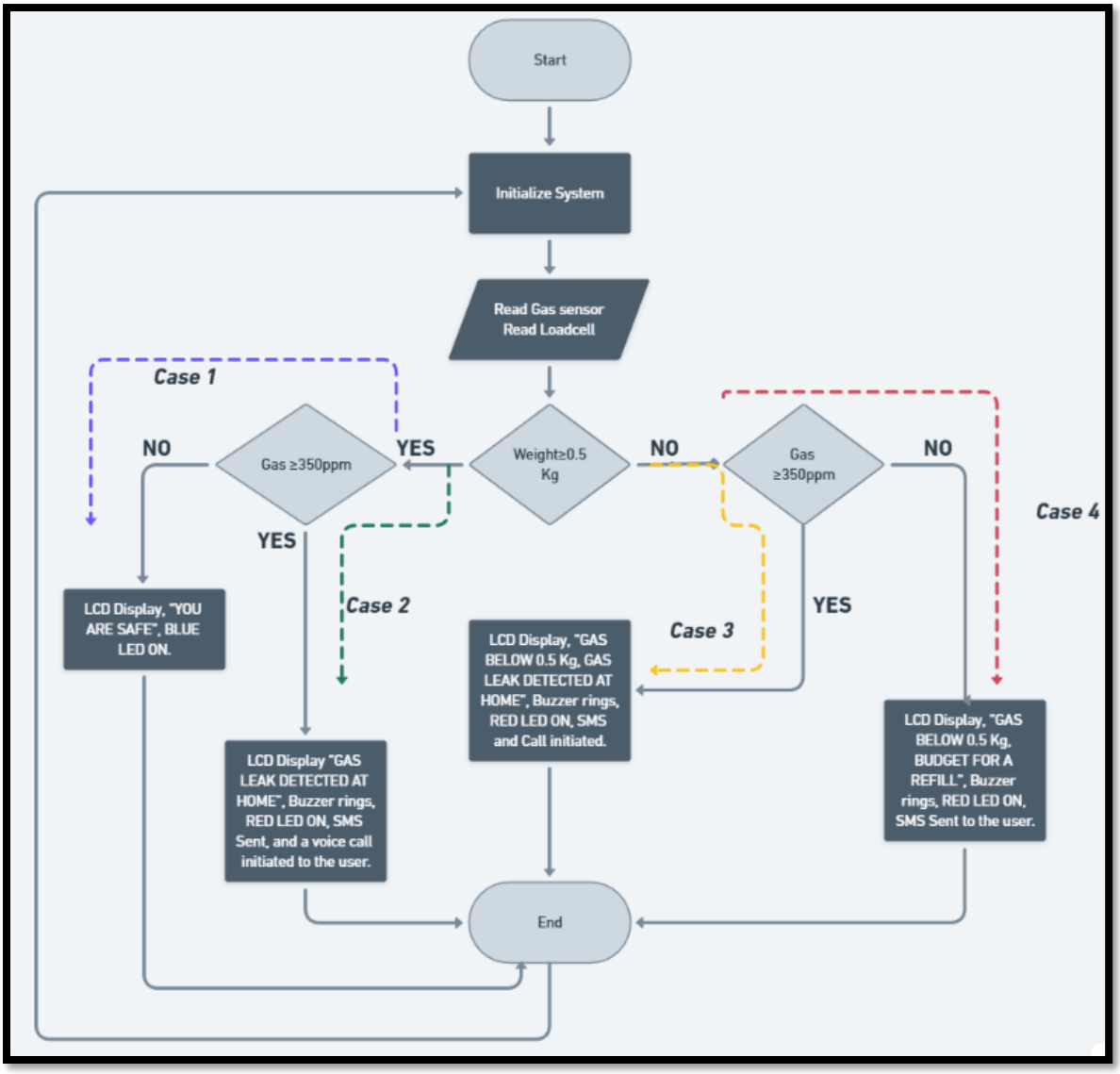

Figure 7.0 LPG System's flowchart

1.4. Protective Enclosures for Electronic Components

To achieve durability and safety of an IoT system, it is important to safeguard the electronic components from harsh environmental conditions such as dust, water, moisture, fluctuating temperatures, and mechanical stress. This requires good protective enclosures that would ensure that electronic components are well protected from such conditions. The quality of the housing casing or enclosures plays a significant role in influencing the components' durability, efficiency, and reliability (Serksnis, 2019). The most used materials for protective enclosures include metals with the most common metals being Aluminum, stainless steel etc. Plastics are also used in creating these protective enclosures. However, these materials have some limitations especially in cost, weight, and design customization.

1.5. Additive Manufacturing

Additive Manufacturing through 3D printing is one of the fastest-growing sectors today. Today, product design and rapid prototyping continue to play a key role in the fabrication of more complex geometries which were not possible with the other types of manufacturing. The use of printing materials such as PLA, ABS, PETG and others made from natural substances such as starch or corn not only helps create quality products but also promotes environmental conservation. Unlike other conventional ways of manufacturing methods, 3D printing is more flexible and innovative in terms of design flexibility, reduced cost and speed (Prashar et al., 2022).

Different and diverse types of printing materials make 3D printing widely acceptable. For example, the use of Hyper PLA for protective enclosures adds more mechanical as well as thermal properties which are very key to the durability of the product. According to a comparative study that sought to compare different types of 3D printing materials in terms of their Young Modulus, it was evident that Hyper PLA had a better Modulus of 3,300MPa as compared to other materials such as ABS, PETG, among others (CNC Kitchen, 2025). According to Spectrum Filaments n.d., Hyper PLA filament material was the preferred choice because of its properties such as high thermal resistance of up to 83oC, superior strength and good flowability (Spectrum Filaments, n.d.).

According to Blanco et al. (2022), incorporating other additional materials into PLA such as the multi-walled carbon fibers (MCFs) can significantly improve mechanical properties, resulting in even higher Young's modulus of 8.56 GPa with higher tensile strength of 64.59 MPa (Blanco et al., 2022). With the growing demand for 3D printed housing enclosures, it's crucial to understand and appreciate the role of Additive Manufacturing in revolutionizing not only the IoT industry in terms of protective enclosures but also other industries such as healthcare, education, Agriculture among others (Prashar et al., 2022). Therefore, by delving into 3D printed protective enclosures for electronic components, this study seeks to unpack the unexplored nature of Additive Manufacturing.

2. METHODOLOGY

This section addresses the PG protective enclosure system with the main focus on the Computer Aided Design (CAD), model optimization, and Computer Aided Manufacturing which are key processes in the design and fabrication of the LPG protective enclosure system. This integrated approach ensured a customized, easy to use and functional system. In addition, the data collected on user preferences, statistical analysis in the Statistical Package for Social Sciences (SPSS) ensured proper and user-centered design and fabrication.

2.1. Computer Aided Design and Optimization

Following the user feedback on design and system functionality, a prototype was developed in CAD. The study took into consideration important aspects such as sensor mounting, system casing for electronics and wiring, and weight support mechanism for accurate weight measurement.

The protective enclosure was designed in SolidWorks 2024 software to ensure customization and precision. SolidWorks 2024 is important software when it comes to design. The software comprises of three main sections, the part, the Assembly, and technical drawing all which have different but related functions (Shih, 2024). In this project, two sections were used, a system model and a technical drawing.

Design key specifications included specific mounting for the gas sensor, an LCD display slot, a 9-12V power supply slot, an antenna slot, and the Arduino uno software slot as shown in Figure 8.0 highlighting the CAD Housing Model of the Enclosure and Figure 9.0 highlighting the CAD representation of the system housing. The key considerations of the design were compactness, and ease of assembly of the system components. The ergonomic features on LCD display, filleted edges, and stability were also integrated with the aim of enhancing safety and usability.

The final model measuring 205 mm × 200 mm × 56 mm was optimized in Creality print version 5.1 slicer software before being converted into a Geometric code (GCODE) which provides key instructions to the printer such as print head movement i.e. the x, y, z axes, extruder control i.e. speed and amount among other key instructions. The GCODE file containing the instructions for the printer was printed on Creality K1 Max 3D printer using the Hyper Polylactic Acid (PLA) filament.

The Hyper PLA filament was chosen because of its good mechanical properties such as high Young's Modulus (E) which is key for strength and durability (Mustafa et al., 2021). The optimization included sparse infill density of 13.5%, layer height of 0.2mm, wall thickness, brim for bed adhesion, and 30o threshold for support structures.

The Creality K1 Max Printer was chosen because of its efficiency and high precision, which allows for the mass production and production of detailed components that meet both functional and aesthetic requirements. Also, the printer has a large build volume, f 300 x 300 x 300 mm, making it ideal for rapid prototyping as well as design verification. Its high-speed capabilities, together with maximum speed of 600 mm/s, make the printer efficient especially in production without compromising the quality of any print ("K1 Max 3D printer," n.d).

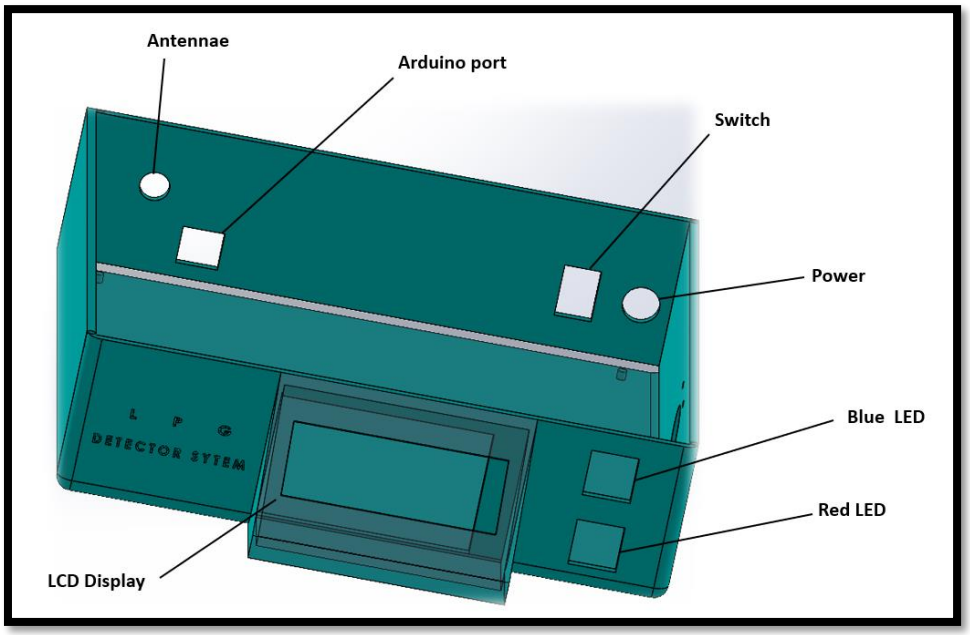

Figure 12.0 LPG CAD Model

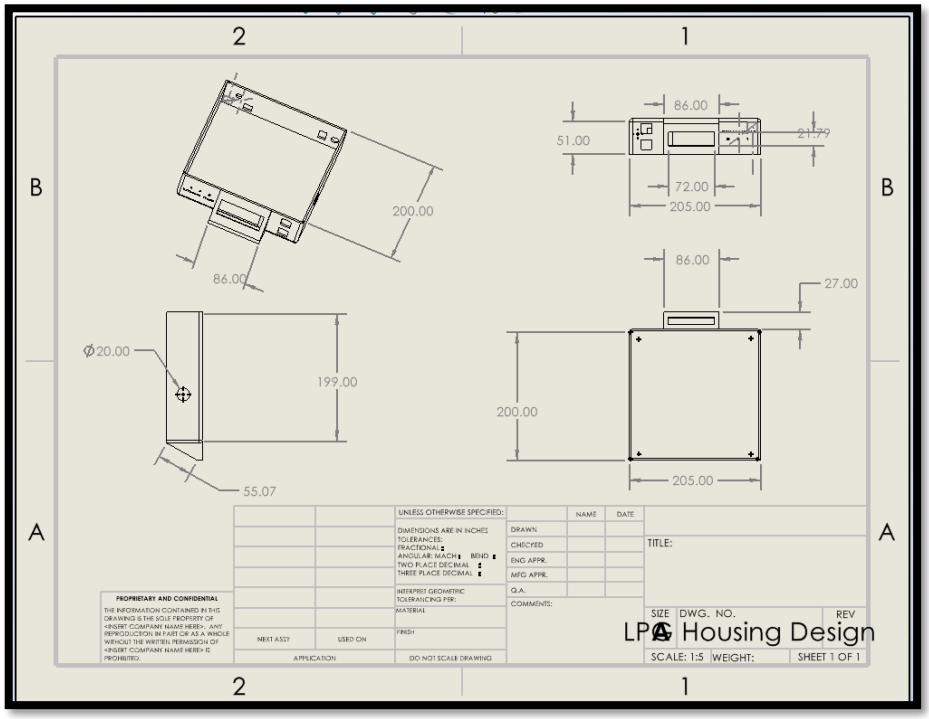

Figure 13.0 CAD Representation of the System Housing

2.2. Fused Deposition Modelling (FDM)

Fused Deposition Modeling is a 3D printing technology that builds objects layer by layer using a thermoplastic filament. The filament was heated and then extruded through a nozzle, which deposited the heated material onto a build platform in a pre-defined path (Siemiński, 2021). As each layer cooled, it bonded to the previous one, gradually forming the final structure as designed in CAD software, SolidWorks. The FDM technique is widely used because of its affordability, material versatility, as well as its ability to create functional prototypes and end-use parts.

SolidWorks 2024 is important software when it comes to Computer Aided Design. The designed model was saved as an STL file before being transferred to a special optimization software called slicer (Creality print v5.1) that modified the designs in terms of the infill density, wall thickness, printer speed, and supports as shown in Figure 10.0. After optimization, the ready to print model was converted into a GCODE file then transferred to the

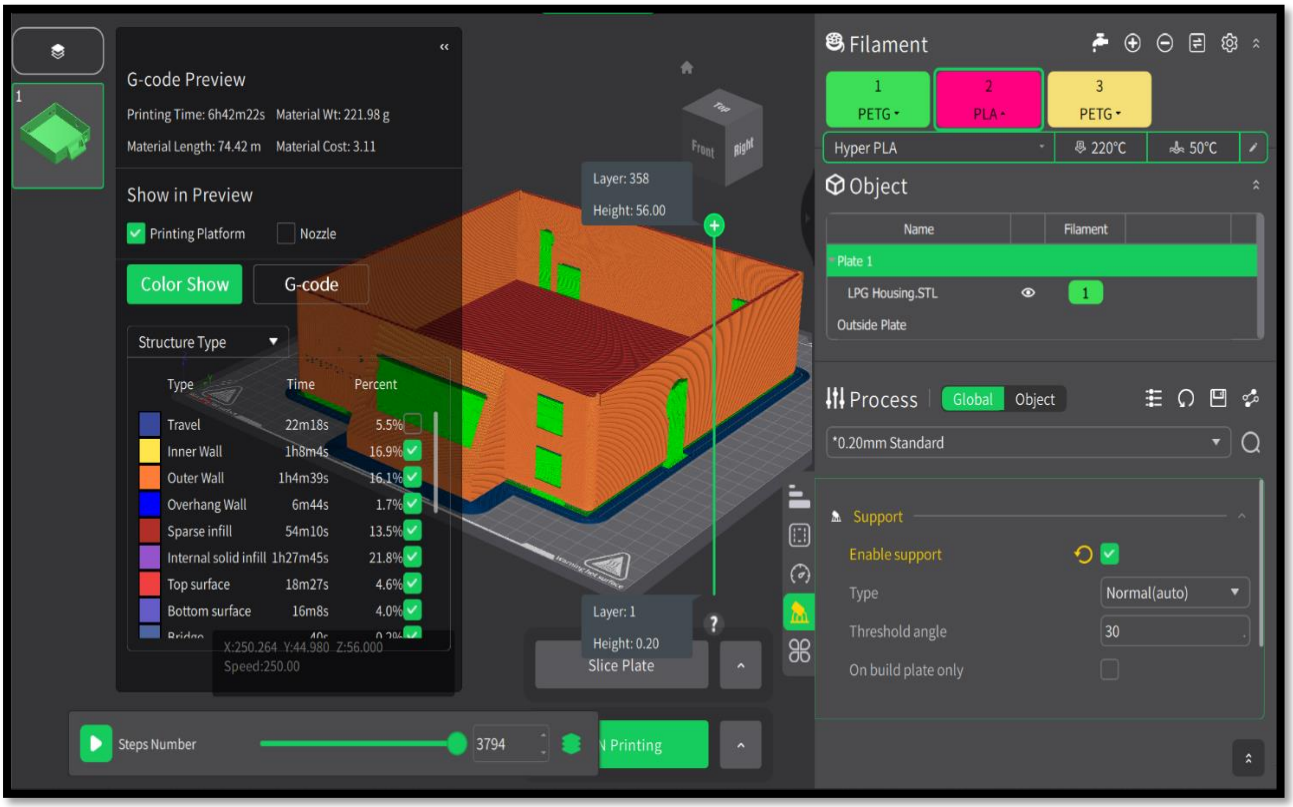

Creality K1

Figure 14.0 LPG CAD Model Optimization

Max Printer for printing through a flash drive (Shih, 2024)

3. RESULTS AND DISCUSSION

3.1. 3D Printing and Fabrication Outcome

The smart LPG usage detection and leakage alert system protective housing was successfully designed and fabricated using a 3D printer, Creality K1 Max 3D printer. The protective housing casing was printed using the Hyper Polylactic Acid (PLA) filament. The designed protective enclosure successfully accommodated all the key components of the LPG system, including the MQ gas sensor, GSM module, load cell, microcontroller (Arduino Uno), 16x2 Liquid Crystal Display, and the buzzer. The clear cutout slots and mounting structures provided perfect alignment, cable management and ease of assembly of the components. The dimension of the protective enclosure were 205 mm × 200 mm × 56 mm, printed using PLA with 13.1% infill density. The final 3D printed product matched the CAD model clearly demonstrating the significance of dimensional accuracy as well as structural integrity which was a key factor consideration during the optimization stage. The achievement of a successful print clearly underscores the efficiency and effectiveness of the slicing software, Creality Print v5.1 and the optimization process which ensured minimal waste of printing material while maintaining good mechanical robustness.

a

b

c

Figure 15.0 a) 3D Printed Protective Enclosure b) Front view c) Back view

The 3D printing process from design to post processing ensured a perfect, and user-customized protective enclosure for the LPG system. The printing parameters that guided the fabrication process included a layer height of 0.2 mm, an infill density of 13.1%, a nozzle temperature of 230°C, bed temperature of 60°C, and lastly the printing speed of 80 mm/s. Throughout the fabrication process, effective monitoring was done to ensure optimum and precise fabrication which helped in preventing defects such as the occurrence of warping and or layer separation. The Computer Aided Manufacturing process took a approximately a total of 6 hours. The GCODE file guided the printer in terms of model design including layer-by-layer fabrication, positioning, material extrusion, and other critical printing parameters (Shih, 2024).

3.2. System Performance with Enclosure

The system was tested using controlled LPG leak simulations and different weights for four possible conditions. The system correctly responded to all four scenarios as illustrated in Table 1.0

Table 1.0 System Response under Various Gas Leakage and Weight Conditions

Case	Condition	Output
1.	No leakage, Weight >0.5Kg	LCD Display, “YOU ARE SAFE”, BLUE LED ON.
2.	Gas leak detected, Weight >0.5Kg	LCD Display, “GAS LEAK DETECTED AT HOME”, Buzzer rings, RED LED ON, SMS Sent, and a voice call initiated to the user.
3.	Gas leak detected, Weight <0.5Kg	LCD Display, “GAS BELOW 0.5 Kg, GAS LEAK DETECTED AT HOME”, Buzzer rings, RED LED ON, SMS Sent “GAS LEAK DETECTED AND GAS LEVEL BELOW 0.5Kg. CLOSE THE GAS VALVE AND BUDGET FOR A REFILL, a voice call is initiated to the user.
4.	No leakage, Weight <0.5Kg	LCD Display, “GAS BELOW 0.5 Kg, BUDGET FOR A REFILL”, Buzzer rings, RED LED ON, SMS Sent to the user.

a

b

Figure 16.0 a) Gas leak and weight below set threshold b) Gas Leak detected alert

a

b

Figure 17.0 a) Gas below set threshold alert b) Low gas weight, Budget for a refill alert

3.3. Material Performance Evaluation

Hyper PLA material is an advanced or enhanced version of the normal or standard PLA material. The enhanced PLA is designed with improved mechanical and thermal properties that makes it stand out as compared to other materials. The hyper PLA supports high speed printing while not affecting the printout properties. The high tensile strength and toughness measured, 1.5 times higher than other materials such as ABS make the hyper PLA an excellent application especially for durable and robust applications (Hotend, n.d.). In addition, hyper PLA has proved to offer high impact resistance and temperature resistance, of up to 83°C after crystallization, for formulations (Hotend, n.d.). These properties make the material versatile and suitable for rapid prototyping as well as artistic applications (Filament2Print, n.d.).

According to Catana et al. (2021), different variants of 3D printed materials were subjected under bending stress and the results and simulations of the experiment were compared. The test strengths of each variant were determined and ranged between 28.87 MPa (G_12_T) to 82.33 MPa (P_E18_T) as shown in Table 1.0. In addition, there were also varied deformations

in the range of 3.37mm to 8.51mm. The simulations obtained had a close match therefore validating the accuracy of the predictions of the Finite Element Method (FEM). The P_E18_T, P_24_T, and P_E16 variants exhibited the highest strength (≥ 50 MPa) with moderate form of deformation. This therefore makes the hyper PLA material ideal for the protective enclosures for the LPG systems among many other enclosures. These results also highlight enhanced performance of the hyper PLA material and its potential in creating protective enclosures (Catana et al., 2021).

Thermal properties is also a key factor in cooling time as well as extrusion speed when dealing with this material among many other advantages of Hyper PLA with comparison to other materials including standard PLA. Also, the high mechanical strength makes the material more flowable which is an enhancement to the bonding quality especially between layers and nozzle clogging when extruded at high speed (Filament2Print, n.d.). The ability of the Hyper PLA in achieving high speed print out and minimal or no clogging in the nozzle makes it ideal in the production of high quality and smooth printed parts while keeping fine details as shown in figure 7.0.

Table 2.0 Comparisons between tests and simulation results for 3D-printed variants under bending stress.

Specimen Code	Test Results		Simulation Results	
	Strength (MPa)	Deformation (mm)	Strength (MPa)	Deformation (mm)
P_24	44.18	4.92	46.70	4.98
G_24	32.84	3.5	34.20	3.70
P_20	39.78	5.54	36.90	4.77
G_20	38.26	4.95	38.70	4.09
P_E18	54.85	5.81	55.30	6.10
G_E18	41.40	4.11	42.50	4.46
P_E16	51.02	6.05	51.80	5.83
G_E16	43.57	4.78	44.10	4.44
P_24_T	63.94	7.5	66.10	8.51
G_24_T	32.16	4.08	34.50	3.94
P_12_T	40.14	7.54	39.40	5.85
G_12_T	28.87	7.75	30.40	3.76
P_E18_T	82.33	6.37	83.10	8.17
G_E18_T	36.07	3.37	36.50	3.22

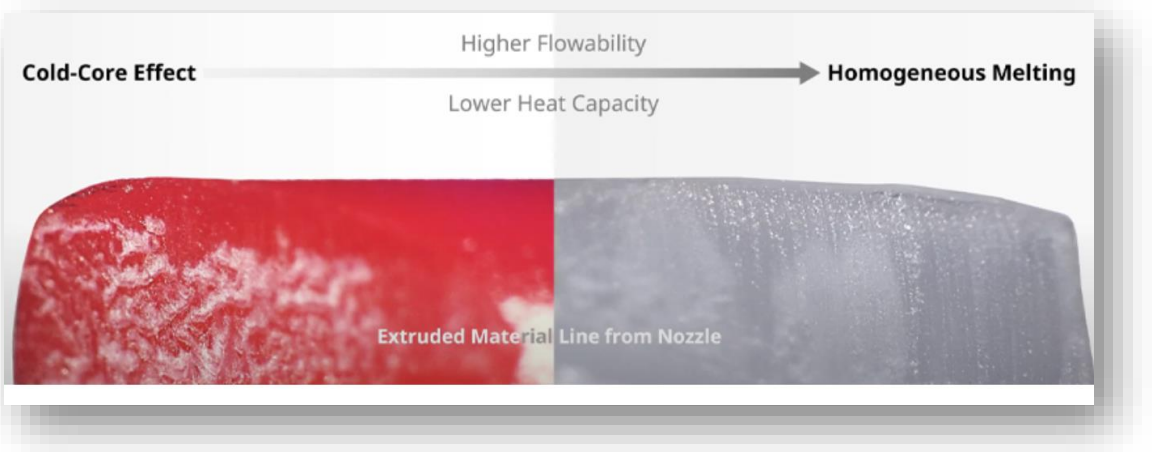

Figure 18.0 Hyper PLA thermal properties

According to Raise3D statistics, prototyping at high speeds, 200% faster increases the number at which design iterations are created by increasing the yield production of a 3D printer to up to four times. When hyper filaments or materials such as Hyper PLA are used for production, the productivity is likely to increase by 500%, thereby reducing the response time (Raise3D, n.d.). There are physical, thermal, electrical, and mechanical properties the material possesses that makes it ideal for many applications. Some of these properties include high extrusion speed capabilities, high mechanical properties i.e. high density of 1.22 g/cm^3, and high-quality surface finish (Raise3D, n.d.).

3.4. Cost and Customization Benefits

The cost and customization of a product is one of the key considerations when it comes to product design. Traditional manufacturing processes such as metal fabrication and injection molded plastic, although important, have many limitations especially on initial costs, lead times, design complexity, customization among other aspects because of the molds and the tooling process (McClements & Paulsen, 2024). The fabrication of these products, i.e. protective housing enclosures, are costly because of the expensive nature of the molds and higher lead time which has a significant impact on the final price of the product as shown in Figure 8. In addition, fabrication of these products lacks customization and therefore leaving users with little or no choice of interest as shown in Table 2.0 (Xometry, n.d.). According to Xometry (n.d.), 3D printing technology offers a more cost-effective approach in terms of design flexibility and faster lead times as compared to traditional manufacturing. On contrary, additive manufacturing, 3D printing allows design customization, rapid prototyping, as well as effective and efficient production especially for small scale, making 3D printing ideal especially for innovative solutions (Siemiński, 2021).

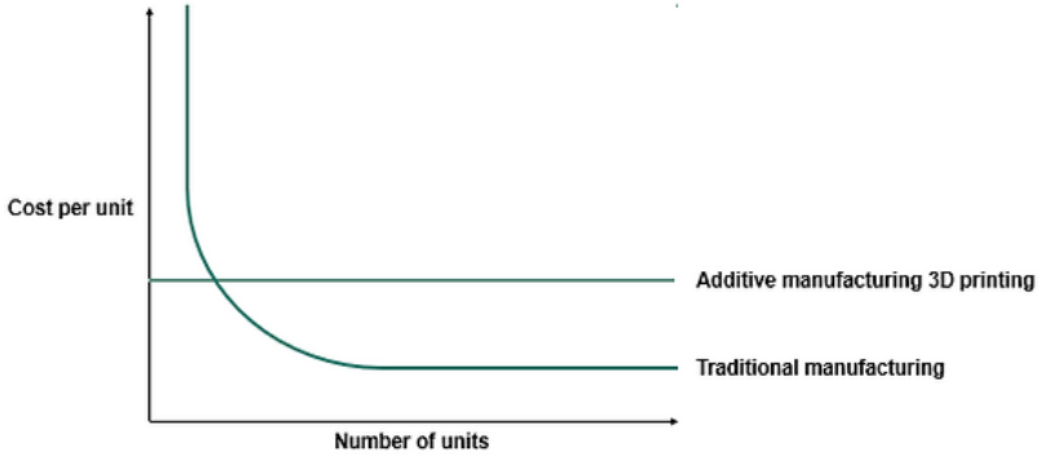

Table 3.0 Comparison of Additive Manufacturing (3D Printing) vs. Traditional Manufacturing

Attribute	3D Printing	Traditional Manufacturing
Lead time	Fast	Slow
Material selection	Good	Excellent
Surface finish	Moderate	Excellent
Profitability	Independent from scale	Large-scale production
Design complexity	Yes	No
Customizability	Yes	No

Figure 19.0 Additive manufacturing (3D printing) vs Traditional manufacturing

3.5. Structural and Ergonomic Considerations

Ergonomics is one of the key considerations to any design work. Design without considering the ergonomics aspect not only affects the user preferences but also market visibility as well as acceptance (Tosi & Tosi, 2020). In this study, the LPG usage detection and leakage alert system final housing casing put into consideration the ergonomic features of the product. These features include a user-friendly interface that is easily operated as well as maintained. System integration and mounting of sensors such as the gas sensor helped in securing the sensor attachment and therefore reducing risks to sensor misalignments or detachment. In addition,

placement of the LCD display at the user's preferred angle ensured that users have an easy and comfortable way of monitoring their LPG without straining.

3.6.Performance Comparison with Conventional Enclosures

According to Vijayalaxmi & Singh (2023), 3D printing offers better output in terms of cost as compared to other conventional ways of production. For example, a study by Vijayalaxmi & Singh (2023) cited a significant reduction in time and cost by 50% while using 3D printing technology as compared to other traditional ways. Other advantages of 3D printing as compared to conventional ways include reduced weight. 3D-printed housing was approximately 40% lighter as compared to metal alternatives (Jordan, 2019). Modular design also enabled easy customization, something that was not possible with traditional or conventional ways. Lastly, environmental conservation is very key when it comes to any design and production. With 3D printing, there was significant reduction in material wastage making production more ecofriendly as compared to the other conventional ways of production (Javaid *et al*., 2021).

4. LIMITATIONS AND FUTURE CONSIDERATIONS

Additive Manufacturing, 3D printing technology is a growing field especially in the continent of Africa and more specifically in Kenya. This is because of the slow adoption of technology in the continent. This technology has the potential to revolutionize every sector of life including healthcare, manufacturing, education among others. However, there is more that needs to be unraveled as far as production is concerned as this will help us to realize the full benefits of Additive Manufacturing. Despite the many advantages discussed, 3D printed housing has some limitations. For example, although the material can withstand temperatures up to 83oC, beyond this temperature, especially in high temperature environs, the material can lose its thermal properties (Raise3D, n.d.). Therefore, more research needs to be conducted, especially in heat resistant materials such as polymers as well as composite materials. Another limitation of 3D printing is scalability. Although 3D offers advantages such as cost and good material usage, scalability remains a big challenge. Research therefore needs to address this issue through hybrid manufacturing (Stavropoulos et al., 2018).

5. CONCLUSION

In conclusion, this study successfully designed and fabricated an effective protective enclosure for a smart LPG detection and leakage alert system using the Additive Manufacturing process, 3D printing technique. The protective enclosure was able to work perfectly with the system

components highlighting the importance of design customization as far as protective enclosures is concerned. The prototype's successful performance in all test scenarios confirms its reliability and practicality. The study is also a clear demonstration that additive manufacturing can offer a cost effective and viable solution in the production of not only protective enclosures for IoT-based safety systems but also other custom-based devices for different applications including medical applications.

The study findings clearly demonstrate the use of Additive Manufacturing and the application of 3D printing in achieving a cost-effective, highly customizable product. The development of a robust LPG enclosure not only underscores the importance of innovative technologies such as 3D printing but also demonstrates the significance of protecting IoT devices in enhancing durability, and performance. The choice of hyper PLA material not only proved to be aesthetic but also contributed to the device's thermal stability and mechanical strength, key contributors to reliable and high device performance (Blanco et al., 2022).

To enhance the work, future research should explore and focus on the use of other advanced 3D printing filaments or materials, such as carbon fiber-reinforced composites to achieve even higher thermal and mechanical properties. In addition, there is a high need for scalability and adoption of such technology-based products. This would help facilitate mass production, especially for commercial purposes. It is very evident from the study that optimization through layer height adjustment, infill patterns, support placement, print speed and cooling to prevent warping and material selection makes Additive Manufacturing, FDM a revolutionary tool in the development of IoT-based protective casing and enclosures for smart systems (Siemiński, 2021).

6. ACKNOWLEDGEMENTS

We thank the management of the Cezeri lab led by Dr. Kenneth Iloka, and Dr. Wairimu, for allowing us to use the lab for our research.

REFERENCES

Barrett, S. F., & Pack, D. J. (2022). *Microchip AVR® Microcontroller Primer: Programming and Interfacing*. Springer Nature.

Blanco, I., Cicala, G., Recca, G., & Tosto, C. (2022). Specific Heat Capacity and Thermal Conductivity Measurements of PLA-Based 3D-Printed Parts with Milled Carbon Fiber Reinforcement. *Entropy*, **24**(5): 654. https://doi.org/10.3390/e24050654

Catana, D., Pop, M. A., & Brus, D. I. (2021). Comparison between the Test and Simulation Results for PLA Structures 3D Printed, Bending Stressed. *Molecules*, **26**(11): 3325. https://doi.org/10.3390/molecules26113325

Javaid, M., Haleem, A., Singh, R. P., Suman, R., & Rab, S. (2021). Role of additive manufacturing applications towards environmental sustainability. *Advanced Industrial and Engineering Polymer Research*, **4**(4): 312–322. https://doi.org/10.1016/j.aiepr.2021.07.005

Prashar, G., Vasudev, H., & Bhuddhi, D. (2022). Additive manufacturing: Expanding 3D printing horizon in industry 4.0. *International Journal on Interactive Design and Manufacturing (IJIDeM)*, **–**: 1–15. https://doi.org/10.1007/s12008-022-00956-4

Rekha, M., Sathishkumar, S., Lakshni, S., Shravani, R., & Sharmitha, V. (2023, November). Revolutionizing Gas Management: An Integrated Approach To Leakage Detection, Monitoring, And Automated Booking System. In *2023 International Conference on Research Methodologies in Knowledge Management, Artificial Intelligence and Telecommunication Engineering (RMKMATE)* (pp. 1–10). IEEE. https://doi.org/10.1109/RMKMATE59243.2023.10368931

Serksnis, T. (2019). *Designing Electronic Product Enclosures*. Springer International Publishing. https://link.springer.com/content/pdf/10.1007/978-3-319-69395-8.pdf

Siemiński, P. (2021). Introduction to fused deposition modeling. In *Additive Manufacturing* (pp. 217-275). Elsevier.

Stavropoulos, P., Foteinopoulos, P., Papacharalampopoulos, A., & Bikas, H. (2018). Addressing the challenges for the industrial application of additive manufacturing: Towards a hybrid solution. International Journal of Lightweight Materials and Manufacture, 1(3), 157-168. https://www.sciencedirect.com/science/article/pii/S2588840418300490

Sujarwo, N. R. F., Kholis, N., Anifah, L., & Baskoro, F. (2021, December). Design Build of IoT Based Smart Liquefied Petroleum Gas Leakage Detector with NodeMCU ESP8266 Module. In *International Joint Conference on Science and Engineering*

2021 (IJCSE 2021) (pp. 688–692). Atlantis Press. https://www.atlantis-press.com/proceedings/ijcse-21/125966467

The Engineering Knowledge. (2021, January 30). *Introduction to Atmega328p Microcontroller*. Retrieved from https://www.theengineeringknowledge.com/introduction-to-atmega328p-microcontroller/

Cavaliere, P. (2023). Safety issues and regulations. In *Water Electrolysis for Hydrogen Production* (pp. 729–791). Cham: Springer International Publishing. https://doi.org/10.1007/978-3-031-37780-8_19

Jordan, J. M. (2019). *3D Printing*. MIT Press.

Shih, R. (2024). *Learning SOLIDWORKS 2024: Modeling, Assembly and Analysis*. SDC Publications.

Siemiński, P. (2021). Introduction to fused deposition modeling. In *Additive Manufacturing* (pp. 217–275). Elsevier.

Tosi, F., & Tosi, F. (2020). Design for ergonomics. In *Design for Ergonomics* (pp. 31–45). Springer International Publishing.

Vijayalaxmi, J., & Singh, P. (2023). Comparative analysis of concrete 3D printing and conventional construction technique for housing. In *Innovative Processes and Materials in Additive Manufacturing* (pp. 177–190). Woodhead Publishing.

Chakaravarthi, C. (2020, May 13). Comparison guide to efficiently fabricate electronic enclosures for your products. *Circuit Digest*. Retrieved March 9, 2025, from https://circuitdigest.com/article/comparision-guide-to-efficiently-fabricate-electronic-enclosures-for-your-products

CNC Kitchen. (2025). Comparing PLA, PETG & ASA [Feat. Prusament]. https://www.cnckitchen.com/blog/comparing-pla-petg-amp-asa-feat-prusament

Creality. (n.d.). K1 Max 3D printer: Fast, smart AI & precision. *Creality*. Retrieved March 10, 2025, from https://www.creality.com/products/creality-k1-max-3d-printer

Filament2Print. (n.d.). Hyper Speed PLA Raise3D. Retrieved March 4, 2025, from https://filament2print.com/en/pla/2053-hyper-speed-pla-raise3d.html

Hotend. (n.d.). 3DPOWER Hyper PLA - Flame Red. Retrieved March 4, 2025, from https://www.hotend.eu/p/3dpower-hyper-pla-flame-red

Illustrate Architecture. (2025). What to look for in durable and affordable electronic enclosures. https://illustrarch.com/articles/41448-what-to-look-for-in-durable-and-affordable-electronic-enclosures.html

K1 Max 3D printer. (n.d.). creality. https://www.creality.com/products/creality-k1-max-3d-printer?utm_source=chatgpt.com

MakerVerse. (n.d.). *3D printing vs. traditional manufacturing: Which is right for your production?* Retrieved May 27, 2025, from https://www.makerverse.com/resources/3d-printing/3d-printing-vs-traditional-manufacturing/#elementor-toc__heading-anchor-3

McClements, D., & Paulsen, G. (2024, October 8). 3D printing vs. traditional manufacturing: Differences and comparison. *Xometry*. https://www.xometry.com/resources/3d-printing/3d-printing-vs-traditional-manufacturing/

Mustafa, A., Aloyaydi, B., Subbarayan, S., & Al-Mufadi, F. A. (2021). Mechanical properties enhancement in composite material structures of poly-lactic acid/epoxy/milled glass fibers prepared by fused filament fabrication and solution casting. Polymer Composites, (12), 6847-6866.

Nakanwagi, S. (2021). Increasing uptake of liquefied petroleum gas in Uganda: Lessons from Morocco. https://pub.nkumbauniversity.ac.ug/xmlui/handle/123456789/901

Raise3D. (n.d.). Hyper Speed Upgrade Kit Overview. *Raise3D Support*. https://support.raise3d.com/RaiseTouch/1-overview-17-727.html

Spectrum Filaments. (n.d.). PLA Pro filament. Retrieved March 4, 2025, from https://spectrumfilaments.com/en/filament/pla-pro/

Xometry. (n.d.). 3D printing vs. traditional manufacturing: Differences and comparison. Retrieved from https://d27ze05algd7ka.cloudfront.net/resources/3d-printing/3d-printing-vs-traditional-manufacturing/

Editorial Committee

Name	Category	Country

Eng. Prof. Lawrence Gumbe	Chair	Kenya
Eng. Prof. Leonard Masu	Secretary	Kenya
Eng. Prof. Ayodeji Oluleye	Member	Nigeria
Eng. Dr. Slah Msahli	Member	Tunisia
Eng. Prof. Bernadette W. Sabuni	Member	Kenya
Prof. Anish Kutien	Member	South Africa

Editorial Board

	Name
Chairperson:	Eng. Prof. Lawrence Gumbe
Members:	Eng. Paul Ochola- Secretary
	Eng. Sammy Tangus- Treasurer
	Eng. Erick Ohaga – IPP, IEK
	Eng. Shammah Kiteme- President, IEK
	Eng. Prof. Leornard Masu
	Eng. Margaret Ogai
	Eng. Nathaniel Matalanga
	Eng. Dr. Samwel Roy Orenge – Technical Editor

INSTRUCTIONS TO CONTRIBUTORS

The editorial staff of the AJERI requests contributors of articles for publication to observe the following editorial policy and guidelines accessible at https://www.iekenya.org/ in order to improve communication and to facilitate the editorial process.

Criteria for Article Selection

Priority in the selection of articles for publication is that the articles:

a. Are written in the English language
b. Are relevant to the application relevant of engineering and technology research and Innovation
c. Have not been previously published elsewhere, or, if previously published are supported by a copyright permission
d. Deals with theoretical, practical and adoptable innovations applicable to engineering and technology
e. Have a 150 to 250 words abstract, preceding the main body of the article
f. The abstract should be followed by a list of 4 to 8 "key Words"
g. Manuscript should be single-spaced under 4,000 words (approximately equivalent to 5-6 pages of A4-size paper)
h. Are supported by authentic sources, references or bibliography

Rejected/Accepted Articles

a. As a rule, articles that are not chosen for AJERI publication are not returned unless writer (s) asks for their return and are covered with adequate postage stamps. At the earliest time possible, the writer (s) is advised whether the article is rejected or accepted.
b. When an article is accepted and requires revision/modification, the details will be indicated in the return reply from the AJERI Editor, in which case such revision/modification must be completed and returned to AJERI within three months from the date of receipt from the Editorial Staff.
c. Complementary copies: Following the publishing, three successive issues are sent to the author(s)

Procedure for Submission

a. Articles for publication must be sent to AJERI on the following address:

The Editor

African Journal of Engineering Research and Innovation

P.O Box 41346- 00100

City Square Nairobi Kenya

Tel: +254 (20) 2729326, 0721 729363, (020) 2716922

E-mail: editor@iekenya.org

b. The article must bear the writer (s) name, title/designation, office/organization, nationality and complete mailing address. In addition, contributors with e-mail addresses are requested to forward the same to the Editor for faster communication.

For any queries, authors are requested to contact by mail (editor@iekenya.org).

PUBLISHER

The Institution of Engineers of Kenya (IEK)

P.O Box 41346- 00100

City Square Nairobi Kenya

Tel: +254 (20) 2729326, 0721 729363, (020) 2716922

Email: editor@iekenya.org

Website: www.iekenya.org

CONTENTS

High Resolution Solar Irradiance Prediction Model for Machakos Town Using Long Short-Term Memory (LSTM) **6**

C. Mwaniki, R. Damoah

Water Resource Allocation: A Comparative Literature Review of Modeling Frameworks for Sustainable Management in River Catchments **15**

A. T. Asava, J. O. Okungu, M. M. Mukolwea, E. K. Kandaa

Rheology of En Masse Grains in Silo Load Computations **46**

L. O. Gumbe

Bio-Inspired Concrete Structures for Enhancing Mechanical Performance **1011**

L. K. Boretor

Design and 3D Printing of a Protective Enclosure System: A Customized Enclosure for a Smart LPG Detection and Leakage Alert System **110**

W. Augustine, M. Mathew, N. Raphael, I. Kenneth, M. Bazil